

**DISTINCT SUBPOPULATIONS OF EXTRACELLULAR VESICLES  
ARE RELEASED FROM THE CILIA OF *C. ELEGANS* SENSORY NEURONS**

by

Michael Clupper

A dissertation submitted to the Faculty of the University of Delaware in partial fulfillment of the requirements for the degree of Doctor of Philosophy in Biological Sciences

Spring 2022

© 2022 Michael Clupper  
All Rights Reserved

**DISTINCT SUBPOPULATIONS OF EXTRACELLULAR VESICLES  
ARE RELEASED FROM THE CILIA OF *C. ELEGANS* SENSORY NEURONS**

by

Michael Clupper

Approved: \_\_\_\_\_  
Velia M. Fowler, Ph.D.  
Chair of the Department of Biological Sciences

Approved: \_\_\_\_\_  
John A. Pelesko, Ph.D.  
Dean of the College of Arts and Sciences

Approved: \_\_\_\_\_  
Louis F. Rossi, Ph.D.  
Vice Provost for Graduate and Professional Education and  
Dean of the Graduate College

I certify that I have read this dissertation and that in my opinion it meets the academic and professional standard required by the University as a dissertation for the degree of Doctor of Philosophy.

Signed:

---

Jessica E. Tanis, Ph.D.  
Professor in charge of dissertation

I certify that I have read this dissertation and that in my opinion it meets the academic and professional standard required by the University as a dissertation for the degree of Doctor of Philosophy.

Signed:

---

Matthew E.R. Butchbach, Ph.D.  
Member of dissertation committee

I certify that I have read this dissertation and that in my opinion it meets the academic and professional standard required by the University as a dissertation for the degree of Doctor of Philosophy.

Signed:

---

Donna S. Woulfe, Ph.D.  
Member of dissertation committee

I certify that I have read this dissertation and that in my opinion it meets the academic and professional standard required by the University as a dissertation for the degree of Doctor of Philosophy.

Signed:

---

Erica M. Selva, Ph.D.  
Member of dissertation committee

I certify that I have read this dissertation and that in my opinion it meets the academic and professional standard required by the University as a dissertation for the degree of Doctor of Philosophy.

Signed:

---

Colin Thorpe, Ph.D.  
Member of dissertation committee

## ACKNOWLEDGMENTS

I would foremost like to thank Dr. Jessica Tanis for the opportunity to undertake my doctoral research in her lab, and for the constant support and guidance that allowed me to navigate a challenging project and emerge as a better scientist. I would also like to thank my project colleagues in the Tanis lab: Denis Touroutine, Rachael Gill, and Malek Elsayyid, without whom my project would not have been completed, and Andy Lam, Kirstin Kervin, and the rest of my lab friends, without whom I would've lost my sanity sometime after my second year of graduate school.

Additionally, I thank Dr. Jeffrey Caplan, Dr. Sylvain le Marchand, Timothy Chaya, and all of the members of the Delaware Bio-imaging Facility. Their assistance in matters small and large was absolutely essential to my experimental endeavors. Of course, thank you to Betty Cowgill and the entire administrative staff for being generally helpful and always awesome. Finally, I thank the individual members of my thesis committee, Dr. Erica Selva, Dr. Donna Woulfe, Dr. Matthew Butchbach, Dr. Colin Thorpe, and Dr. Matthew Hudson, for being insightful and asking the important questions.

To my wife, Meredith, and my family and friends, I give thanks for giving unwavering support and distraction, which was always appreciated and often necessary.

## TABLE OF CONTENTS

LIST OF TABLES .....	viii
LIST OF FIGURES .....	ix
ABSTRACT .....	xiv

### Chapter

1	INTRODUCTION .....	1
1.1	Extracellular vesicles and their subclasses .....	1
1.2	EV physiology and pathophysiology.....	2
1.3	EV biogenesis and molecular cargo sorting .....	4
1.4	Primary cilia as platforms for EV shedding .....	6
1.5	<i>In vivo</i> models of EV biology.....	8
1.6	<i>C. elegans</i> as a model for EV biology.....	9
1.7	Hypothesis and Specific Aims.....	15
2	MATERIALS AND METHODS .....	16
2.1	<i>C. elegans</i> culture and genetics .....	16
2.2	Generation of transgenic strains .....	17
2.3	Imaging and analysis of EVs.....	19
2.4	Imaging and analysis of male tail cilia .....	20
2.5	EV isolation and characterization.....	21
2.6	LC-MS/MS proteomic analysis of isolated EVs .....	22
2.7	Strep-tag protein blot.....	24
2.8	Statistics and Graphing.....	25
3	CLHM-1 IS CONTAINED WITHIN A DISTINCT SUBPOPULATION OF EVS RELEASED FROM SENSORY NEURON CILIA .....	32
3.1	CLHM-1 localizes to the cilia of EV-releasing sensory neurons .....	33
3.2	CLHM-1 is novel cargo in EVs released from sensory neuron cilia.....	36
3.3	CLHM-1 and PKD-2 are contained within quantifiably distinct subpopulations of EVs released from the same EVNs.....	41
3.4	Physiological factors differentially impact the release of EVs enriched with CLHM-1 and PKD-2.....	48

4	KINESIN-II MOTOR ACTIVITY DIFFERENTIALLY AFFECTS CLHM-1 AND PKD-2 CILIA LOCALIZATION AND EV BIOGENESIS.....	52
4.1	PKD-2, but not CLHM-1, is enriched to the distal tip of EVN cilia.....	52
4.2	Individual kinesin-II motor activity differentially impacts biogenesis of CLHM-1 and PKD-2 EVs.....	57
4.3	Release of EVs containing PKD-2, but not CLHM-1, is dependent on joint OSM-3 and heterotrimeric kinesin-II activity.....	66
4.4	MKS-5 and the transition zone are required for maintaining EV biogenesis .....	71
5	ALX-1 AND ARF-6 PLAY DISTINCT ROLES IN CILARY EV BIOGENESIS AND CARGO SORTING.....	74
5.1	The ubiquitin binding protein ALX-1 is a regulator of EV biogenesis...	74
5.2	ARF-6 is required for biogenesis of CLHM-1 EVs .....	78
6	ISOLATION AND LC-MS/MS CHARACTERIZATION OF EV PARTICLES FROM <i>C. ELEGANS</i> CULTURE .....	80
6.1	NTA and TEM characterization of EVs isolated from <i>C. elegans</i> culture using differential ultracentrifugation.....	80
6.2	LC-MS/MS analysis of EVs isolated from ultracentrifugation reveals presence of contaminating EVs.....	84
6.3	Engineering a Strep-tag into CLHM-1 to pull down CLHM-1 EVs via Streptavidin affinity beads.....	89
7	DISCUSSION.....	95
	REFERENCES.....	102

## LIST OF TABLES

Table 1: List of strains used in this study .....	26
Table 2: List of oligonucleotide primers used in this study .....	29
Table 3: List of transgenic alleles generated for use in this study.....	31
Table 4: List of <i>C. elegans</i> proteins represented in LC-MS/MS samples .....	86
Table 5: List of <i>E. coli</i> proteins represented in LC-MS/MS samples .....	87

## LIST OF FIGURES

- Figure 1: Exosomal and ectosomal EVs contain multiple species of functional biological macromolecule, including proteins, lipids, nucleic acids, and metabolites..... 12
- Figure 2: Exosomes and endosomes arise by different mechanisms, but both use the ESCRT complex as a means of cargo sorting and excision (Monguió-Tortajada et al., 2019)..... 13
- Figure 3: The cilia of IL2, CEM, RnB, and HOB sensory neurons shed ectosomal EVs into a lumen formed by surrounding glial cells. These EV are then released into the environment through a pore in the outer cuticle. . 14
- Figure 4: (A) *Pclhm-1::gfp* is expressed in a number of ciliated sensory neurons in the head (left) and tail (right) of adult males. (B) *Pklp-6::mCherry* is expressed in IL2, CEM, RnB (R1B-R9B, excluding R6B), and HOB neurons. (C) Expression of the two transgenes overlaps in the IL2, CEM, RnB, and HOB neurons. Scale bar = 10  $\mu\text{m}$ ..... 34
- Figure 5: tdTomato-tagged CLHM-1 localizes to the cilia of IL2 and CEM neurons of the male head (left) and the RnB and HOB neurons of the male tail (right), as denoted by colocalization with the ends of a *Pklp-6::gfp* transgene. Scale bars = 10  $\mu\text{m}$ ..... 35
- Figure 6: Environmental release of EVs containing PKD-2::GFP does not significantly change between wild-type and *clhm-1(tm4071)* mutant animals. Error bars show SEM. Mann-Whitney test;  $n \geq 15$ . ..... 38
- Figure 7: Structured Illumination microscopy shows CLHM-1::GFP in environmental EVs (A). TIRF microscopy shows EVs containing CLHM-1::GFP are released into the environment from EVNs of the adult male head (B) and tail (C), as well as from the hermaphrodite head (D). EVs are released from a over 80 percent of male animals and 60 percent of hermaphrodite animals (E). Scale bars = 3  $\mu\text{m}$ . Error bars show SEM.  $n \geq 23$ . ..... 39

Figure 8: Linear unmixing shows emission from CLHM-1::GFP (A,D), autofluorescence (B), and merged with transmitted light (C). Normalized fluorescence emission from EVs containing CLHM-1::GFP matches an eGFP reference emission spectrum, showing the signal is not autofluorescence emission or background noise (E). Scale bars = 10  $\mu$ m. .... 40

Figure 9: TIRF imaging shows fluorescently tagged proteins in EVs released from the same ciliated neurons. (A) CLHM-1::tdTomato and CLHM-1::GFP frequently colocalize in environmental EVs. (B) PKD-2::tdTomato and PKD-2::GFP frequently colocalize in environmental EVs. (C) CLHM-1::tdTomato and PKD-2::GFP colocalize less frequently in environmental EVs. Scale bars = 10  $\mu$ m. .... 44

Figure 10: (Top) Imaris spot detector was used to quantify GFP and tdTomato in released environmental EVs. (Bottom) Quality thresholds for analysis were calculated by imaging animals lacking GFP or tdTomato transgenes. Scale bar = 10  $\mu$ m. Error bar show SEM.  $n \geq 5$ . .... 45

Figure 11: The average number of released environmental EVs containing CLHM-1::tdTomato released does not significantly change between different *clhm-1::tdTomato* SCI transgenes (henSi2 & henSi17), or when *clhm-1::tdTomato* transgenes are paired with different *gfp* SCI transgenes (drSi33, henSi20, henSi21). Error bars show SEM. Kruskal-Wallis test;  $n \geq 35$ . .... 46

Figure 12: (Left) CLHM-1::GFP is significantly more likely than PKD-2::GFP to coincide with CLHM-1::tdTomato in released environmental EVs. (Right) PKD-2::tdTomato is significantly more likely than CLMH-1::tdTomato to coincide with PKD-2::GFP in released environmental EVs. Error bars show SEM. Kruskal-Wallis test;  $n \geq 35$ . \*=  $p < 0.05$ , \*\*= $p < 0.01$ , \*\*\*= $p < 0.005$ . .... 47

Figure 13: (Top) The average number of environmental EVs containing CLHM-1::tdTomato released from the adult male tail significantly decreases in male-only populations, while the average number of PKD-2::GFP EVs released significantly increases. (Bottom) The probability of PKD-2::GFP coinciding with CLHM-1::tdTomato in released environmental EVs significantly increases in male-only populations. Error bars show SEM. Mann-Whitney test,  $n \geq 20$ . \*=  $p < 0.05$ , \*\*= $p < 0.01$ . .... 50

Figure 14: The average number of environmental EVs containing CLHM-1::tdTomato released from the adult male head does not significantly change, while the average number of PKD-2::GFP EVs released significantly increases. Error bars show SEM. Mann-Whitney test; $n \geq 20$ . *= $p < 0.05$ , **= $p < 0.01$ .....	51
Figure 15: (Top) CLHM-1::tdTomato and CLHM-1::GFP colocalize in the PCMC (triangle) and middle segment of the cilia proper (bracket). (Bottom) CLHM-1::tdTomato and PKD-2::GFP colocalize in the PCMC and middle segment of the cilia proper, but PKD-2 alone localizes to the distal segment (arrow). Scale bars = 3 $\mu\text{m}$ . .....	54
Figure 16: Average normalized fluorescence intensity of CLHM-1::tdTomato and PKD-2::GFP along the length of RnB cilia shows that PKD-2 alone localizes to the cilia distal segment. Error bars show SEM. $n \geq 15$ . .....	55
Figure 17: (A) PKD-2::GFP, but not CLHM-1::tdTomato, is found in EVs shed from the cilia distal segment (arrowhead). (B) An EV containing CLHM-1::tdTomato, but not PKD-2::GFP, is shed from the PCMC (arrowhead). (C) Schematic representation of differential cilia localization leading to EV enrichment of CLHM-1::tdTomato and PKD-2::GFP. Scale bars = 3 $\mu\text{m}$ . .....	56
Figure 18: (Left) Environmental release of EVs containing PKD-2::GFP is not significantly changed in <i>kfp-11</i> or <i>osm-3</i> mutant backgrounds. (Right) Environmental release of EVs containing CLHM-1::tdTomato is significantly increased in both <i>kfp-11</i> and <i>osm-3</i> mutant males. Error bars show SEM. Kruskal-Wallis test; $n \geq 24$ . *= $p < 0.05$ , **= $p < 0.01$ , ***= $p < 0.005$ . .....	61
Figure 19: Average normalized fluorescence intensity of CLHM-1::tdTomato and PKD-2::GFP along the length of RnB cilia shows that PKD-2 alone localizes to the cilia distal segment in <i>kfp-11</i> (left) and <i>osm-3</i> (right) mutant males. Error bars show SEM. $n \geq 15$ .....	62
Figure 20: The probability of PKD-2::GFP coinciding with CLHM-1::tdTomato in released environmental EVs does not significantly change in <i>kfp-11</i> mutants but significantly increases in two different <i>osm-3</i> mutant alleles. Error bars show SEM. Kruskal-Wallis test; $n \geq 24$ . *= $p < 0.05$ , **= $p < 0.01$ , ***= $p < 0.005$ .....	63

- Figure 21: The M2 coefficient is significantly lower in the cilium proper (left) and PCMC (right) of RnB neuron cilia in *klp-11*, but not *osm-3*, mutant males. Error bars show SEM. Kruskal-Wallis test;  $n \geq 20$ . \*=  $p < 0.05$ , \*\*= $p < 0.01$ , \*\*\*= $p < 0.005$ . ..... 64
- Figure 22: The average number of released environmental EVs containing either CLHM-1 and PKD-2 significantly decreases in *klp-6* mutant males. Error bars show SEM. Mann-Whitney test;  $n \geq 20$ . \*=  $p < 0.05$ , \*\*= $p < 0.01$ , \*\*\*= $p < 0.005$ . ..... 65
- Figure 23: The average number of released environmental EVs containing PKD-2::GFP, but not CLHM-1::tdTomato, significantly decreases in *klp-11;osm-3* mutant males. Scale bars = 3  $\mu\text{m}$ . Error bars show SEM. Mann-Whitney test;  $n \geq 25$ . \*=  $p < 0.05$ , \*\*= $p < 0.01$ , \*\*\*= $p < 0.005$ . ..... 68
- Figure 24: The probability of PKD-2::GFP coinciding with CLHM-1::tdTomato in released environmental EVs significantly decreases change in *klp-11;osm-3* mutant males. Mann-Whitney test;  $n \geq 25$ . \*=  $p < 0.05$ , \*\*= $p < 0.01$ , \*\*\*= $p < 0.005$ . ..... 69
- Figure 25: Average normalized fluorescence intensity of CLHM-1::tdTomato and PKD-2::GFP along the length of RnB cilia shows that CLHM-1 alone enters the cilia proper in *klp-11;osm-3* mutant males. Error bars show SEM.  $n \geq 14$ . ..... 70
- Figure 26: The average number of released environmental EVs containing PKD-2 (left), but not CLHM-1 (right), significantly decreases in *mks-5(tm3100)* mutant males. Error bars show SEM. Mann-Whitney test;  $n \geq 20$ . \*=  $p < 0.05$ , \*\*= $p < 0.01$ , \*\*\*= $p < 0.005$ , \*\*\*\*= $p < 0.001$ . ..... 72
- Figure 27: The probability of PKD-2::GFP coinciding with CLHM-1::tdTomato in released environmental EVs significantly decreases change in *mks-5(tm3100)* mutant males. Mann-Whitney test;  $n \geq 20$ . \*=  $p < 0.05$ , \*\*= $p < 0.01$ . ..... 73
- Figure 28: The average number of released environmental EVs containing CLHM-1 (right), but not PKD-2 (left), significantly increases in *alx-1(gk338)* mutant males. Error bars show SEM. Student's t-test;  $n \geq 14$ . \*=  $p < 0.05$ . ..... 76
- Figure 29: ALX-1::mKate shows nonspecific punctate distribution in the head of an adult male hermaphrodite (white arrow). ..... 77

Figure 30: The average number of released environmental EVs containing CLHM-1, significantly decreases in *arf-6(tm1447)* mutant males. Error bars show SEM. Mann-Whitney test;  $n \geq 20$ .  $*= p < 0.05$ ,  $**= p < 0.01$ . ..... 79

Figure 31: TEM image of pelleted EVs negative stained with uranyl acetate shows EVs are circular and wrapped in membrane-like structure. Scale bar = 0.2  $\mu\text{m}$ . ..... 82

Figure 32: Nanoparticle Tracking Analysis shows that the majority of pelleted EVs are  $135.7 \pm 35.6$  nm in diameter. Graph is an average of 5 technical replicates. .... 83

Figure 33: Protein blot shows Streptactin-HRP conjugate against lysate of animals expressing CLHM-1::tdTomato with internal Strep-tag. Bands appear at approximately 100 kDa and 75 kDa in transgenic lanes but not wild-type lane. .... 92

Figure 34: CLHM-1(STII)::GFP localizes to the cilia of adult male head and tail EVNs. Scale bars = 10  $\mu\text{m}$ . .... 93

Figure 35: The average number of released environmental EVs containing CLHM-1(STII)::GFP is not significantly different than the number containing CLHM-1::GFP. Scale bars = 10  $\mu\text{m}$ .  $n \geq 20$ . Mann-Whitney test. .... 94

## ABSTRACT

Extracellular vesicles (EVs) are shed from primary cilia in multiple systems, yet their role in regulating physiological processes is unclear. As the functionality of an EV is dependent upon its molecular cargo; understanding how cargo is sorted into ciliary EVs is fundamental to understanding their physiological potential.

I discovered that the CLHM-1 ion channel is novel cargo in EVs shed from the cilia of *C. elegans* sensory neurons. Using TIRF super-resolution microscopy, I showed that tdTomato-tagged CLHM-1 is enriched into a subpopulation of EVs distinct from those containing GFP-tagged PKD-2, a well-characterized EV cargo. Analysis of fluorescent cilia images shows that PKD-2 and CLHM-1 differentially localize to distinct subregions of the cilia, leading to their EV enrichment.

To understand how the cilia achieves discrete ciliary sublocalization and EV enrichment, I examined EV release in kinesin-II loss-of-function mutants and found that individual loss of the kinesin OSM-3 or heterotrimeric kinesin-II had differential effects on release of CLHM-1 and PKD-2 EVs, as well as their ciliary colocalization. Loss of both OSM-3 and heterotrimeric kinesin-II prevented cilia entry and EV inclusion of PKD-2, but not CLHM-1. Deleting the transition zone ciliary diffusion barrier also impacted release of PKD-2, but not CLHM-1, EVs.

To characterize other molecular cargo in the CLHM-1 EV subpopulation, I engineered a chimeric CLHM-1 protein containing a Strep-tag in an extracellular loop domain for affinity isolation. I confirmed that Strep-tagged CLHM-1 localizes to the

cilia, is included in EVs, and binds to Streptactin affinity resin, indicating the potential of Strep-tagged CLHM-1 as a tool for isolating intact ciliary EVs.

Ultimately, my work develops *C. elegans* as an *in vivo* model for studying protein packaging into EVs shed from cilia and describes TIRF imaging as a novel technique for super-resolution imaging of fluorescently labeled EVs. I discovered that enrichment of protein cargo into ciliary EVs is a consequence of protein ciliary sublocalization. Future works include using super-resolution microscopy to explore other molecular mechanisms that alter protein ciliary distribution and EV enrichment, and to isolate intact EVs to characterize their molecular cargo and physiological potential.

# Chapter 1

## INTRODUCTION

### 1.1 Extracellular vesicles and their subclasses

Extracellular vesicles (EVs) are subcellular, membrane-wrapped particles that can contain mRNA, miRNA, soluble and transmembrane proteins, metabolites, and are often enriched in unique lipids (**Figure 1**)(Colombo et al., 2014; van Niel et al., 2018). EVs allow cells to jettison unwanted material, and to deliberately exchange functional biological macromolecules and cytoplasmic material as a means of intercellular communication. In this sense, EVs play an active role in many physiological and pathophysiological processes by changing the environmental or gene expression state of target cells (van Niel et al., 2018; Yáñez-Mó et al., 2015).

There are three subclasses of EVs – exosomes, ectosomes (also known as microvesicles), and apoptotic bodies – delineated primarily by size and mechanism of biogenesis (**Figure 2**). Exosomes are the smallest EV subclass (ranging from 40-100 nanometers) and arise when intraluminal vesicles (ILVs) bud into a late endosome, forming a multivesicular body (MVB). Exosomes are released into the external space when the MVB binds to the plasma membrane. Ectosomes range from 100 - 500 nanometers in diameter and are formed by budding directly from the plasma membrane. Apoptotic bodies vary in size and are formed when cells undergoing

programmed cell death bleb off parts of the dying cell (van Niel et al., 2018; Yáñez-Mó et al., 2015). As the mechanism of biogenesis, function, and morphology of apoptotic bodies are distinct from that of ectosomes and exosomes, they will be excluded forthwith from my definition of ‘extracellular vesicles’.

## **1.2 EV physiology and pathophysiology**

An increasing body of research has made it apparent that both exosomes and ectosomes play a role in many human physiological processes. Exosomes regulate reticulocyte maturation by coordinated protein jettison (Harding, 1983; Lespagnol et al., 2008; Rieu et al., 2000). In reproduction, exosomes dubbed ‘prostasomes’ promote fertility by stimulating the acrosomal reaction and suppressing the female immune system (Palmerini et al., 2003; Skibinski et al., 1992). Exosomes can also modulate the adaptive immune system by providing information to antigen presenting cells and T cells (Giri & Schorey, 2008; Izquierdo-Useros et al., 2012; Montecalvo et al., 2012; Morelli et al., 2004; Théry et al., 1999). In the nervous system, exosomes provide an additional means of neuron-neuron communication (Chivet et al., 2014; Lachenal et al., 2011), and can promote neuroprotection and axon regeneration when released from glial cells (Frohlich et al., 2014; Frühbeis et al., 2013; Lopez-Verrilli et al., 2013).

The role of ectosomes has been studied intensively in hemostasis, where they can have both pro- and anti-coagulation effects (Berckmans et al., 2001; Castaman et

al., 1996; Toti et al., 1996). Ectosomes from the epididymis play a role in sperm maturation (Schwarz et al., 2013). In the nervous system, ectosomes released from microglia can regulate synaptic activity of target neurons (Antonucci et al., 2012; Gabrielli et al., 2015).

Despite these seminal findings, by-and-large the roles that EVs play in human physiology are still poorly understood. Additionally, many EV-related physiology studies are conducted exclusively *in vitro*, meaning definitive *in vivo* evidence is needed for these suggested physiological EV roles.

EVs also play an active role in pathophysiology. Their role in cancer has drawn significant interest, as tumor-derived EVs can promote formation of a metastatic niche in target tissues and tumor cell differentiation (Kucharzewska et al., 2013; Webber et al., 2010). In the context of Alzheimer's disease, EVs can carry neurotoxic misfolded amyloid- $\beta$  or tau proteins. It is currently unclear whether this propagates or ameliorates disease progression, with evidence supporting both models (Bahrini et al., 2015; Bulloj et al., 2010; Guo & Lee, 2011; Joshi et al., 2014). EVs also play a role in cardiac, renal, and musculoskeletal pathologies, among many others (Borges et al., 2013; Halkein et al., 2013; Kolhe et al., 2017). As the concentration of many EV cargoes changes in disease states, EVs are also seen as a promising biomarker for diagnosis for diseases for which clinical detection is difficult (Lane et al., 2018; Prabu et al., 2019; Spitzer et al., 2019).

### **1.3 EV biogenesis and molecular cargo sorting**

The molecular function of EVs is to modulate the cellular environment and/or gene expression of a target cell by delivering molecular cargo including proteins and RNAs (Yáñez-Mó et al., 2015). The function of any EV is dependent upon contained cargo and thus the parent cell type. Herein lies the complexity of EVs: both exosomes and ectosomes are released from a large suite of cell types and can contain an extremely broad spectrum of cargo. Nearly all cell types release EVs, which are found circulating in numerous bodily fluids (Admyre et al., 2003; Gonzalez-Begne et al., 2009; Pisitkun et al., 2004; Street et al., 2012). The potential molecular content of EVs is extremely heterogeneous: the database Vesiclepedia has recorded 349,988 proteins, 27,646 mRNAs, 10,520 miRNAs and 639 lipids types from over 1000 studies across 41 different species as of 2021.

Recent literature suggests that within any individual subclass of EVs released from a single cell, there exist heterogenous subpopulations varying in morphology and cargo enrichment. Exosomes released by B16F10 melanoma cells can be separated by density gradient ultracentrifugation, and the resulting exosome fractions are differentially enriched in protein cargo (Willms et al., 2016). Additionally, breast cancer cells have been found to release specialized EVs enriched in specific miRNAs (Palma et al., 2012). These and other findings suggest that selectivity of EV cargo is intensely regulated and speaks to the remarkable potential for EVs as a complex, nuanced form of cell signaling (Jeppesen et al., 2019).

Several independent molecular mechanisms exist to sort molecular cargo into exosomes or ectosomes. The most well-characterized pathway is dependent upon the endosomal sorting complexes required for transport (ESCRT) machinery: conserved protein complexes that play a role in both exosomes and ectosome cargo sorting and biogenesis (**Figure 2**)(Hurley, 2015). In the ESCRT-dependent pathway of exosome biogenesis, the ESCRT-0 complex initiates ILV formation by binding to and sequestering ubiquitinated cargo on the late endosomal membrane (Mayers et al., 2011). The ESCRT-I complex forms a bridge between ESCRT-0 and ESCRT-II, and is able to bind to ubiquitinated protein cargo and lipid molecules with low affinity (Kostelansky et al., 2007). The ESCRT-II complex binds to ESCRT-I and the endosomal membrane, promoting membrane budding (Im & Hurley, 2008; Kostelansky et al., 2007). Together, these three complexes direct the sorting of exosome cargo. ESCRT-II also recruits the highly conserved ESCRT-III/ Vps4 complex, which regulates membrane scission and ESCRT complex disassembly (Han & Hill, 2019; Scott et al., 2005; Wollert et al., 2009).

Recently, it has been shown that EV formation can also proceed through additional ESCRT-dependent pathways. In HEK293T cells, the arrestin domain containing protein 1 (ARRDC1) acts to initiate ectosome budding by associating with the plasma membrane and recruiting the ESCRT-I complex. This process is also dependent upon ESCRT-III/ Vps4 activity (Nabhan et al., 2012). ARRDC1 knockout also causes differential cargo enrichment in ectosomes, and ARRDC1 ectosomes mediate non-canonical NOTCH signaling (Anand et al., 2018; Q. Wang & Lu, 2017).

An important auxiliary factor in ESCRT-dependent pathways is the ALG interacting protein X, or ALIX (Bissig & Gruenberg, 2014). ALIX can bind ubiquitinated cargo and ESCRT-III subunits to promote ESCRT-dependent exosome biogenesis (Baietti et al., 2012; Odorizzi, 2006).

Several other ESCRT-independent pathways of EV biogenesis have been described. The tetraspanin CD63 can coordinate ILV budding independent of the ESCRT machinery (van Niel et al., 2011). Interestingly, ALIX can sort the GPCR Par1 into exosomes in a ubiquitin-independent manner, bypassing the need for ESCRT-0, -I, or -II (Dores et al., 2012). The ADP ribosylation factor 6 (ARF6) can also promote ectosome budding in an ESCRT-independent manner (Muralidharan-Chari et al., 2009).

While some of the machinery that regulates the sorting of EV cargo during biogenesis have been elucidated, there are many contextually specific mechanisms that are still poorly understood. Additionally, it is still unclear how certain EV cargoes are enriched and EV subpopulations are specified.

#### **1.4 Primary cilia as platforms for EV shedding**

Ectosomes are also shed from primary cilia (Nager et al., 2017; Phua et al., 2017; J. Wang et al., 2014; Wood et al., 2013), which are highly conserved microtubule-based organelles that protrude from most eukaryotic cells to provide a platform for organizing both signal transduction (Delling, DeCaen, et al., 2013; Jiang et al., 2019;

Loktev & Jackson, 2013; Wheway et al., 2018) and signal transmission (Volz et al., 2021; J. Wang et al., 2014; J. Wang & Barr, 2016; Wood et al., 2013). The protein composition of primary cilia is dynamically mediated by intraflagellar transport (IFT), which employs both plus-end and minus-end tracking microtubule-binding motor proteins and cargo adaptor proteins to translocate signaling components along the ciliary ultrastructure (Blacque et al., 2004; Kobayashi et al., 2020; Prevo et al., 2017; Qin et al., 2005; Singh et al., 2020).

Free diffusion of certain proteins and lipids into the cilia is prevented by a multi-protein complex known as the transition zone (TZ). Assembly of the transition zone complex is dependent on the conserved assembly factor MKS-5.(Jensen et al., 2015a; C. Li et al., 2016). IFT motors and associated cargo adaptors are selectively required to bypass the transition zone (Fu et al., 2016; Hirano et al., 2017), and IFT itself is required for the maintenance of the transition zone (Jensen et al., 2018). In this way, the transition zone and IFT specify ciliary protein compartmentalization and enrichment.

Certain conserved IFT proteins are required for the shedding and release of most ciliary EVs (Akella et al., 2020; Nager et al., 2017; O'Hagan et al., 2017; J. Wang et al., 2014, 2021), although the specific contribution of individual IFT proteins to ciliary EV biogenesis and selective cargo enrichment has not been explored.

## 1.5 *In vivo* models of EV biology

Although the study of physiological and molecular characteristics of EVs *in vitro* has greatly contributed to our understanding of EV biology, there remains the question of the physiological relevance of *in vitro* findings. Thus, it is imperative to study basic questions of EV biology *in vivo*. In complex systems, however, this can be difficult, as EV studies are often conducted using fluid samples, and EVs from multiple cell types can be released into the same bodily fluid (Ramirez et al., 2018). As such, there is great value in seeking *in vivo* answers from simpler eukaryotic model systems.

Some progress has already been made where this is concerned. Studies have been conducted in *Chlamydomonas reinhardtii*, *Drosophila melanogaster*, and *Caenorhabditis elegans*, showing that EVs are physiologically relevant to these organisms in both development and behavior (Gross et al., 2012; Hyenne et al., 2015; Koles et al., 2012; J. Wang et al., 2014). Additionally, the core EV biogenesis machinery – the ESCRT complexes and small GTPases – are conserved between lower- and higher-order eukaryotic systems (Corrigan et al., 2014; Hyenne et al., 2015).

The advantages of using such simple, genetically tractable models cannot be understated; the study of *C. elegans* alone has contributed vastly to our understanding of many fundamental aspects of biology. Since its first use as a model organism in 1974, the free-dwelling non-parasitic nematode *C. elegans* has become an immensely popular model organism. Compared to higher-order systems, care and maintenance *C.*

*elegans* is simple and cost-effective. It was the first metazoan organism to have its entire genome sequenced; since then, a remarkably diverse genetic toolkit has been developed to manipulate the *C. elegans* genome. Additionally, these animals are transparent, allowing for easy visualization of fluorescently tagged proteins in a living specimen (Corsi et al., 2015).

### 1.6 *C. elegans* as a model for EV biology

In the context of EV biology, *C. elegans* release exosomes from seam cells (Hyenne et al., 2015). In embryonic cells, controlled ectosome shedding regulates cell adhesion and morphogenesis, and is dependent on the ATPase TAT-5 and the ESCRT complex (Wehman et al., 2011).

EVs are also shed from the cilia of a subset of *C. elegans* sensory neurons (**Figure 3**), including the inner labial type 2 (IL2) and male-specific cephalic male (CEM), bilateral ray B-type (RnB), and hook B-type (HoB) neurons (Nikonorova et al., 2021; Razzauti & Laurent, 2021; J. Wang et al., 2014). Release of ciliary EVs containing GFP-tagged PKD-2, a conserved TRP polycystin channel, is dependent on genes that maintain cilia structure and function, but not upon ESCRT-0 subunit *stam-1* or ESCRT-1 subunit *mvp-12*. Additionally, electron tomography shows no MVBs in the cilia or surrounding lumen and that EVs bud directly from the cilia membrane, identifying these EVs as ectosomes. These EVs are biologically active: when plated on solid medium, they induce higher frequency of a male-specific mating behavior

known as tail-chasing (J. Wang et al., 2014). Release of EVs containing PKD-2 from the adult male tail is dependent on mechanical stimulus and male-derived EVs accumulate in the hermaphrodite uterus following copulation (J. Wang et al., 2020). *C. elegans* ciliated neuron EVs provide a unique, relatively novel opportunity to study several poorly explored aspects of EV biology *in vivo*, including biogenesis of EVs released from neurons, trafficking and packaging of EV cargo, and the release of EVs from primary cilia.

The maintenance of primary cilia structure and function is orchestrated by multiple molecular processes, including IFT (Bader et al., 2012; Prevo et al., 2017; van der Burght et al., 2020). How IFT and other processes work together to control ciliary EV biogenesis and cargo sorting is an active area of investigation (O'Hagan et al., 2017; Silva et al., 2017; J. Wang et al., 2014, 2021). While studies have shown the importance of IFT as a whole to be important for ciliary EV biogenesis and release, how individual IFT components contribute to these aspects of EV biology is not well understood.

An obstacle to studying ciliary EV biology is the lack of well-described EV markers. Although density gradient ultracentrifugation and subsequent proteomic profiling has revealed many potential protein cargoes enriched in *C. elegans* ciliary EVs, only a handful have been validated or explored in detail (Nikonorova et al., 2021). To date, no studies have been published exploring the transcriptomic, metabolomic, or lipidomic contents of these EVs. One factor that obfuscates the study of any EV population, including those shed from ciliated neurons, is the presence of

contaminating EVs from multiple sources. Outer membrane vesicles are shed in vast quantities by bacteria, which serve as the primary food source of all laboratory strains of *C. elegans*. These vesicles are vital to bacterial function and released in large quantities, and roughly overlap with the reported size of *C. elegans* neuron-derived vesicles (Schwechheimer & Kuehn, 2015). Recent work shows that OMVs vastly outnumber any vesicles released by *C. elegans*, and that *C. elegans* EVs arise from many cell types (Russell et al., 2020). To overcome these obstacles, there is a pressing need for additional biological tools and markers to be established that allow for specific identification, observation, and isolation of these EVs.

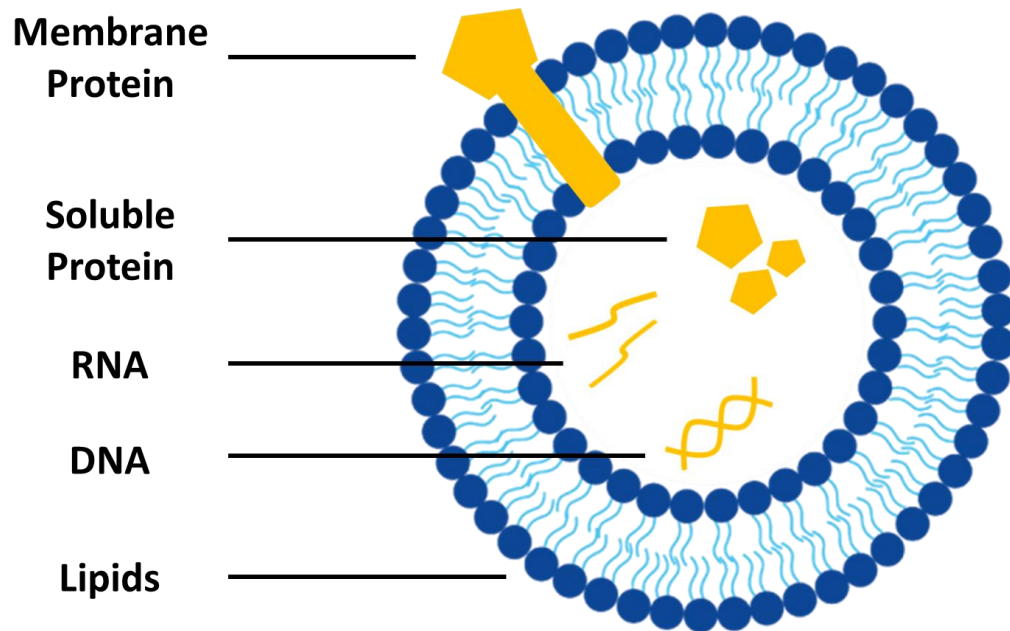


Figure 1: Exosomal and ectosomal EVs contain multiple species of functional biological macromolecule, including proteins, lipids, nucleic acids, and metabolites.

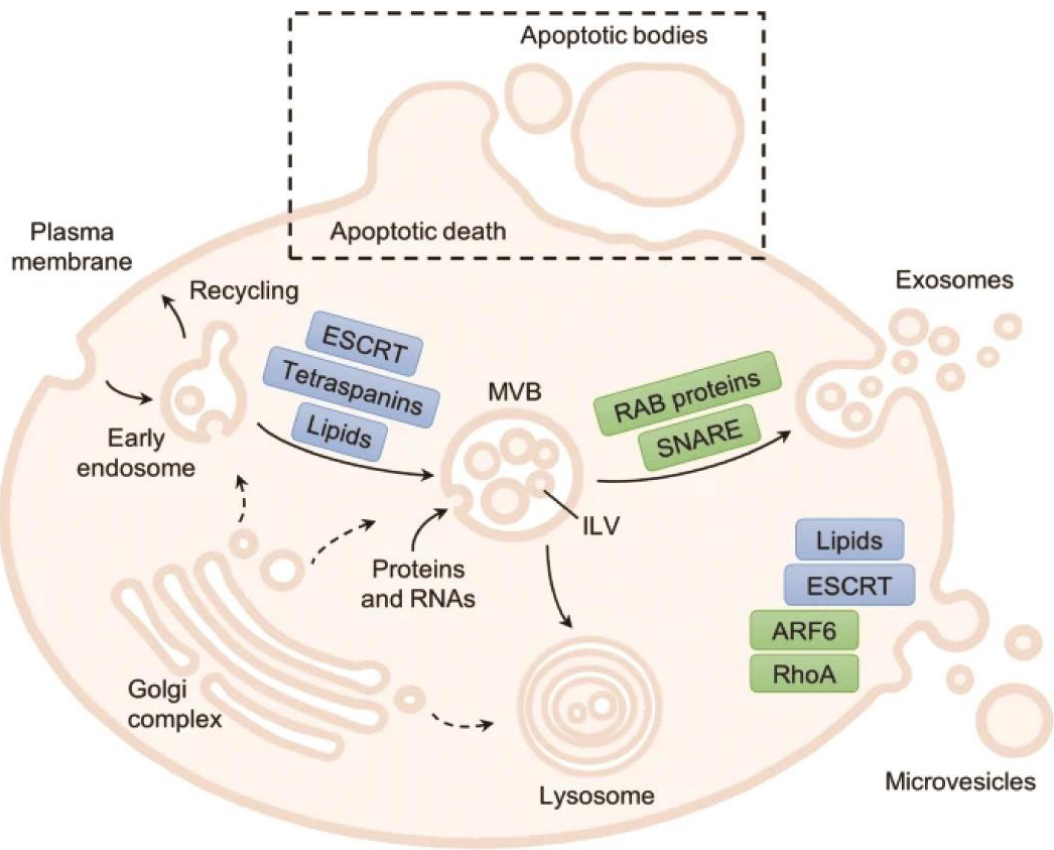


Figure 2: Exosomes and endosomes arise by different mechanisms, but both use the ESCRT complex as a means of cargo sorting and excision (Monguió-Tortajada et al., 2019).

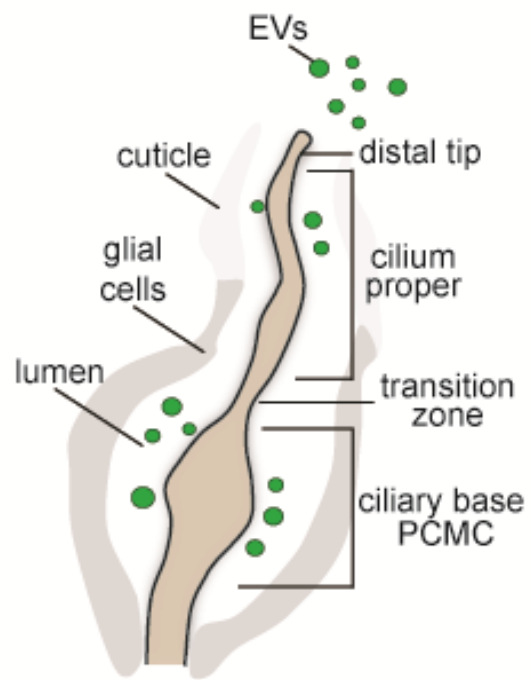


Figure 3: The cilia of IL2, CEM, RnB, and HOB sensory neurons shed ectosomal EVs into a lumen formed by surrounding glial cells. These EV are then released into the environment through a pore in the outer cuticle.

## 1.7 Hypothesis and Specific Aims

Using super-resolution imaging, I discovered that the conserved ion channel CLHM-1 is found in EVs released from the sensory neuron cilia of both males and hermaphrodites. In contrast to EVs containing PKD-2, which are only released from male-specific neurons, EVs containing CLHM-1 are released from hermaphrodite neurons and in differential quantities. Thus, **I hypothesized that molecular mechanisms exist to enrich CLHM-1 into a distinct subpopulation of EVs shed and released from sensory neuron cilia.** To test this hypothesis, I formulated several specific research aims:

**Aim 1:** Use super-resolution microscopy to show that CLHM-1 and PKD-2 are quantifiably enriched in different populations of ciliary EVs released from the same neurons

**Aim 2:** Use super-resolution microscopy to determine the role of IFT and ciliary protein localization in CLHM-1 EV enrichment

**Aim 3:** Use super-resolution microscopy to determine the potential role of ALX-1 and ARF-6 ectosome budding factors in CLHM-1 EV enrichment

**Aim 4:** Isolate ciliary EVs containing CLHM-1 and analyze protein content using LC-MS/MS analysis

## Chapter 2

### MATERIALS AND METHODS

#### 2.1 *C. elegans* culture and genetics

All *C. elegans* strains were cultured at 20°C on Nematode Growth Media (NGM) plates seeded with *E. coli* OP50 as previously described (Brenner, 1974). N2 Bristol was used as the wild-type reference strain. The following mutant alleles were used: *clhm-1(tm4071)* II, *mks-5(ok3582)* II, *mks-5(tm3100)* II, *alx-1(gk338)* III, (*klp-6(sy511)* III, *osm-3(mn391)* IV, *osm-3(p802)* IV, *klp-11(tm324)* IV and *lin-15(n765ts)*. Most strains used in this work contain the *him-5(e1490)* mutation, which causes increased frequency of male offspring (Hodgkin et al., 1979). A comprehensive list of all strains used in this work can be found in **Table 1**.

Standard duplex PCR genotyping was used to detect the following alleles: *clhm-1(tm4071)*, *klp-11(tm324)*, *mks-5(ok3582)*, *mks-5(tm3100)*, *alx-1(gk338)*, *drSi33*, *henSi2*, *henSi17*, *henSi20*, and *henSi26*. SuperSelective genotyping was used to detect *klp-6(sy511)*, *osm-3(mn391)* IV, and *osm-3(p802)* IV (Touroutine & Tanis, 2020). A list of oligonucleotide primers used for genotyping can be found in **Table 2**.

## 2.2 Generation of transgenic strains

The transgene used to examine the *clhm-1* expression pattern was generated using standard germline transformation (Mello et al., 1991). The following constructs were injected into the syncytial germline of MT8189 *lin-15(n765ts)* adult hermaphrodites: pJT46, a construct 3 kb *clhm-1* promoter::*gfp*::*unc-54* 3' UTR (50 ng/μl), pENM1, a 1.58 kb *kfp-6* promoter::*mCherry*::*unc-54* 3' UTR construct (50 ng/μl), and the *lin-15* rescuing construct pL15EK (80 ng/μl). Progeny displaying *lin-15* rescue were cultivated and males for imaging were generated by heat shock.

Plasmid constructs for single-copy insertion were generated using a combination of TOPO, restriction enzyme, Gateway cloning, and Gibson assembly. pCFJ910, which contains an MCS, minimal Mos1 transposon elements and Neomycin/G418 resistance sequences, was used as the backbone for all constructs. Constructs made for this study by postdoctoral researcher Denis Touroutine include: pDT285 (3 kb *clhm-1* promoter::*clhm-1*::tdTomato::*let-858* 3'UTR), pDT290 (1.3 kb *pkd-2* promoter::*pkd-2*::*gfp*::*let-858* 3'UTR), pDT292 (1.3 kb *pkd-2* promoter::*pkd-2*::tdTomato::*let-858* 3'UTR), pDT299 (1.6 kb *kfp-6* promoter::*clhm-1*::tdTomato::*let-858* 3'UTR).

I designed the constructs pMEC16(3 kb *clhm-1* promoter::*clhm-1*(internal Strep-tag II)::tdTomato::*let-858* 3'UTR) and pMEC20 (3 kb *clhm-1* promoter::*clhm-1*(internal Strep-tag II)::GFP::*let-858* 3'UTR) by ordering a synthesized DNA fragment containing the Strep-tag II sequence and inserting it into existing miniMos vectors using Gibson assembly.

Single copy insertion strain transgenes were integrated into the genome using the minimal Mos1 (miniMos) insertion protocol (Frøkjær-Jensen et al., 2014). Briefly, adult hermaphrodites were injected with a DNA mix containing the construct for the desired transgene (10 ng/μL), pGH8 (*rab-3* promoter::*mCherry*::*unc-54* 3'UTR; 10 ng/μL), pCFJ90 (*myo-2* promoter::*mCherry*:: *unc-54* 3'UTR; 2.5 ng/μL), pCFJ104 (*myo-3* promoter::*mCherry*:: *unc-54* 3'UTR; 10 ng/μL), pCFJ601 (*eef-1A.1* promoter::*Mos1* transposase; 50 ng/μL), and pMA122 (*hsp-16.41* promoter::*peel-1*::*tbb-2* 3'UTR; 10 ng/μL). Successful integration was positively selected for by aliquoting 375 μL of 25 mg/mL G418 (GoldBio Cat no. G-418-5), a neomycin analogue, directly onto plates. Animals retaining an extrachromosomal array were killed by heat-shock (2 hours at 34°C) induced *peel-1* toxicity. Surviving animals were rescued onto G418 plates and allowed to propagate. Genomic DNA was extracted from transgenic lines (QIAGEN Genra Puregene Tissue Kit), digested with DpnII, and ligated with T4 DNA ligase. Two rounds of inverse PCR were run using ligation as template (see **Table 2**) and run on agarose gel to determine appropriate purification method. PCR products were submitted for Sanger sequencing with appropriate sequencing primer (see **Table 2**). Sequencing reads were fed into a *C. elegans*-specific BLAST engine ([https://wormbase.org/tools/blast\\_blat](https://wormbase.org/tools/blast_blat)) to identify the genomic context of the miniMos insert. A comprehensive list of single-copy transgenic alleles generated for this work can be found in **Table 3**.

### 2.3 Imaging and analysis of EVs

To image EV release from adult male tails, 8 transgenic L4 hermaphrodites carrying the *him-5(e1490)* mutation were staged onto to 6 cm NGM plates and allowed to grow for four days, resulting in a mixed population of adult males and hermaphrodites. Prior to imaging, adult males were picked to an unseeded NGM plate and allowed to crawl for several seconds to clear bacteria, then picked into 20 mM levamisole (100 mM diluted in Image-iT FX Signal Enhancer medium; ThermoFisher Item no. I36933) on 3% agarose pads and covered with Zeiss high-performance cover glass (D=0.17 mm, 22x22mm; item no.: 474030-9020-000). Wild-type and mutant transgenic animals were staged on plates from the same batch and imaged on the same day to control for batch-to-batch culture variations. For analysis of EV release from virgin males, 20-30 L4 males were placed on a new plate on the third day of culturing and imaged to the following day.

Spectral imaging of EVs was performed using a Zeiss LSM880 confocal microscope equipped with a standard spectral detector at 63X magnification. ZEN black (Zeiss) was used for linear unmixing of single emission spectra. All other images of EVs were acquired with total internal reflection fluorescence (TIRF) microscopy by using an Andor Dragonfly super-resolution microscope and 63x oil objective equipped with an Andor Zyla sCMOS detector (1.5X zoom, 98  $\mu\text{m}$  x 98  $\mu\text{m}$  with 2048 x 2048 pixel resolution). The TIRF angle of incidence was manually adjusted for each animal to achieve a critical IR angle. Images were taken using a 10%

laser power for both 488 and 561 nm wavelengths and 200 ms exposure time. All EV images were taken within 40 minutes of animal mounting, to account for EV passive diffusion.

Imaris (Oxford Instruments), a comprehensive image analysis software package, was used for quantitative EV analysis. EVs were identified and labeled using the “Spot” function, setting approximate object size to 0.350  $\mu\text{m}$  in diameter (as determined by averaging manual measurements of many fluorescent spots) and a quality threshold of 4 (for GFP) and 10 (for RFP). Selected cutoffs for quality threshold, a measure of intensity at the center of the spot, filtered out the maximum amount of noise in negative controls with minimal impact on detection of real signal in positive controls. Hot pixels and any spots that intersected with animal cuticle were manually removed. To identify intersecting/ co-localized vesicles, GFP and RFP spots were filtered by distance to each other with a maximum distance of 0.3  $\mu\text{m}$ .

## **2.4 Imaging and analysis of male tail cilia**

To image fluorescent ciliated sensory neurons, staged adult males were imaged 24 hours after reaching late fourth larval (L4) stage. Transgenic *C. elegans* were immobilized with 10 mM levamisole (Sigma) on 3% agarose pads. *clhm-1* expression pattern images were obtained with a Zeiss LSM880 confocal microscope. Images of splayed male tails were acquired as Z stacks using a Zeiss LSM880 confocal microscope and 63x oil objective equipped with an Airyscan GaAsP-PMT area

detector (1.8X zoom, 73.95 x 73.95  $\mu\text{m}$  with 1740 x 1740 pixel resolution).

Representative cilia images were acquired with an Andor Dragonfly microscope and Andor Zyla sCMOS camera as described for EV imaging.

ImageJ (NIH) was used to plot normalized fluorescence intensity distribution profiles. Starting beyond the distal tip, a linear ROI was drawn through the entirety of each individual cilium. ROIs were sampled from a collection of R2B-R4B cilia across multiple animals. The “multi plot” function was used to collect fluorescence intensity distribution profiles; each profile was normalized individually to the maximum ROI value. Individual cilium profiles were manually aligned using Microsoft Excel.

## **2.5 EV isolation and characterization**

Differential ultracentrifugation was used to isolate EVs for downstream characterization and analysis. To scale up animal culture for sufficient isolation, 8 adult hermaphrodite animals were transferred to 10 cm NGM plates seeded with 1 mL of OP50 grown in LB medium, which were incubated at 20°C for 4 days to achieve mixed population of adult males and hermaphrodites. At least 100 plates were used for each isolation.

Animals were removed from each plate with 1 mL of M9 media into multiple 15 mL conical tubes, where they were incubated at 20°C for 1 hour. Animals were pelleted at 2000 RPM for 1 minute. The supernatant was transferred to fresh 50 mL conical tubes and centrifuged at 2500 x  $g$  for 5 minutes at 4°C. The supernatant was

transferred to a sterile polypropylene ultracentrifuge tube(s) and centrifuged at 15,000 x g for 30 minutes at 4°C to pellet smaller debris, and again transferred to sterile polypropylene ultracentrifuge tubes and centrifuged at 100,000 x g for 90 minutes at 4°C to pellet EVs. All liquid was discarded, and the EV pellet was resuspended in 50 µL of sterile M9.

Size analysis of isolated EVs was conducted using nanoparticle tracking analysis on a NanoSight NS300 (Malvern Panalytical). 5 µL of sample was diluted into 700 µL of sterile water and thoroughly mixed. Data acquisition was conducted for one minute with screen gain of 3 and camera height of 12 and repeated 5 times. Analysis was performed with a detection threshold of 3.

TEM of EV isolate stained with uranyl acetate was performed by Shannon Modla at the Delaware Bio-imaging Center using a Libra 120 transmission electron microscope (Carl Zeiss Instruments).

## **2.6 LC-MS/MS proteomic analysis of isolated EVs**

EVs isolated via differential ultracentrifugation were prepared for LC-MS/MS analysis by in-gel trypsin digestion as previously described (Gundry et al., 2010; Subedi et al., 2019). An equal volume of 2X RIPA buffer (50 mM Tris-HCl pH 7.6, 300 mM NaCl, 2% NP-40, 2% sodium deoxycholate, 5% SDS) was added to sample and allowed to incubate on ice for 15 minutes and then spun at 14,000 RPM for 20 minutes at 4°C. The supernatant was removed, combined with 2 µL of 4X Laemmli

buffer (used here as a loading dye), and loaded onto pre-cast SDS-polyacrylamide gel and run for 10 minutes at 120 V. Kaleidoscope prestained protein standard (Bio-Rad, Cat no. 1610375) was loaded alongside samples for size comparison

Protein bands were stained using colloidal blue dye (Colloidal Blue Staining Kit, ThermoFisher Cat no. LC6025), cut with sterile metal gel cutters, and transferred to low protein binding ultracentrifuge tubes (ThermoFisher, Cat no. 90410). Gel bands were de-stained with a 50% methanol solution for 30 minutes.

Gel bands were then reduced with 5 mM TCEP bond-breaker solution (10  $\mu$ L 0.5 M in 1 mL 100 mM ammonium bicarbonate pH 8) at 60°C for 10 minutes and alkylated with 100 mM IAA solution (9.3 mg IAA in 1 mL 100 mM ammonium bicarbonate pH 8). Gel bands were washed by incubating in wash solution (50% acetonitrile, 50% 100 mM ammonium bicarbonate pH 8) twice for 15 minutes, and once in 100% acetonitrile for 15 minutes (room temperature). Gel bands were digested in trypsin solution (0.01 mg/mL in 100 mM ammonium bicarbonate pH 8) overnight at 37°C. Additional digested fragments were extracted with extraction solution (50% acetonitrile, 49% water, 1% TFA) for 30 minutes (room temperature). Fragments were then purified using Pierce C-18 Spin Columns (ThermoFisher, Cat no. 89870) according to manufacturer protocol. All solutions were prepared fresh in lab the day before procedure.

C-18 purified peptide fragments were dried using a Speedvac (ThermoFisher) and submitted for LC-MS/MS analysis, which was performed using a Q-Exactive Orbitrap mass spectrometer (ThermoFisher).

Analyzed peptide fragments were identified using Proteome Discoverer Software (ThermoFisher), using the the Uniprot database of *C. elegans* proteins (<https://www.uniprot.org/proteomes/UP000001940>).

## **2.7 Strep-tag protein blot**

Approximately 10,000 transgenic animals were cultured on 10 cm NGM plates seeded with OP50. Animals were washed into 15 mL conical tubes using M9, pelleted at room temperature, and frozen at -80°C. 100 µL of lysis buffer (0.15 M NaCl, 1% NP-40, 50 mM Tris pH 7.5, with crushed Roche protease inhibitor tab added (Cat no. 04693159001)) was added to thawed pellets and animals were sonicated on ice until visibly cleared. Sample was centrifuged at 13,500 x *g* for 10 minutes at 4°C and supernatant was removed. Protein concentration was determined using BCA protein quantitation assay (ThermoFisher, Cat no. 23227).

4X Laemmli buffer was activated by adding BME (final concentration 10%) and urea sulfate (final concentration 8 M). At least 2 µg of protein sample was incubated in activated Laemmli buffer (3 sample: 1 buffer) at 95°C for 5 minutes, centrifuged at 13,500 x *g* for 2 minutes at room temperature, and loaded onto pre-cast SDS-polyacrylamide gel. Electrophoresis was run at 60 V for 20 minutes and 90 V for 60 minutes. Sample was transferred onto a 0.45 µm pore nitrocellulose membrane (Bio-Rad, Cat no. 1620145) for 1 hour at 75 V.

The membrane was blocked with PBS-blocking buffer (3% BSA, 0.05% Tween 20 in PBS) overnight at 4°C, and washed with PBS-Tween buffer (0.1% Tween 20 in PBS). During the last wash, 10 µL of Biotin Blocking Buffer (IBA Lifesciences, Cat no. 2-0501-002) was added and incubated for 10 minutes at room temperature.

Strep-Tactin HRP conjugate (IBA Lifesciences, Cat no. 2-1502-001) was diluted 1:100 and added to PBS-Tween buffer, and then incubated with membrane for 60 minutes at room temperature. Membrane was washed twice with PBS-Tween buffer for one minute, then imaged with a 5-minute exposure.

## **2.8 Statistics and Graphing**

Dataset normality was determined using the Anderson-Darling normality test. Depending on normality, either the Student's t-test or Mann-Whitney U test was used when comparing two data sets and one-way ANOVA or Kruskal-Wallis test with multiple comparisons when comparing three or more datasets. For comparing EV release in virgin and mated males, a Mann-Whitney test was used rather than a Kruskal-Wallis test because data sets from animals carrying different transgenes were presented on the same graphs. All statistical analyses and graphing were performed with GraphPad Prism 9. Significant differences are indicated as \* $p < 0.05$ , \*\* $p < 0.01$ , \*\*\* $p < 0.001$ .

Table 1: List of strains used in this study

Genotype	Source	Strain name
<i>him-5(e1490)</i> V	CGC	DR466
<i>klp-6(sy511)</i> III; <i>him-5(e1490)</i> V	CGC	PT442
drSi33[P <i>clhm-1::clhm-1::GFP::unc-54 3'UTR</i> ] IV	Jessica Tanis	OG599
drSi36[P <i>clhm-1::GFP::unc-54 3'UTR</i> ] IV	Jessica Tanis	OG609
myIs4[P <i>klp-6::pkd-2::GFP + cc::GFP</i> ]; <i>him-5(e1490)</i> V	Maureen Barr	PT621
<i>him-5(e1490)</i> V; myIs10 [P <i>klp-6::KLP-6::GFP + pBX1</i> ]	Maureen Barr	PT2332
henEx1 [P <i>clhm-1::GFP::unc-54 UTR + Pklp-6::mCherry::unc-54 3'UTR</i> ]	This study	UDE3
henEx7 [P <i>clhm-1::GFP::unc-54 UTR + Pnpr-5::mCherry::unc-54 3'UTR</i> ]	This study	UDE10
drSi33[P <i>clhm-1::clhm-1::GFP::unc-54 3'UTR</i> ] IV; <i>him-5(e1490)</i> V	This study	UDE27
henSi2[P <i>clhm-1::clhm-1::tdTomato::let858 3'UTR</i> ] I	This study	UDE49
henSi2[P <i>clhm-1::clhm-1::tdTomato::let858 3'UTR</i> ] I; <i>him-5(e1490)</i> V	This study	UDE62
henSi2[P <i>clhm-1::clhm-1::tdTomato::let858 3'UTR</i> ] I; drSi33[P <i>clhm-1::clhm-1::GFP::unc-54 3'UTR</i> ] IV; <i>him-5(e1490)</i> V	This study	UDE76
henSi2[P <i>clhm-1::clhm-1::tdTomato::let858 3'UTR</i> ] I; <i>him-5(e1490)</i> V; myIs10 [P <i>klp-6::KLP-6::GFP + pBX1</i> ]	This study	UDE77
henSi20[P <i>pkd-2::pkd-2::GFP::let858 3' UTR</i> ]; <i>pkd-2 (sy606)</i> IV; <i>him-5(e1490)</i> V	This study	UDE93
henSi17[P <i>klp-6::clhm-1::tdTomato::let858 3'UTR</i> ] I; <i>clhm-1(tm4071)</i> II	This study	UDE100
henSi20[P <i>pkd-2::pkd-2::GFP::let858 3' UTR</i> ]; <i>pkd-2 (sy606)</i> IV	This study	UDE103
<i>pkd-2 (sy606)</i> IV; henSi21[P <i>pkd-2::pkd-2::GFP::let858 3' UTR</i> ] V	This study	UDE104
<i>alx-1(gk338)</i> III; <i>him-5(e1490)</i> V	This study	UDE116

che-3(cas443[gfp::che-3]); henSi2[Pclhm-1::clhm-1::tdTomato::let858 3'UTR] I; him-5(e1490) V	This study	UDE119
henSi24 [Pclhm-1::clhm-1(internal Strep-II tag)::tdTomato::let858 3'UTR] V	This study	UDE134
alx-1(gk338) III; drSi33[Pclhm-1::clhm-1::GFP::unc-54 3'UTR] IV; him-5(e1490) V	This study	UDE138
henSi20[Ppkd-2::pkd-2::GFP::let858 3' UTR]; pkd-2 (sy606) IV; henSi26[Pklp-6::pkd-2::tdTomato::let858 3'UTR]; him-5(e1490) V	This study	UDE150
henSi17[Pklp-6::clhm-1::tdTomato::let858 3'UTR] I; mks-5(ok3582) II; henSi20[Ppkd-2::pkd-2::GFP::let858 3' UTR] IV; him-5(e1490) V	This study	UDE151
henSi27 [Pclhm-1::clhm-1(internal Strep-II tag)::GFP::let858 3'UTR]; him-5(e1490) V	This study	UDE160
henSi21[Ppkd-2::pkd-2::GFP::let858 3' UTR]; him-5(e1490) V	This study	UDE162
henSi17[Pklp-6::clhm-1::tdTomato::let858 3'UTR] I; him-5(e1490) V	This study	UDE163
henSi17[Pklp-6::clhm-1::tdTomato::let858 3'UTR] I; henSi20[Ppkd-2::pkd-2::GFP::let858 3' UTR] IV; him-5(e1490) V	This study	UDE165
henSi17[Pklp-6::clhm-1::tdTomato::let858 3'UTR] I; henSi21[Ppkd-2::pkd-2::GFP::let858 3' UTR]; him-5(e1490) V	This study	UDE175
henSi17[Pklp-6::clhm-1::tdTomato::let858 3'UTR] I; alx-1(gk338) III; henSi20[Ppkd-2::pkd-2::GFP::let858 3' UTR] IV; him-5(e1490) V	This study	UDE177
henSi17[Pklp-6::clhm-1::tdTomato::let858 3'UTR] I; mks-5(tm3100) II; henSi20[Ppkd-2::pkd-2::GFP::let858 3' UTR] IV; him-5(e1490) V	This study	UDE183
henSi17[Pklp-6::clhm-1::tdTomato::let858 3'UTR] I; osm-3(mn391) IV; henSi21[Ppkd-2::pkd-2::GFP::let858 3' UTR]; him-5(e1490) V	This study	UDE184
henSi17[Pklp-6::clhm-1::tdTomato::let858 3'UTR] I; klp-6(sy511) III; henSi20[Ppkd-2::pkd-2::GFP::let858 3' UTR] IV; him-5(e1490) V	This study	UDE193

henSi17[P <i>klp-6::clhm-1::tdTomato::let858 3'UTR</i> ] I; <i>klp-11(tm324)</i> IV; henSi21[P <i>pkd-2::pkd-2::GFP::let858 3' UTR</i> ]; <i>him-5(e1490)</i> V	This study	UDE195
henSi17[P <i>klp-6::clhm-1::tdTomato::let858 3'UTR</i> ] I; <i>osm-3(p802)</i> IV; henSi21[P <i>pkd-2::pkd-2::GFP::let858 3' UTR</i> ]; <i>him-5(e1490)</i> V	This study	UDE198
<i>clhm-1(tm4071)</i> II; henSi21[P <i>pkd-2::pkd-2::GFP::let858 3' UTR</i> ]; <i>him-5(e1490)</i> V	This study	UDE206
henSi17[P <i>klp-6::clhm-1::tdTomato::let858 3'UTR</i> ] I; <i>klp-11(tm324)</i> ; <i>osm-3(p802)</i> IV; henSi21[P <i>pkd-2::pkd-2::GFP::let858 3' UTR</i> ]; <i>him-5(e1490)</i> V	This study	UDE207

Table 2: List of oligonucleotide primers used in this study

<b>Allele</b>	<b>Primer 1 (recognizes WT)</b>	<b>Primer 2 (recognizes mutant)</b>	<b>Primer 3 (shared)</b>	<b>T<sub>an</sub> (C°)</b>
<i>clhm-1(tm4071)</i> II	agagctagtcgatgcataa c	gacacacctgatacc aatc	gggctgtggaaatg gttatg	51
<i>klp-6(sy511)</i> III	gattggaaactgttctcc acatcgggctcacttgcg tcagactttg	gaaactgttctccac atcaatcaaatgggct cagcttta	gcattgtgtaggcag gttg	58
<i>alx-1(gk338)</i> III	ccaacaatctgctggagta ttcg	gcctcgtatgactc actcg	tgatactgggagct gcttgg	50
<i>mks-5(ok3582)</i> II	ccaaagattgatcgc gg	cataatccggcagt aac	none	50
<i>mks-5(tm3100)</i> II	tgcaactgctacggatg	ccgaagtattgtg cg	agccaagtcattct ca gc	51
<i>osm-3(mn391)</i> IV	cctgcttctctctccaa at ctgagatctcg	cctgcttctctctcc aatctgagatctta	agactctctccact tcg	55
<i>osm-3(p802)</i> IV	ggatccaaaggatgct tctt agcttcgagtacc	ggatccaaaggatg ctttagcttcgagtact	ctgatcttggagct gtg	59
<i>klp-11(tm324)</i> IV	tggtccattagcatgc	gcaggttcttattct ca c	caccgaattgtctc g agc	49
<i>drSi33</i> IV	accctgattctgtcaagcc	tcgaatcctgaacat c attccc	cgagaaatagtacag caaacgc	53
<i>henSi2</i> I	tctgtattatctaacaagc g atgg	agctagcgcgacgg caa atact	cgagtttaagagata gtcgtc	49
<i>henSi17</i> I	gctttgctgactccgaaga g	cgataaatatttacgtt g gcgagac	cggaattcatgattc gttcgca	50
<i>henSi20</i> IV	cctttggagggacttctg tac	cgataaatatttacgtt g gcgagac	gacttctgacggta atgacg	50
<i>henSi21</i> V	none	cgataaatatttacgtt g gcgagac	ccttactccaatcct ctc acaacc	50
<i>henSi26</i> V	gtgagaaaactatatcc ct cacg	cgataaatatttacgtt g gcgagac	ccaggctgtctcatta cg	50
Inverse PCR round 1 (5' insertion)	atagtttggcgcaattga g	gggtgttcgacagtca aggt		64

Inverse PCR round 2 (5' insertion)	agagcaaacgcgacag tat	cgataaatattacgtt gcgagac	<b>Sequencing:</b> cgataaatattacgtt tgcgagac	64
Inverse PCR round 1 (3' insertion)	aaaaatggctcgatgaatg g	taagaatcgaagcgt gctc		64
Inverse PCR round 2 (3' insertion)	agctagcgacggcaaata ct	catcgaagcgaatag gtggt	<b>Sequencing:</b> catcgaagcgaatag gtggt	64

Table 3: List of transgenic alleles generated for use in this study

<b>Genotype</b>	<b>Chromosomal location</b>	<b>Allele name</b>
<i>Pclhm-1::GFP::unc-54 UTR + Pklp-6::mCherry::unc-54 3'UTR</i>	Extrachromosomal	henEx1
<i>Pclhm-1::GFP::unc-54 UTR + Pnpr-5::mCherry::unc-54 3'UTR</i>	Extrachromosomal	henEx7
<i>Pclhm-1::clhm-1::tdTomato::let858 3'UTR</i>	I:6,674,502..6,680,525	henSi2
<i>Pklp-6::clhm-1::tdTomato::let858 3'UTR</i>	I:12,316,637..12,322,659	henSi17
<i>Ppkd-2::pkd-2::GFP::let858 3' UTR</i>	IV:10,788,289..10,794,310	henSi20
<i>Ppkd-2::pkd-2::GFP::let858 3' UTR</i>	V:20,070,640..20,076,662	henSi21
<i>Pclhm-1::clhm-1(internal Strep-II tag)::tdTomato::let858 3'UTR</i>	V: 20,536,869...20,542,888	henSi24
<i>Pklp-6::pkd-2::tdTomato::let858 3'UTR</i>	V:3,715,983..3,722,005	henSi26
<i>Pclhm-1::clhm-1(internal Strep-II tag)::GFP::let858 3'UTR</i>	Unmapped	henSi27

### Chapter 3

#### **CLHM-1 IS CONTAINED WITHIN A DISTINCT SUBPOPULATION OF EVS RELEASED FROM SENSORY NEURON CILIA**

Calcium homeostasis modulator 1 (CALHM1) is a calcium and ATP permeable ion channel that modulates neuron excitability and is required for gustatory neuron signaling from type II taste cells (Ma et al., 2012; Taruno et al., 2013; Vingtdeux et al., 2016). Human genetic studies suggest the P86L polymorphism in *CALHM1* lowers the age of Alzheimer's disease onset (Dreses-Werringloer et al., 2008; Lambert et al., 2010). The exact physiological function of CALHM1 in the human central nervous system is still unclear.

A single CALHM1 homolog is expressed in *C. elegans*: CLHM-1. Human CALHM1 and *C. elegans* CLHM-1 share biophysical properties when expressed in *Xenopus* oocytes and functional conservation when expressed in *C. elegans* (Tanis et al., 2013). CLHM-1 localizes to *C. elegans* body wall muscles as well as the cilia of inner labial type 2 (IL2) and amphid sensory (AS) neurons of the hermaphrodite head (Tanis et al., 2013).

### 3.1 CLHM-1 localizes to the cilia of EV-releasing sensory neurons

EVs are shed from IL2 and AS neurons of the hermaphrodite head, as well as from the CEM neurons of the male head and the RnB and HOB neurons of the male tail (Razzauti & Laurent, 2021; J. Wang et al., 2014, 2015). Collectively, these neurons are known as the EV-releasing neurons (EVNs).

As CLHM-1 localizes to the cilia of several known hermaphrodite EVNs (Tanis et al., 2013), I wanted to assess whether CLHM-1 was expressed in male-specific EVNs. To do this, I created transgenic animals coexpressing *gfp* under the *clhm-1* regulatory sequences and promoter (*Pclhm-1::gfp*) with *mCherry* under the *klp-6* promoter (*Pklp-6::mCherry*), which drives expression in the IL2, CEM, RnB, and HOB neurons (Peden & Barr, 2005). I used confocal microscopy to image the adult male head and tail and observed overlap in *clhm-1* and *klp-6* expression in these neurons (**Figure 4**).

To determine if CLHM-1 also localizes to the cilia of male-specific EVNs, I created a transgenic strain co-expressing a tdTomato-tagged CLHM-1 fusion protein with a *Pklp-6::GFP* reporter and imaged the adult male head and tail. I observed that CLHM-1::tdTomato localizes to the cilia of IL2, CEM, RnB, and HOB neurons (**Figure 5**). Thus, CLHM-1 is expressed in most known EVNs and localizes to the site of EV shedding, indicating potential involvement in ciliary EV biology.

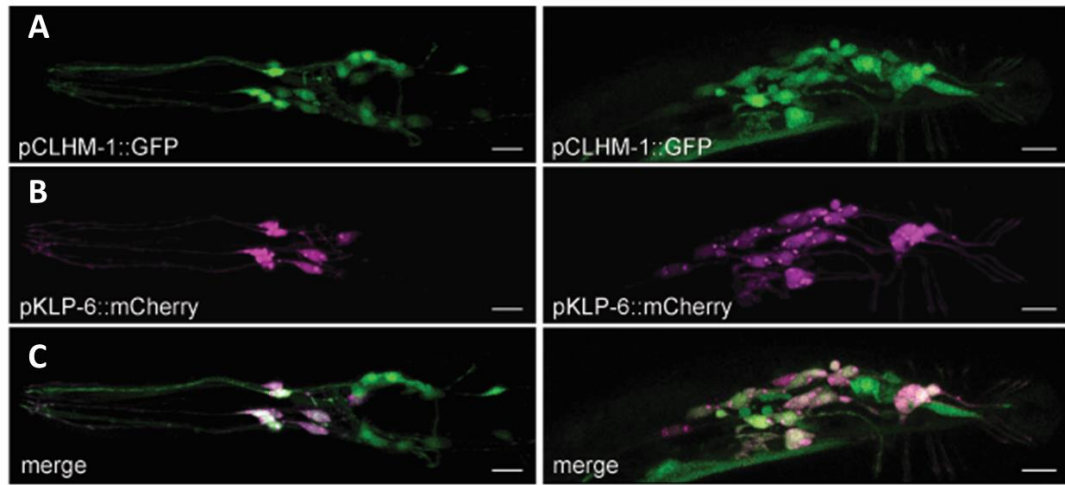


Figure 4: (A) *Pclm-1::gfp* is expressed in a number of ciliated sensory neurons in the head (left) and tail (right) of adult males. (B) *Pklp-6::mCherry* is expressed in IL2, CEM, RnB (R1B-R9B, excluding R6B), and HOB neurons. (C) Expression of the two transgenes overlaps in the IL2, CEM, RnB, and HOB neurons. Scale bar = 10  $\mu$ m.

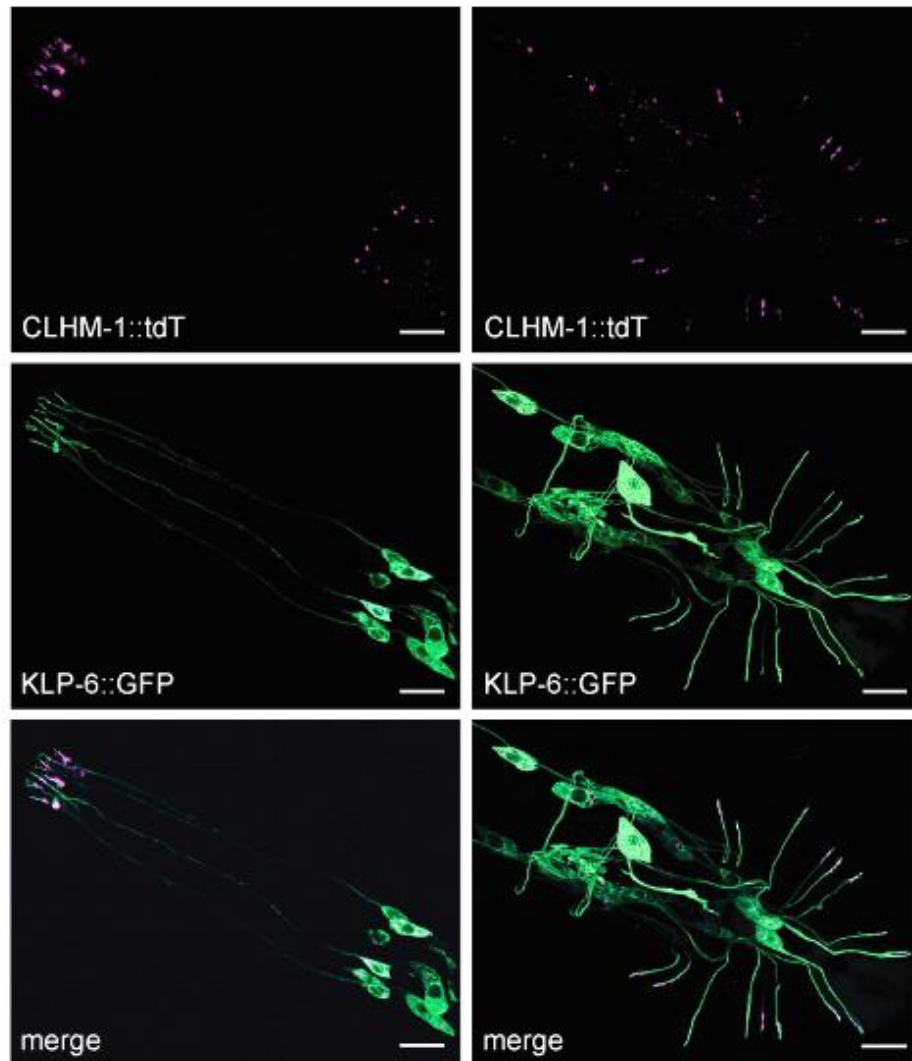


Figure 5: tdTomato-tagged CLHM-1 localizes to the cilia of IL2 and CEM neurons of the male head (left) and the RnB and HOB neurons of the male tail (right), as denoted by colocalization with the ends of a *Pklp-6::gfp* transgene. Scale bars = 10  $\mu$ m.

### 3.2 CLHM-1 is novel cargo in EVs released from sensory neuron cilia

As CLHM-1 is permeable to both calcium and ATP (Ma et al., 2012; Tanis et al., 2013; Taruno et al., 2013), both of which are involved in EV biogenesis (Lombardi et al., 2021; Nabhan et al., 2012; Taylor et al., 2020), I reasoned that CLHM-1 may be involved in ciliary EV biogenesis. To assess this, I crossed a strain expressing GFP-tagged PKD-2, an EV cargo, with the *clhm-1(tm4071)* null deletion mutant and used super-resolution microscopy to image release of EVs containing PKD-2::GFP into the environment from adult male tail EVNs. I found no significant difference in release of PKD-2::GFP EVs between wild-type and *clhm-1(tm4071)* males (**Figure 6**), indicating that CLHM-1 is not required for release of these ciliary-derived EVs under basal conditions.

I then considered that CLHM-1 may be found as cargo in EVs shed from neuron cilia. Using a confocal microscope equipped with an Airyscan super-resolution detector, I imaged the tails of adult males expressing CLHM-1::GFP at single copy and observed environmental release of EVs containing CLHM-1::GFP. I confirmed this observation using two other modalities of super-resolution imaging: structured illumination microscopy and total internal reflection fluorescence (TIRF) microscopy, with TIRF providing the largest field-of-view and highest resolution per image. I observed EVs containing CLHM-1::GFP are released from the adult male head and tail, as well as from the hermaphrodite head, with high frequency (**Figure 7**).

To confirm that observed CLHM-1::GFP in environmental EVs was legitimate signal and not background noise or artefact, I used lambda spectral imaging to collect the entire fluorescence emission spectrum of a representative transgenic animal sample, followed by linear unmixing to delineate all fluorescence emission lines. I found that the signal emitted from EVs matched the shape and intensity of a reference eGFP emission spectrum and was not a product of background noise or bacterial autofluorescence (**Figure 8**).

GFP-tagged CLHM-1 is functional (Tanis et al., 2013), and as it was expressed at single copy, it indicates that CLHM-1::GFP localization to EVs is not the result of aberrant protein folding or over-expression. Further, not all ciliary-localized proteins expressed in EVNs are found in EVs (J. Wang et al., 2014, 2015, 2021), indicating that CLHM-1 is a new, selectively packaged EV cargo.

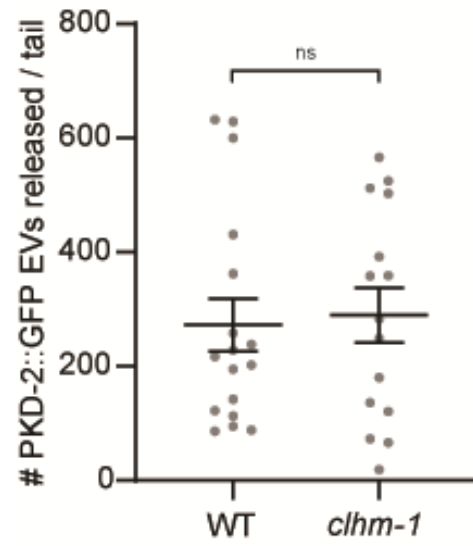


Figure 6: Environmental release of EVs containing PKD-2::GFP does not significantly change between wild-type and *clhm-1(tm4071)* mutant animals. Error bars show SEM. Mann-Whitney test;  $n \geq 15$ .

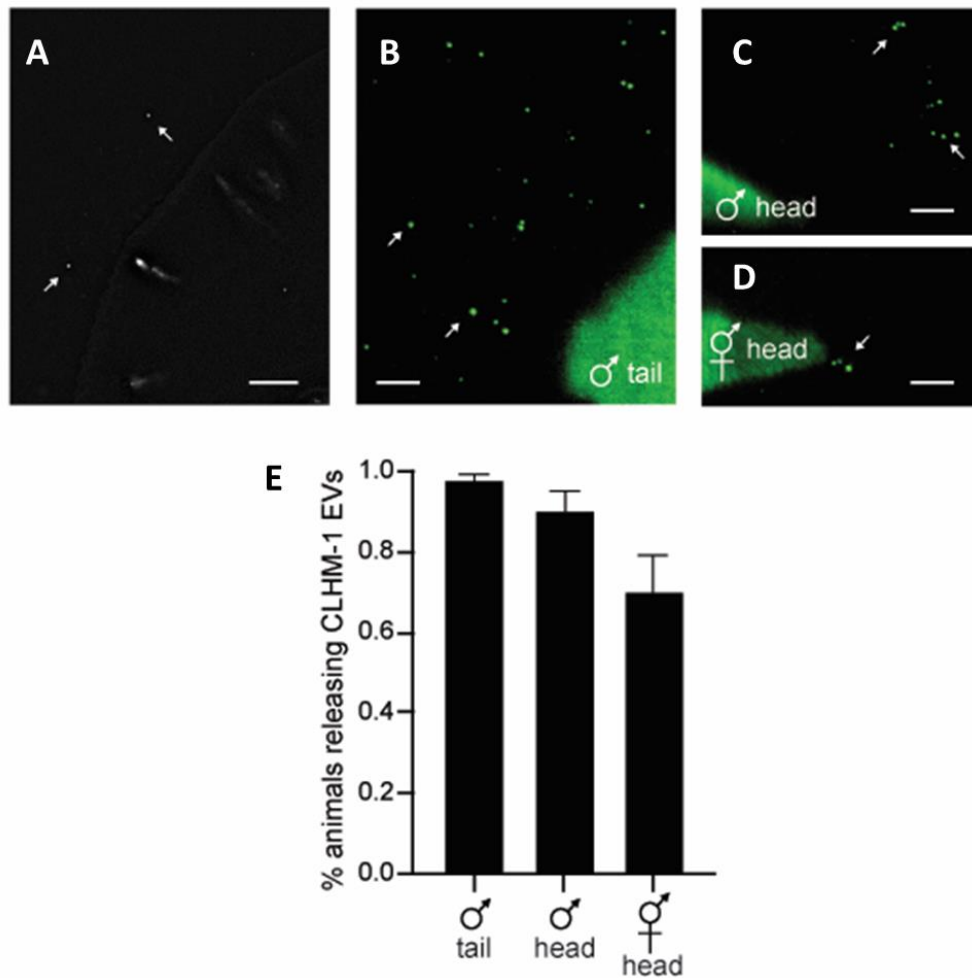


Figure 7: Structured Illumination microscopy shows CLHM-1::GFP in environmental EVs (A). TIRF microscopy shows EVs containing CLHM-1::GFP are released into the environment from EVNs of the adult male head (B) and tail (C), as well as from the hermaphrodite head (D). EVs are released from over 80 percent of male animals and 60 percent of hermaphrodite animals (E). Scale bars = 3  $\mu$ m. Error bars show SEM.  $n \geq 23$ .

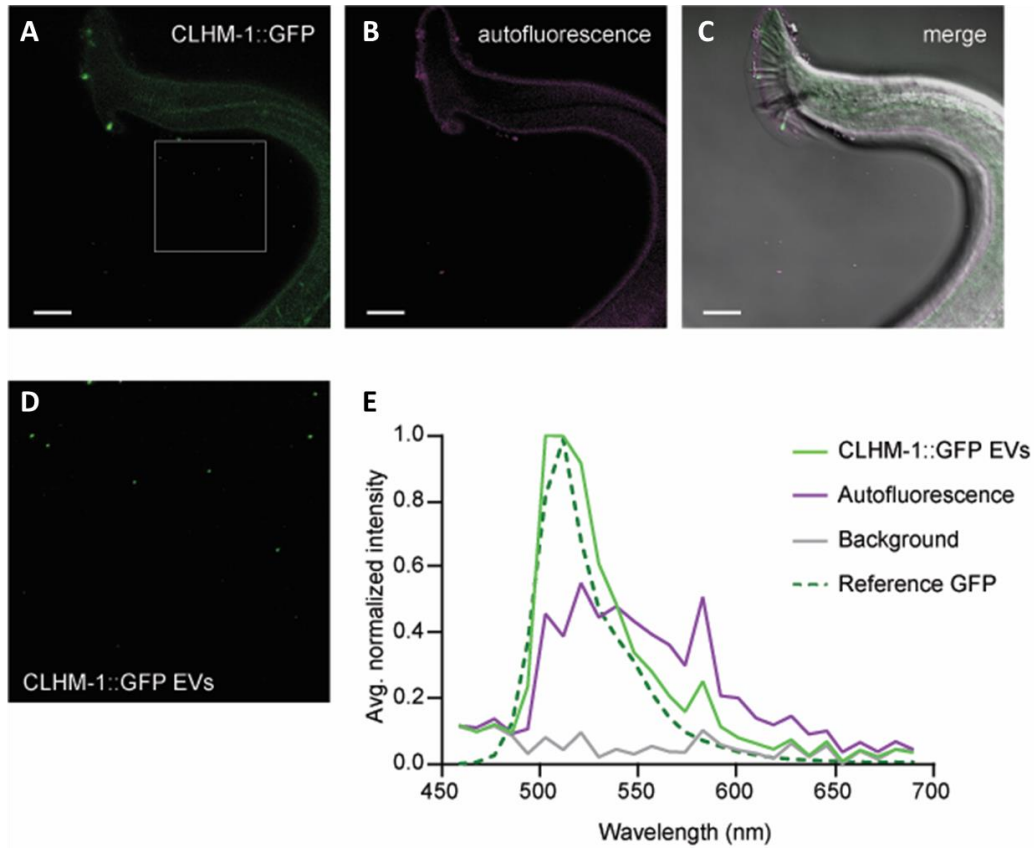


Figure 8: Linear unmixing shows emission from CLHM-1::GFP (A,D), autofluorescence (B), and merged with transmitted light (C). Normalized fluorescence emission from EVs containing CLHM-1::GFP matches an eGFP reference emission spectrum, showing the signal is not autofluorescence emission or background noise (E). Scale bars = 10  $\mu$ m.

### 3.3 CLHM-1 and PKD-2 are contained within quantifiably distinct subpopulations of EVs released from the same EVNs

In imaging environmental EVs containing either CLHM-1::GFP or PKD-2::GFP, I observed release of both PKD-2::GFP and CLHM-1::GFP EVs from nearly all animals; however, EVs containing CLHM-1::GFP appeared fewer in quantity but seemingly larger compared to PKD-2::GFP. Expression of *pkd-2* is restricted to male-specific neurons, while *clhm-1* is expressed in a wider subset of both male and hermaphrodite EVNs. These observations led me to hypothesize that CLHM-1 could be enriched in a different environmentally-released EV subset than PKD-2, as a single cilium can release multiple EV subpopulations containing distinct protein cargo (Nikonorova et al., 2021; J. Wang et al., 2021).

To test this observation, I required strains simultaneously expressing fluorescently tagged CLHM-1 and PKD-2 in the same ciliated sensory neurons. I created these strains by using transposon-mediated genomic insertion. I used molecular techniques to clone either *clhm-1::tdTomato* or *pkd-2::GFP/tdTomato* sequences between flanking Mos1 transposon elements, which insert randomly into the *C. elegans* genome to create single-copy insertion (SCI) transgenes when transformed into the adult hermaphrodite germline (Frøkjær-Jensen et al., 2014). By crossing together animals containing single fluorescent SCI transgenes, I created one strain coexpressing CLHM-1::GFP with CLHM-1::tdTomato, a second strain

coexpressing PKD-2::GFP with PKD-2::tdTomato, and two strains coexpressing PKD-2::GFP with CLHM-1::tdTomato.

EVs are released from the adult male tail in high abundance, and accumulate in the hermaphrodite uterus following copulation, indicating physiological potential (Nikonorova et al., 2021; J. Wang et al., 2020). Thus, all strains were created in a high incidence of males (*him*) background (Hodgkin et al., 1979) and all SCI transgenes were designed to express in the same overlapping set of male tail EVNs.

I then used TIRF super-resolution microscopy to image EVs released from the tails of adult male animals of all three aforementioned strains. I observed that CLHM-1::GFP largely colocalized with CLHM-1::tdTomato in environmentally-released EVs, as did PKD-2::GFP and PKD-2::tdTomato. Notably, I observed fewer incidences of CLHM-1::tdTomato and PKD-2::GFP together in EVs (**Figure 9**).

To quantify these observations, I used the Imaris image analysis suite to identify objects in both the GFP and RFP channels and their overlap. I imaged EVs containing exclusively CLHM-1::GFP or CLHM-1::tdTomato to develop detection thresholds that maximized the counting of discernable signal and minimized the counting of noise or background (**Figure 10**). I used these parameters to quantify images of released EVs.

I first quantified the number of EVs containing CLHM-1::tdTomato released from strains containing two different *clhm-1::tdTomato* SCI transgenes: *henSi2* (containing native *clhm-1* promoter) and *henSi17* (containing *kfp-6* promoter). and determined that transgene promoter had no significant effect on the number of CLHM-

1::tdTomato EVs released (**Figure 11**). Interestingly, this experiment also showed that pairing a *clhm-1::tdTomato* SCI transgene with either a *clhm-1::GFP* (*drSi33*) or *pkd-2::GFP* SCI transgene(s) (*henSi20* & *henSi21*) does not alter the detection of CLHM-1::tdTomato EVs (**Figure 11**). This shows that the presence of GFP-labeled CLHM-1 does not alter the number of detectable CLHM-1::tdTomato EVs and suggest that CLHM-1 oligomerization is not a significant contributor to EV detection. These results also demonstrate that our imaging and analysis pipeline generates reproducible quantitative data with multiple independent transgene combinations.

Using this pipeline to quantify the signal overlap in EVs, I found that CLHM-1::GFP is significantly more likely than PKD-2::GFP to colocalize with CLHM-1::tdTomato, despite PKD-2::GFP being the more abundant EV cargo (**Figure 12**). Likewise, PKD-2::tdTomato is significantly more likely than CLHM-1::tdTomato to colocalize with PKD-2::GFP in EVs (**Figure 12**). These data indicate that PKD-2 and CLHM-1 are deliberately enriched into distinct subpopulations of ciliary EVs shed from the same sensory neuron cilia.

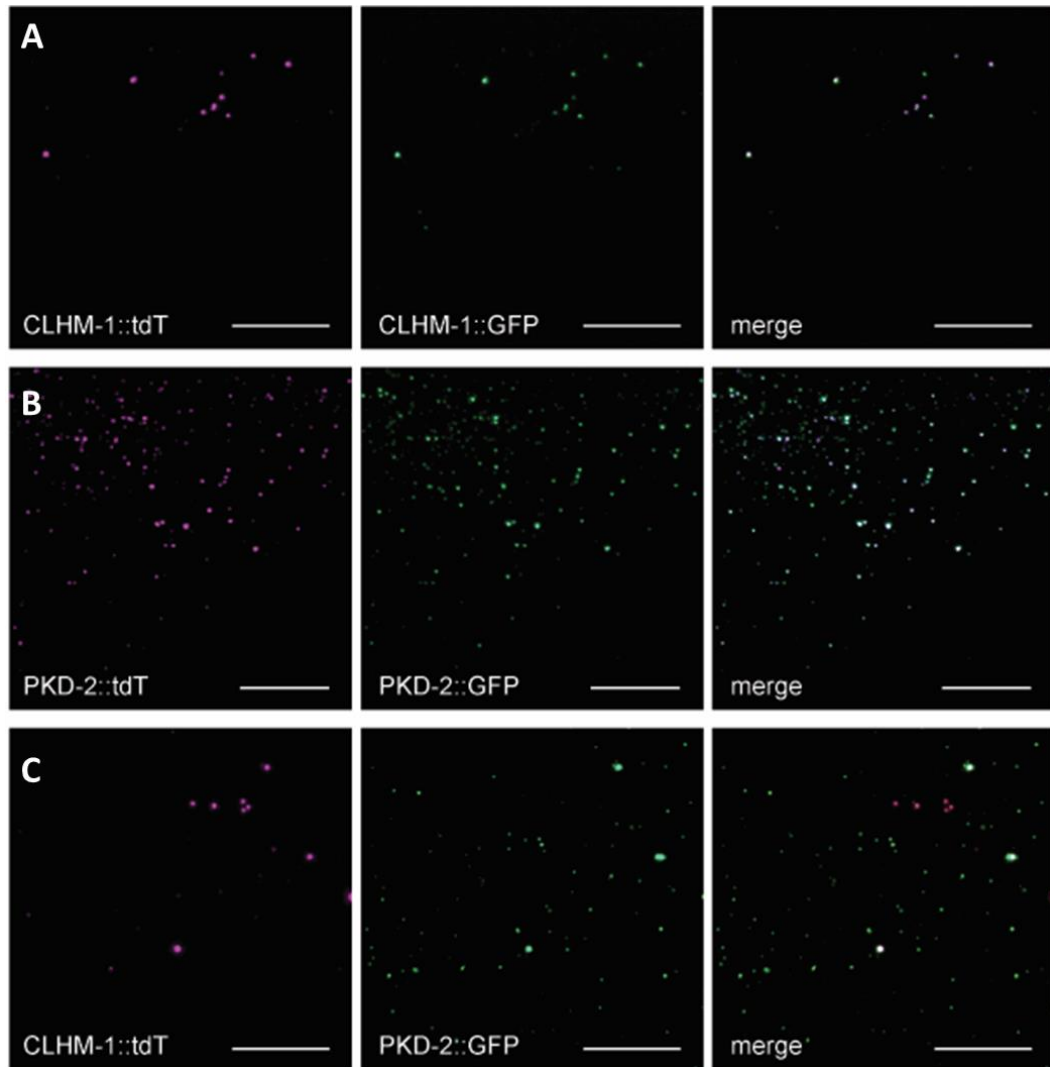


Figure 9: TIRF imaging shows fluorescently tagged proteins in EVs released from the same ciliated neurons. (A) CLHM-1::tdTomato and CLHM-1::GFP frequently colocalize in environmental EVs. (B) PKD-2::tdTomato and PKD-2::GFP frequently colocalize in environmental EVs. (C) CLHM-1::tdTomato and PKD-2::GFP colocalize less frequently in environmental EVs. Scale bars = 10  $\mu$ m.

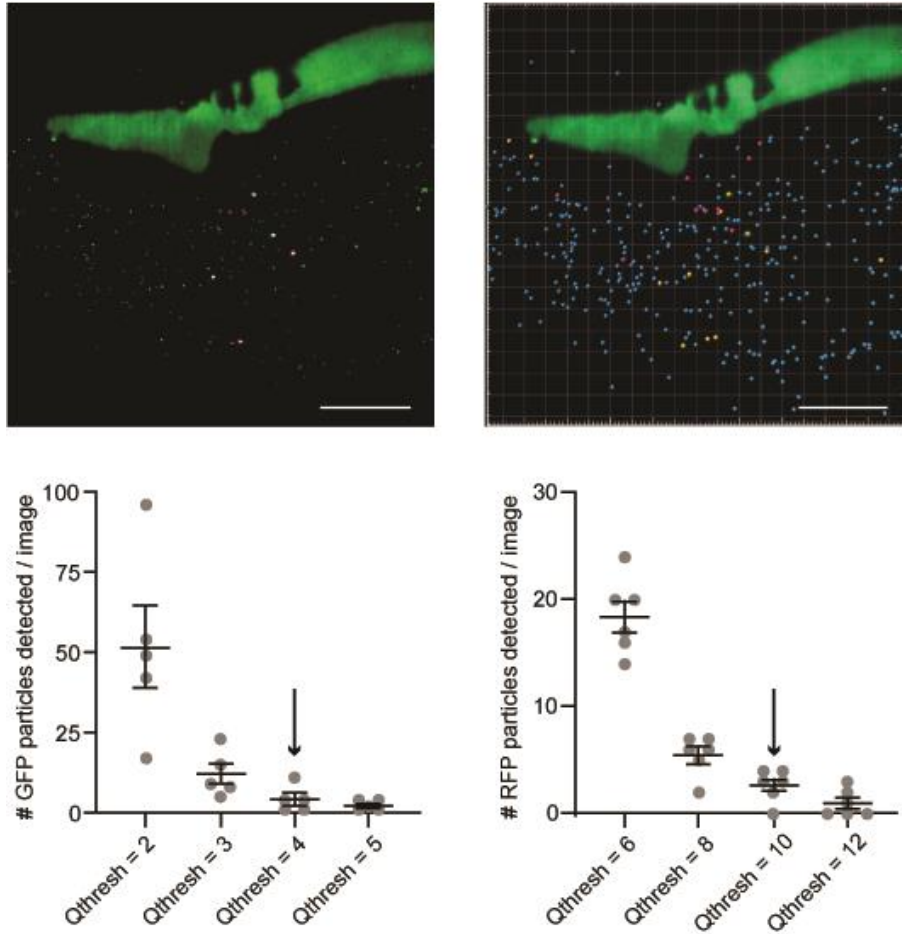


Figure 10: (Top) Imaris spot detector was used to quantify GFP and tdTomato in released environmental EVs. (Bottom) Quality thresholds for analysis were calculated by imaging animals lacking GFP or tdTomato transgenes. Scale bar = 10  $\mu$ m. Error bar show SEM.  $n \geq 5$ .

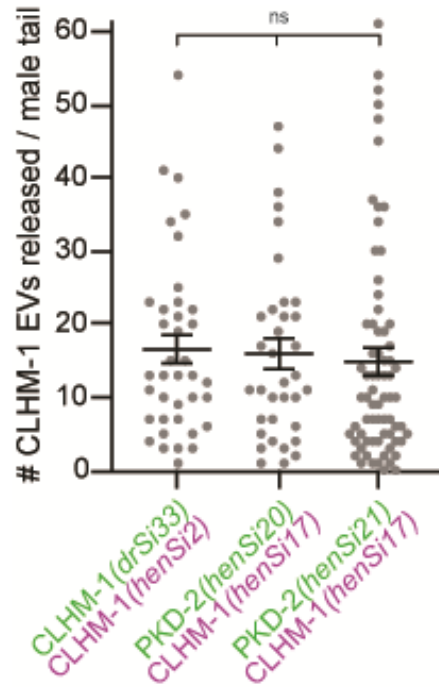


Figure 11: The average number of released environmental EVs containing CLHM-1::tdTomato released does not significantly change between different *clhm-1::tdTomato* SCI transgenes (henSi2 & henSi17), or when *clhm-1::tdTomato* transgenes are paired with different *gfp* SCI transgenes (drSi33, henSi20, henSi21). Error bars show SEM. Kruskal-Wallis test;  $n \geq 35$ .

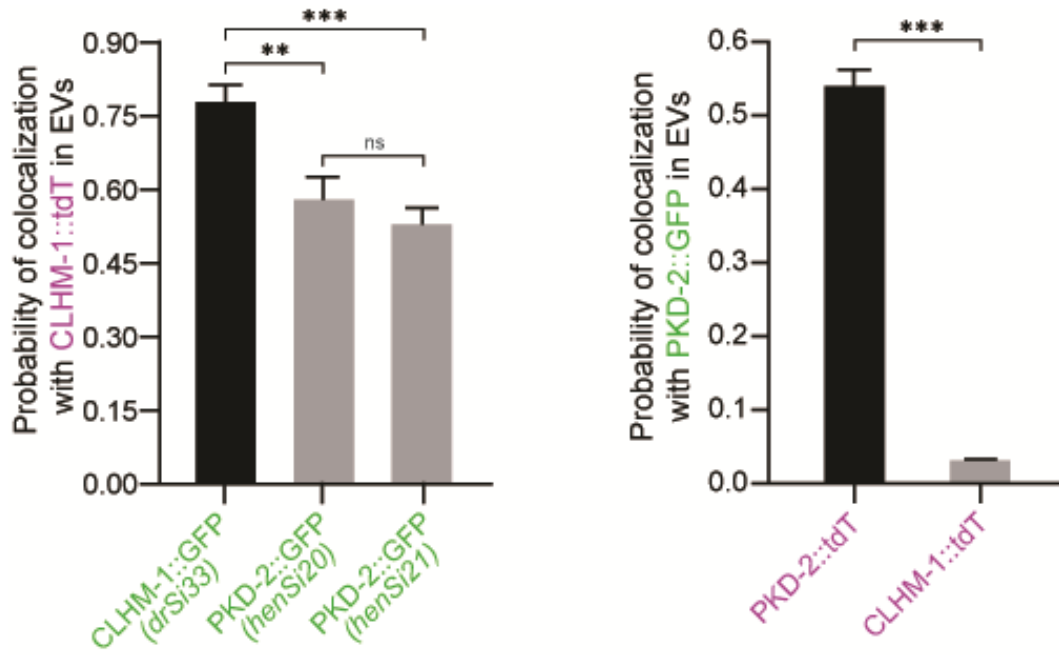


Figure 12: (Left) CLHM-1::GFP is significantly more likely than PKD-2::GFP to coincide with CLHM-1::tdTomato in released environmental EVs. (Right) PKD-2::tdTomato is significantly more likely than CLM-1::tdTomato to coincide with PKD-2::GFP in released environmental EVs. Error bars show SEM. Kruskal-Wallis test;  $n \geq 35$ . \* =  $p < 0.05$ , \*\* =  $p < 0.01$ , \*\*\* =  $p < 0.005$ .

### 3.4 Physiological factors differentially impact the release of EVs enriched with CLHM-1 and PKD-2

Given the observation of CLHM-1 and PKD-2 in distinct EV subpopulations, I wondered if these EVs were differentially shed in response to environmental cues. The presence of hermaphrodite mating partners has been shown to modulate relative abundance of PKD-2-containing EVs (J. Wang et al., 2021).

To test this, I compared the number of CLHM-1::tdTomato EVs shed from tail sensory neurons of males cultured with adult hermaphrodites to the number released by virgin males separated from hermaphrodites at the fourth larval (L4) stage. The absence of mating partners significantly reduced CLHM-1 EV release (**Figure 13**). Conversely, release of PKD-2 EVs from virgin males was significantly higher compared to males cultured with hermaphrodites (**Figure 13**). I also observed a significant increase in the probability of PKD-2::GFP being present in CLHM-1::tdTomato EVs released from virgin adult males, possibly due to the concurrent increase in PKD-2 and decrease in CLHM-1 EV shedding (**Figure 13**).

Male tail EVNs respond to mechanosensory cues, while many head EVNs respond to chemosensory cues (Johnson et al., 2017; Liu & Sternberg, 1995; White et al., 2007). Thus, I also examined if the presence of mating partners had a differential impact on EV release from neurons that respond to different stimuli. Hermaphrodite presence did not impact release of CLHM-1 EVs from male head EVNs (**Figure 14**). However, just as observed for the tail neurons, PKD-2 EV release from head EVNs of

virgin males was significantly higher than from males cultured with hermaphrodites **(Figure 14)**.

In conclusion, CLHM-1 and PKD-2 EV release is differentially altered by mating partner availability, demonstrating that cargo abundance within these EVs is a dynamically regulated and not just the result of non-specific ciliary membrane shedding. These observations also strengthen my hypothesis that CLHM-1 and PKD-2 are deliberately enriched into subpopulations of EVs shed from the same ciliated neurons.

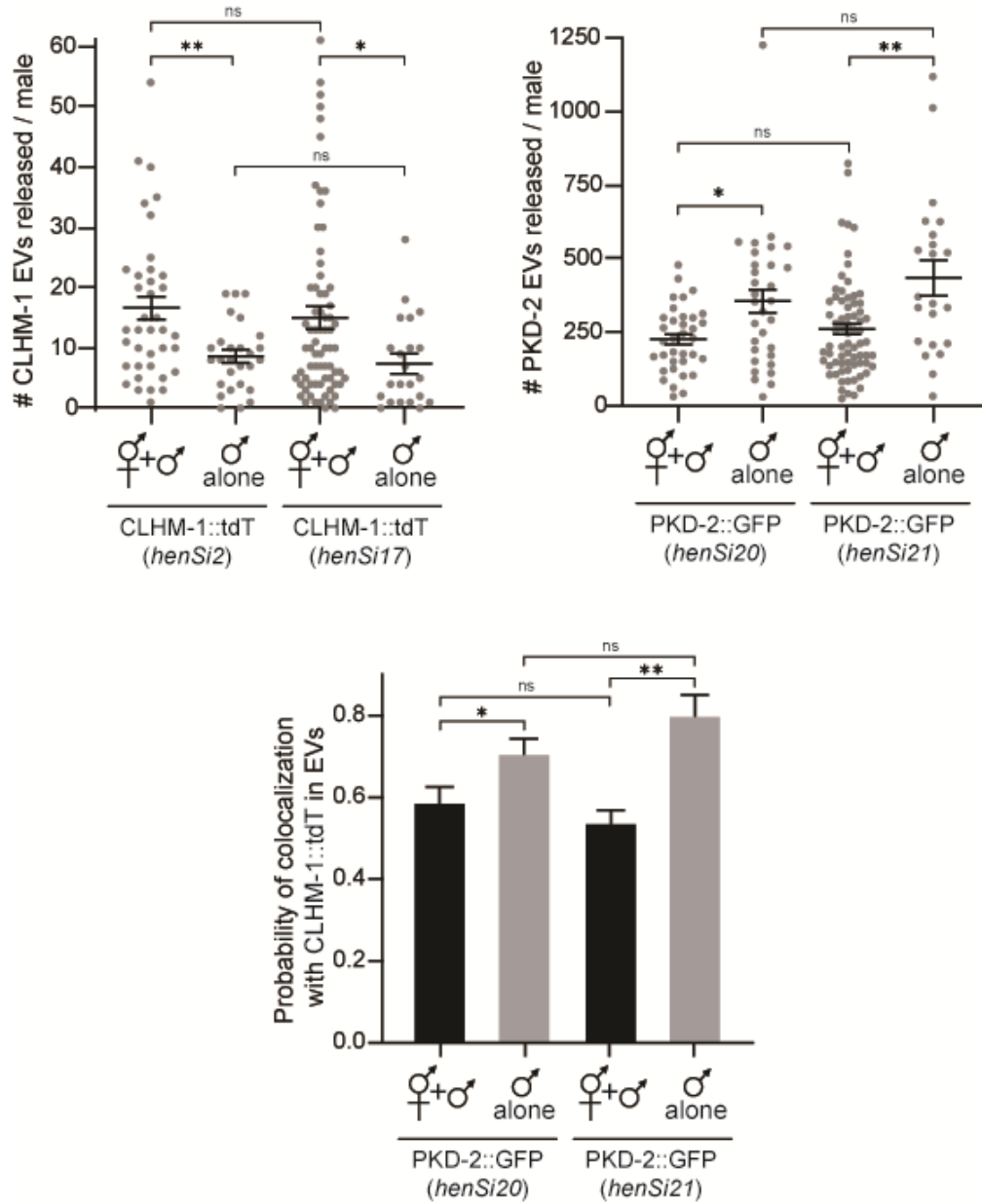


Figure 13: (Top) The average number of environmental EVs containing CLHM-1::tdTomato released from the adult male tail significantly decreases in male-only populations, while the average number of PKD-2::GFP EVs released significantly increases. (Bottom) The probability of PKD-2::GFP coinciding with CLHM-1::tdTomato in released environmental EVs significantly increases in male-only populations. Error bars show SEM. Mann-Whitney test,  $n \geq 20$ . \* =  $p < 0.05$ , \*\* =  $p < 0.01$ .

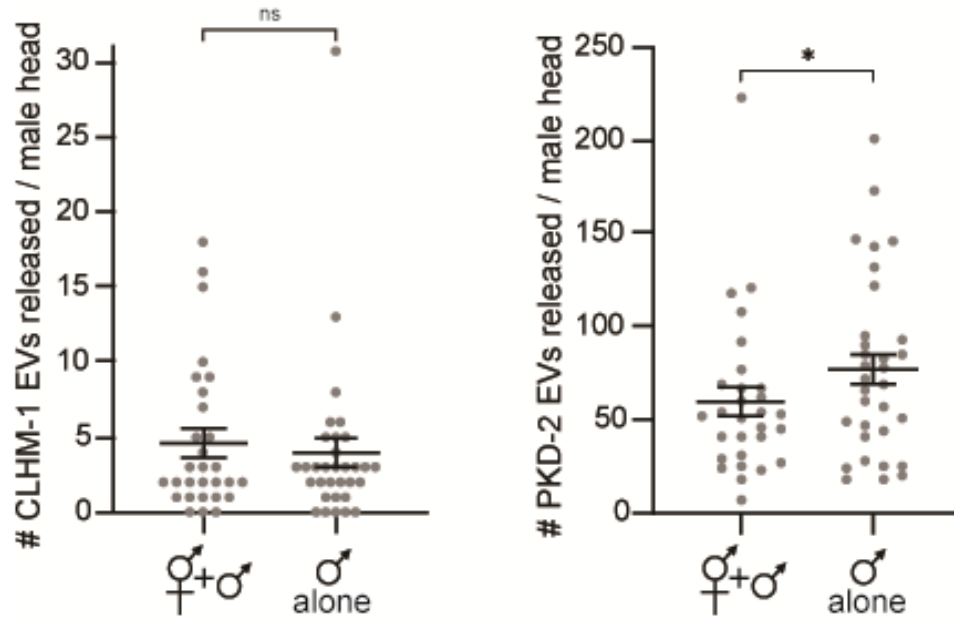


Figure 14: The average number of environmental EVs containing CLHM-1::tdTomato released from the adult male head does not significantly change, while the average number of PKD-2::GFP EVs released significantly increases. Error bars show SEM. Mann-Whitney test;  $n \geq 20$ . \* =  $p < 0.05$ , \*\* =  $p < 0.01$ .

## Chapter 4

### **KINESIN-II MOTOR ACTIVITY DIFFERENTIALLY AFFECTS CLHM-1 AND PKD-2 CILIA LOCALIZATION AND EV BIOGENESIS**

#### **4.1 PKD-2, but not CLHM-1, is enriched to the distal tip of EVN cilia**

In lower-and-higher order eukaryotes, primary cilia are comprised of multiple distinct signaling compartments. These compartments are differentiated by their microtubule ultrastructure as well as their lipid and protein composition. The enrichment of specific proteins and lipid species allows for the concentration of signaling molecules (Blacque & Sanders, 2014; Doroquez et al., 2014; Jensen et al., 2015b; Kaplan et al., 2012; Silva et al., 2017).

In *C. elegans*, the cilia of sensory neurons consist of a periciliary membrane compartment (PCMC), middle segment and distal segment; certain proteins, such as PKD-2, are specifically enriched at the distal segment of these cilia (van der Burght et al., 2020; J. Wang et al., 2021). I reasoned that enrichment of CLHM-1 and PDK-2 in distinct EV subpopulations could result from their differential localization to specific ciliary compartments microdomains, and thus sought to define relative CLHM-1 and PKD-2 localization.

To do this, members of my lab imaged RnB neurons in adult males coexpressing CLHM-1::tdTomato and PKD-2::GFP. We observed that both CLHM-1

and PKD-2 localize to the PCMC and middle segment of the cilium proper, while PKD-2::GFP alone localizes to the distal tip (**Figure 15**).

To quantitate this observation, I used ImageJ (NIH) to analyze PKD-2::GFP and CLHM-1::tdTomato fluorescence intensity along the cilia in two-dimensional image projections. The resulting normalized fluorescence distribution profiles showed that PKD-2::GFP alone extends into the distal tip where CLHM-1::tdTomato is typically absent, consistent with my visual observations (**Figure 16**).

EVs containing PKD-2 are shed from the cilia distal region as well as the PCMC; however, EVs derived from the PCMC are thought to be phagocytosed by neighboring glia cells and not released into the environment (Akella et al., 2020; Razzauti & Laurent, 2021; J. Wang et al., 2021). I observed EVs exclusively containing PKD-2::GFP being shed from the cilia distal region. I also occasionally observed EVs exclusively containing CLHM-1::tdTomato being shed from the cilia middle region and PCMC (**Figure 17**). This suggests that environmentally-released EVs enriched with CLHM-1 are not derived from the cilia distal tip and rather originate at secondary sites, either the cilia middle segment or the PCMC. Thus, I posit that enrichment of CLHM-1 and PKD-2 into discrete subpopulations of EVs derived from multiple sites on the same cilium is a product of differential ciliary localization.

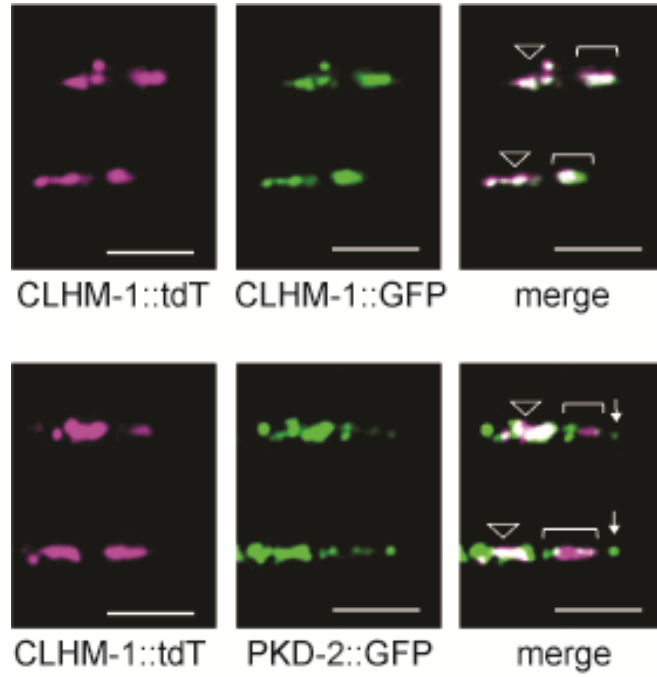


Figure 15: (Top) CLHM-1::tdTomato and CLHM-1::GFP colocalize in the PCMC (triangle) and middle segment of the cilia proper (bracket). (Bottom) CLHM-1::tdTomato and PKD-2::GFP colocalize in the PCMC and middle segment of the cilia proper, but PKD-2 alone localizes to the distal segment (arrow). Scale bars = 3  $\mu$ m.

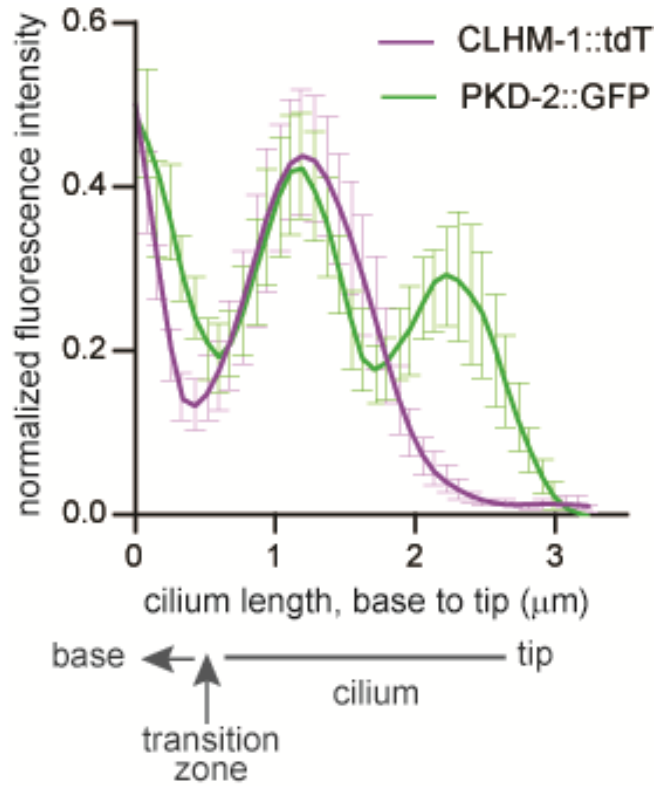


Figure 16: Average normalized fluorescence intensity of CLHM-1::tdTomato and PKD-2::GFP along the length of RnB cilia shows that PKD-2 alone localizes to the cilia distal segment. Error bars show SEM.  $n \geq 15$ .

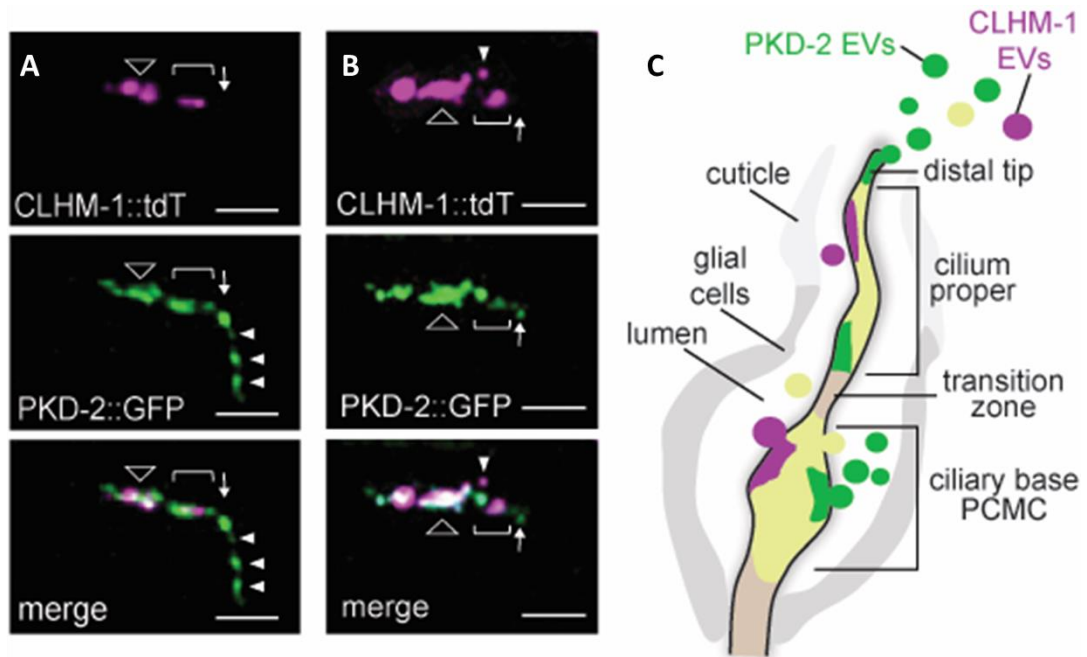


Figure 17: (A) PKD-2::GFP, but not CLHM-1::tdTomato, is found in EVs shed from the cilia distal segment (arrowhead). (B) An EV containing CLHM-1::tdTomato, but not PKD-2::GFP, is shed from the PCMC (arrowhead). (C) Schematic representation of differential cilia localization leading to EV enrichment of CLHM-1::tdTomato and PKD-2::GFP. Scale bars = 3  $\mu$ m.

## 4.2 Individual kinesin-II motor activity differentially impacts biogenesis of CLHM-1 and PKD-2 EVs

IFT, the bi-directional movement of proteins along ciliary microtubules, is required for establishing and maintaining cilium ultrastructure and compartmentalization (Prevo et al., 2017). Anterograde IFT in *C. elegans* cilia is driven by two members of the kinesin-II family: homodimeric kinesin OSM-3 and a heterotrimeric kinesin comprised of KLP-11, KLP20, and KAP-1 (Pan et al., 2006; Snow et al., 2004). In IL2 and male-specific EVNs, the kinesin-3 KLP-6 also participates in anterograde IFT (Morsci & Barr, 2011). As IFT is required for translocation of many ciliary membrane proteins, I considered whether could serve as a mechanism to enrich PKD-2 and CLMH-1 into different ciliary regions and thus EV subpopulations.

To test this, I crossed strains expressing both PKD-2::GFP and CLHM-1::tdTomato with either the *osm-3(mn391)* or *osm-3(p802)* null alleles, or the *klp-11(tm324)* hypomorphic loss-of-function allele (Snow et al., 2004). I observed no significant change in average environmental release of EVs containing PKD-2::GFP from male tail cilia between wild type and *osm-3(mn391)*, *osm-3(p802)*, or *klp-11(tm324)* mutant animals. Interestingly, I did observe a significant increase in average environmental release of EVs containing CLHM-1::tdTomato in both *osm-3* and *klp-11* mutant alleles (**Figure 18**).

To determine whether this relative change was the result of CLHM-1 mislocalization, I analyzed the distribution of GFP and tdTomato fluorescent signal along the cilia in both *osm-3* and *klp-11* mutants. I found no significant change in either CLHM-1::tdTomato or PKD-2::GFP fluorescence distribution; PKD-2 alone is still trafficked to the cilia distal region in both *osm-3* and *klp-11* mutants (**Figure 19**). Thus, individual loss of function for either kinesin-II motor does not cause ciliary mislocalization or significant loss of EV release.

I then analyzed the how loss of OSM-3 or KLP-11 affects the coincidence of PKD-2::GFP and CLHM-1::tdTomato in environmentally released EVs. I found that the probability of PKD-2::GFP being found in a CLHM-1::tdTomato EV increased in both *osm-3* mutant alleles but was unchanged in the *klp-11* mutant compared to wild type (**Figure 20**).

Although I had previously determined that loss of OSM-3 or KLP-11 does not result in aberrant CLHM-1 or PKD-2 mislocalization, I wondered whether smaller changes in ciliary colocalization could be detected that would explain the observed changes in EV colocalization. To do this, Rachael Gill, another graduate student in the lab imaged RnB cilia in either *osm-3* or *klp-11* mutants and measured net colocalization between CLHM-1::tdTomato and PKD-2::GFP in both the cilia proper and PCMC. Colocalization was measured with the Manders 2 (M2) coefficient, which indicates the percentage of red pixels that co-occur with green pixels within a given region.

Compared to wild type, we observed a significant decrease in the M2 coefficient in both the cilium proper and PCMC of *klp-11* mutants, indicating an increase in CLHM-1::tdTomato that did not colocalize with PKD-2::GFP. No change in ciliary colocalization of CLHM-1 and PKD-2 was detected in either *osm-3* mutant (**Figure 21**).

These data show an interesting correlation between the ciliary colocalization of CLHM-1 and PKD-2 and their coincidence in EVs. The increase in CLHM-1 EV release in the *osm-3* mutant is associated with an increase in colocalization of PKD-2 and CLHM-1 in EVs. Conversely, loss of *klp-11* reduces ciliary colocalization of these cargoes, suggesting that the additional CLHM-1-containing EVs released in the *klp-11* mutant are shed from membrane regions that contain only CLHM-1.

*C. elegans* male-specific EVNs also employ the kinesin-3 KLP-6, which is necessary for release of PKD-2 EVs into the environment but does not prevent ciliary EV shedding into the lumen (Morsci & Barr, 2011; J. Wang et al., 2014). To determine whether KLP-6 is also required for release of both PKD-2 and CLHM-1 EVs, I crossed a strain expressing both PKD-2::GFP and CLHM-1::tdTomato with the *klp-6(sy511)* loss-of-function mutant (Peden & Barr, 2005). I observed a significant decrease in CLHM-1 EVs released into the environment in the *klp-6* mutant compared to the wild type, suggesting that KLP-6 is required for environmental release for multiple EV subpopulations (**Figure 22**).

Together, my data demonstrate that each kinesin plays a distinct role in EV biogenesis, differentially impacting ciliary colocalization and enrichment of EV cargoes as well as release of EV subpopulations into the environment.

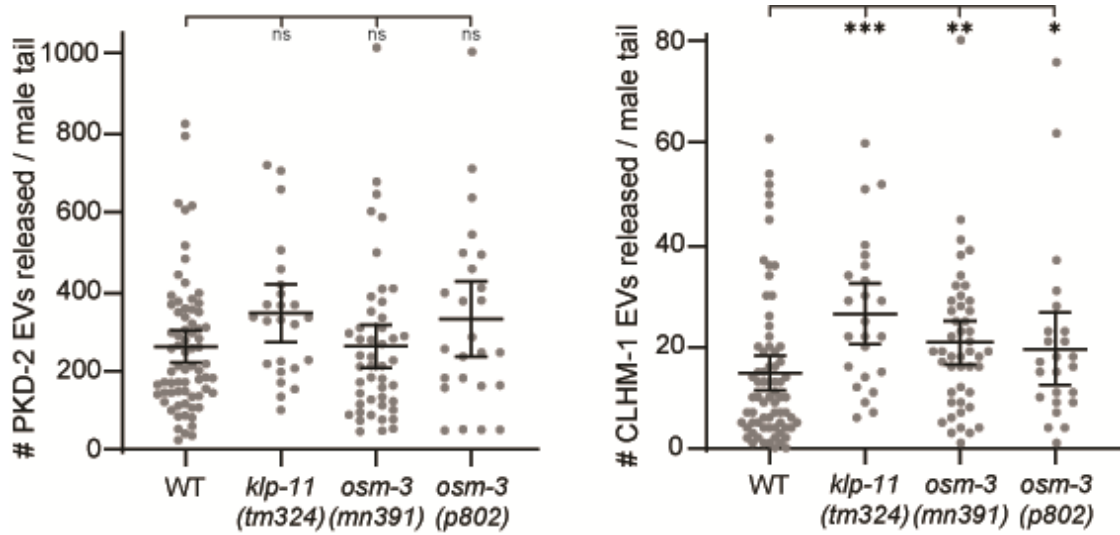


Figure 18: (Left) Environmental release of EVs containing PKD-2::GFP is not significantly changed in *klp-11* or *osm-3* mutant backgrounds. (Right) Environmental release of EVs containing CLHM-1::tdTomato is significantly increased in both *klp-11* and *osm-3* mutant males. Error bars show SEM. Kruskal-Wallis test;  $n \geq 24$ . \* =  $p < 0.05$ , \*\* =  $p < 0.01$ , \*\*\* =  $p < 0.005$ .

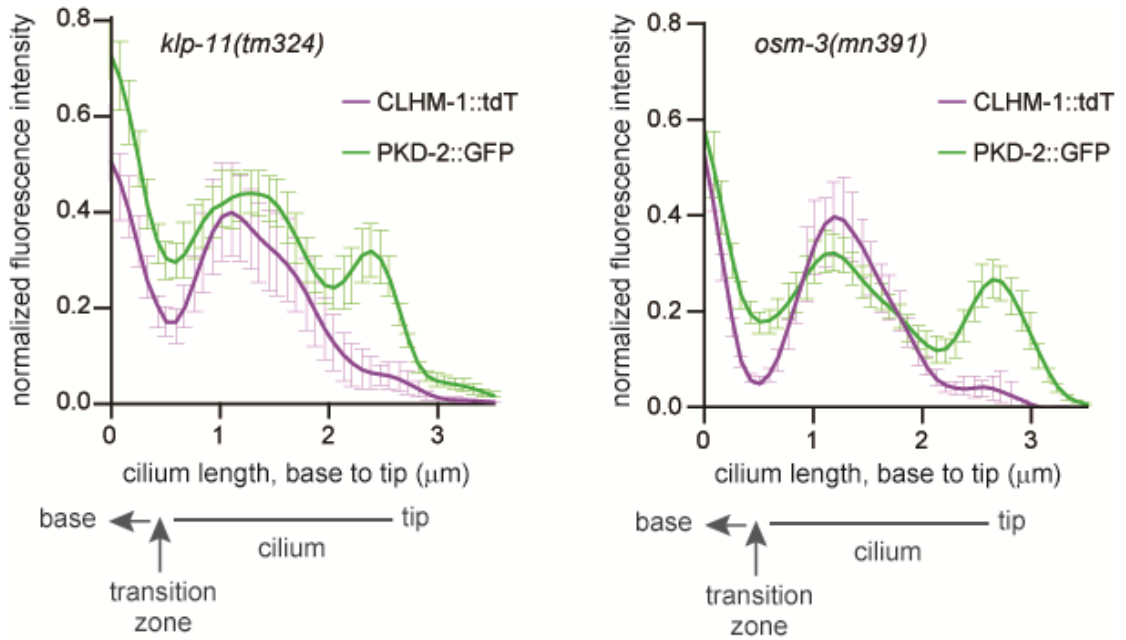


Figure 19: Average normalized fluorescence intensity of CLHM-1::tdTomato and PKD-2::GFP along the length of RnB cilia shows that PKD-2 alone localizes to the cilia distal segment in *klp-11* (left) and *osm-3* (right) mutant males. Error bars show SEM.  $n \geq 15$ .

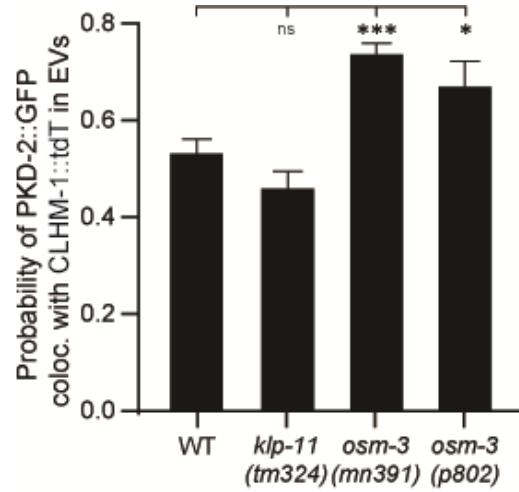


Figure 20: The probability of PKD-2::GFP coinciding with CLHM-1::tdTomato in released environmental EVs does not significantly change in *klp-11* mutants but significantly increases in two different *osm-3* mutant alleles. Error bars show SEM. Kruskal-Wallis test;  $n \geq 24$ . \* =  $p < 0.05$ , \*\* =  $p < 0.01$ , \*\*\* =  $p < 0.005$ .

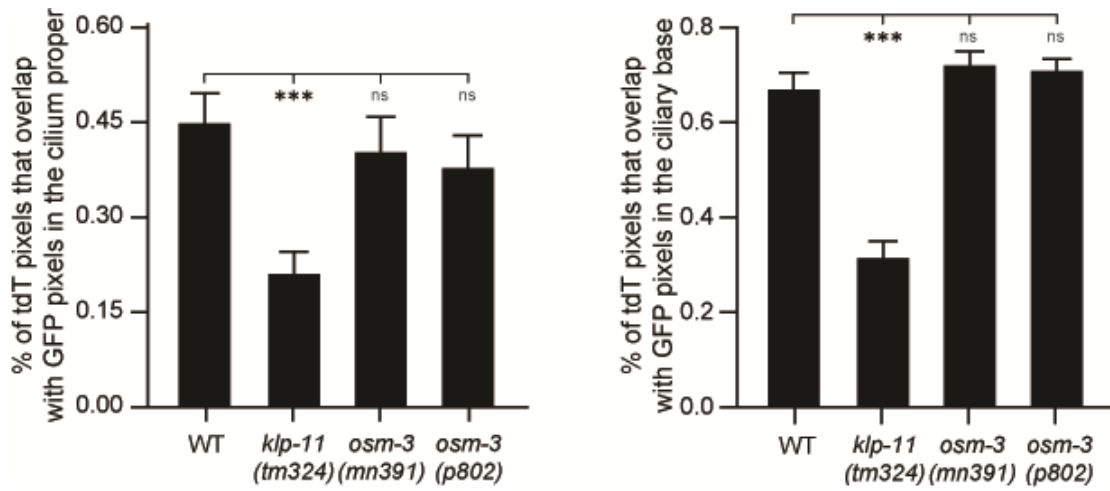


Figure 21: The M2 coefficient is significantly lower in the cilium proper (left) and PCMC (right) of RnB neuron cilia in *klp-11*, but not *osm-3*, mutant males. Error bars show SEM. Kruskal-Wallis test;  $n \geq 20$ . \* =  $p < 0.05$ , \*\* =  $p < 0.01$ , \*\*\* =  $p < 0.005$ .

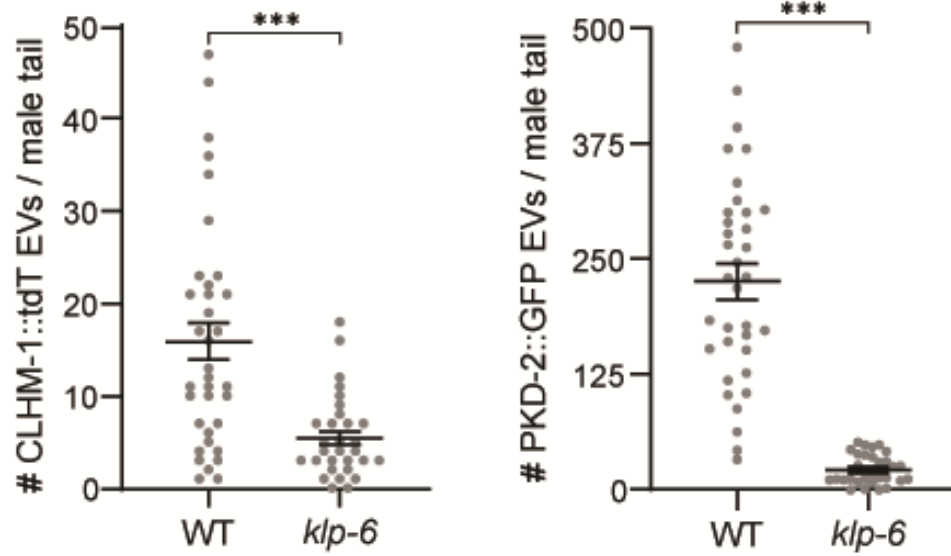


Figure 22: The average number of released environmental EVs containing either CLHM-1 and PKD-2 significantly decreases in *klp-6* mutant males. Error bars show SEM. Mann-Whitney test;  $n \geq 20$ . \* =  $p < 0.05$ , \*\* =  $p < 0.01$ , \*\*\* =  $p < 0.005$ .

### 4.3 Release of EVs containing PKD-2, but not CLHM-1, is dependent on joint OSM-3 and heterotrimeric kinesin-II activity

Loss of kinesin-II mediated anterograde IFT in *osm-3; klp-11* double mutants dramatically decreases shedding of EVs containing PKD-2::GFP without impacting the length of male-specific CEM cilia (Morsci & Barr, 2011; J. Wang et al., 2014, 2021). I wondered whether environmental CLHM-1 EVs, which do not originate at the ciliary distal tip like PKD-2 EVs, are similarly dependent on the cooperative action of kinesin-II motors.

To test this, I crossed a strain expressing both PKD-2::GFP and CLHM-1::tdTomato with a strain containing the *osm-3(p802)* and *klp-11(tm324)* mutations, and imaged environmental EV release from the adult male tail. I found that loss of OSM-3 & KLP-11 drastically reduces the average number of PKD-2::GFP EVs released into the environment, as previously reported, but does not significantly change environmental release of CLHM-1::tdTomato EVs (**Figure 23**). I also observed a significant decrease in the probability of PKD-2::GFP being present with CLHM-1::tdTomato in EVs released from *osm-3; klp-11* animals (**Figure 24**). This shows that loss of cooperating OSM-3 and heterotrimeric kinesin-II motors has a subpopulation-specific impact on EV release.

To determine if the observed changes in EV release were the result of changes in ciliary protein distribution, fellow graduate students Rachael Gill and Malek Elsayyid imaged RnB cilia in *osm-3; klp-11* mutants. We observed that CLHM-1::tdTomato was

still trafficked into the cilium proper while PKD-2::GFP was often excluded entirely and rarely found at the distal tip in *osm-3; klp-11* mutants (**Figure 25**). Fluorescence intensity distribution profiles confirm that CLHM-1:tdTomato, but not PKD-2::GFP, is able to enter the cilia in these mutants (**Figure 25**), explaining the significant decrease in PKD-2::GFP environmental release. Taken together, my data suggests that discrete ciliary localization, mediated by anterograde IFT, results in specific protein enrichment into EVs shed from primary cilia.

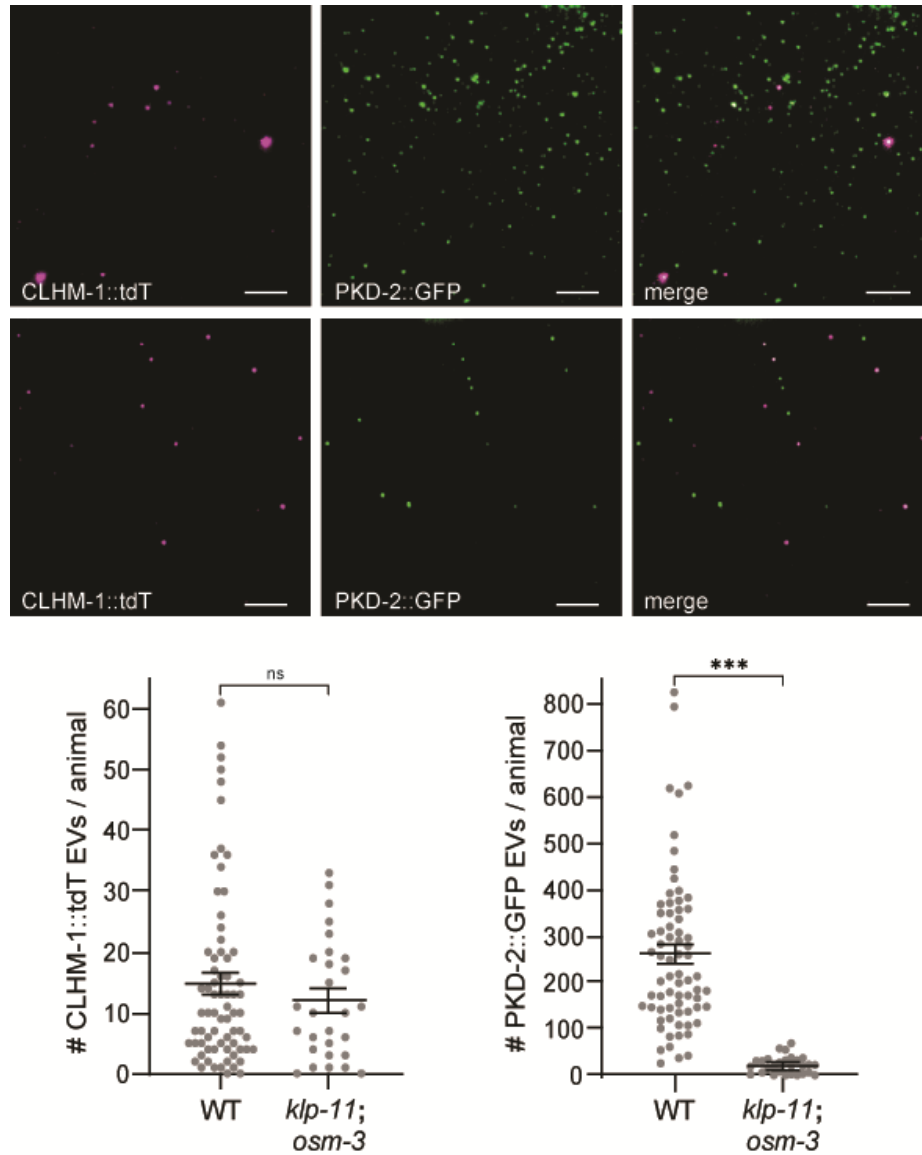


Figure 23: The average number of released environmental EVs containing PKD-2::GFP, but not CLHM-1::tdTomato, significantly decreases in *klp-11; osm-3* mutant males. Scale bars = 3 μm. Error bars show SEM. Mann-Whitney test;  $n \geq 25$ . \* =  $p < 0.05$ , \*\* =  $p < 0.01$ , \*\*\* =  $p < 0.005$ .

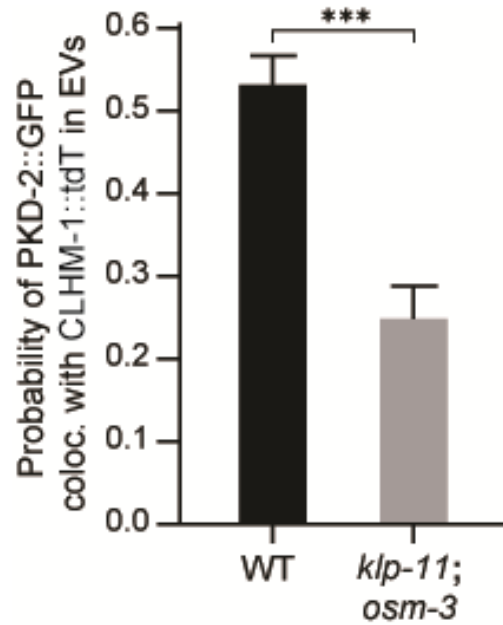


Figure 24: The probability of PKD-2::GFP coinciding with CLHM-1::tdTomato in released environmental EVs significantly decreases change in *klp-11;osm-3* mutant males. Mann-Whitney test;  $n \geq 25$ . \* =  $p < 0.05$ , \*\* =  $p < 0.01$ , \*\*\* =  $p < 0.005$ .



#### 4.4 MKS-5 and the transition zone are required for maintaining EV biogenesis

Selective transport of proteins and lipids into the cilia organelle is gated by the conserved transition zone (TZ) complex (Jensen & Leroux, 2017; Lee & Chung, 2015). Construction of the TZ is dependent on the assembly factor MKS-5 as loss of this protein results in free diffusion of various proteins and lipid species into the ciliary space (Jensen et al., 2015a; C. Li et al., 2016).

How loss of the TZ affects EV biogenesis or cargo sorting is unknown. However, as my data shows that ciliary sublocalization of EV cargo proteins contributes to their specific EV enrichment, I reasoned that loss of MKS-5 would impact ciliary EV biogenesis and/or cargo sorting. To test this, I crossed a strain expressing both PKD-2::GFP and CLHM-1::tdTomato into the *mks-5(tm3100)* loss-of-function mutant and imaged release of EVs from the adult male tail.

Interestingly, I found that loss of MKS-5, and thus, the transition zone, caused a significant decrease in the release of EVs containing PKD-2::GFP but no significant change in release of EVs containing CLHM-1::tdTomato (**Figure 26**). I also observed a significant decrease in the average probability of PKD-2::GFP coinciding with CLHM-1::tdTomato in environmental EVs (**Figure 27**), likely because of the decreased presence of PKD-2::GFP. These data indicate that a functional transition zone and maintenance of cilia compartmentalization is fundamental to selective EV cargo enrichment.

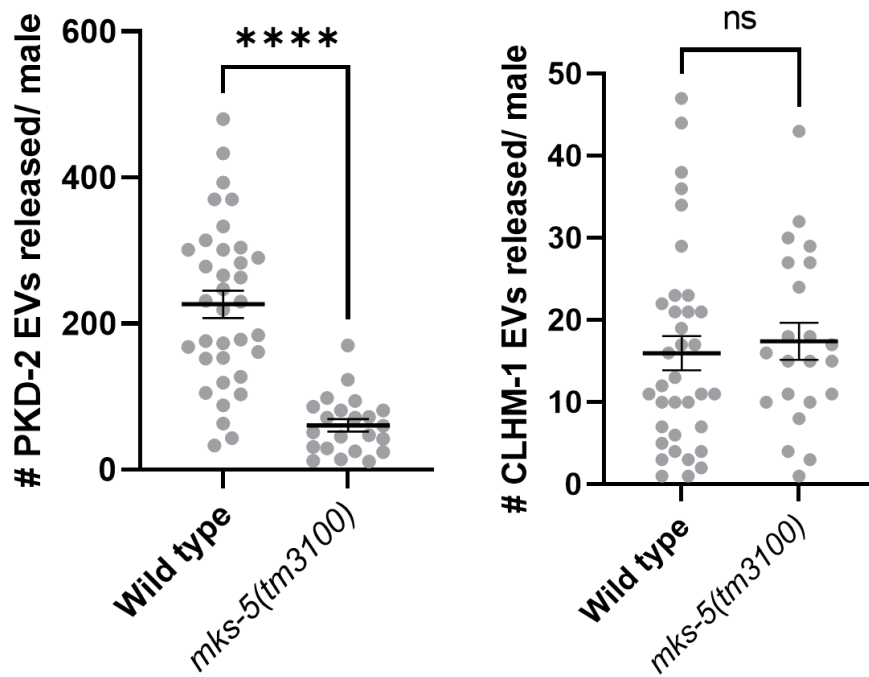


Figure 26: The average number of released environmental EVs containing PKD-2 (left), but not CLHM-1 (right), significantly decreases in *mks-5(tm3100)* mutant males. Error bars show SEM. Mann-Whitney test;  $n \geq 20$ . \* =  $p < 0.05$ , \*\* =  $p < 0.01$ , \*\*\* =  $p < 0.005$ , \*\*\*\* =  $p < 0.001$ .

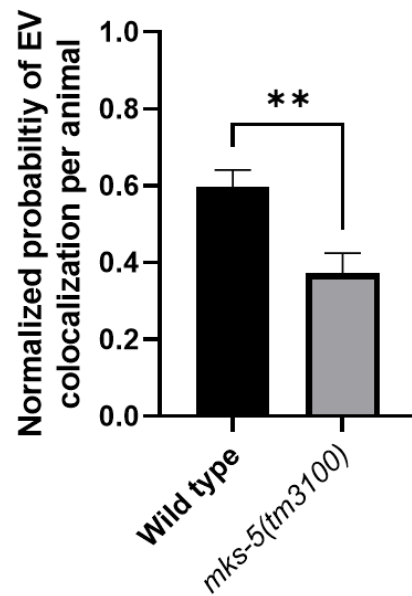


Figure 27: The probability of PKD-2::GFP coinciding with CLHM-1::tdTomato in released environmental EVs significantly decreases change in *mks-5(tm3100)* mutant males. Mann-Whitney test;  $n \geq 20$ . \*=  $p < 0.05$ , \*\*= $p < 0.01$ .

## Chapter 5

### ALX-1 AND ARF-6 PLAY DISTINCT ROLES IN CILARY EV BIOGENESIS AND CARGO SORTING

#### 5.1 The ubiquitin binding protein ALX-1 is a regulator of EV biogenesis

The ALG-2 Interacting Protein X (ALIX) is a soluble cytoplasmic protein that contains a Bro1 ubiquitin binding domain and regulates ESCRT-dependent and ESCRT-independent exosome biogenesis (Baietti et al., 2012; Bissig & Gruenberg, 2014; Dores et al., 2012). ALIX also plays a role in ectosome biogenesis and is required for HIV-1 ectosome-like budding (Morita et al., 2011). ALIX homologs are involved in EV biogenesis in non-mammalian systems. In *Chlamydomonas*, PDCD6 and PDCD6IP (ALG-2 and ALIX homologs, respectively) were found overrepresented in flagellar ectosomes compared to flagellar membranes.

*C. elegans* expresses a single ALIX homolog, designated ALX-1. The *alx-1* gene appears to be expressed in multiple cell types and ALX-1 is required for RME-1 mediated endosomal recycling of cell receptors and also localizes to MVBs in intestinal cells (Shi et al., 2007). Whether *alx-1* is expressed in ciliated neurons or plays a role in ciliary EV biogenesis has not been explored.

I sought to determine whether ALX-1 plays a role in ciliary EV budding or cargo sorting. To test this, I crossed a strain expressing PKD-2::GFP and CLHM-

1::tdTomato with the *alx-1(gk338)* loss-of-function mutant and imaged ciliary EVs released from the adult male tail. Interestingly, I found that loss of *alx-1* results in a significant increase in release of EVs containing CLHM-1::tdTomato, but no significant change in release of EVs containing PKD-2::GFP (**Figure 28**). This indicates that ALX-1 plays a selective role in cargo sorting, cargo delivery, or EV biogenesis of specific EV subpopulations.

Based on previous studies (Dores et al., 2012; Long et al., 2016), I reasoned that ALX-1 regulates ciliary EV biogenesis by either localizing to the cilia and directly binding to and clustering cargo, or by selectively regulating ciliary protein abundance via the endosomal recycling pathway. To determine which of these possibilities is more likely, I sought to determine where ALX-1 localizes in ciliated sensory neurons. Thus, we ordered a strain containing a CRISPR/Cas9 generated knock-in of mKate at the endogenous *alx-1* locus.

Super-resolution imaging of ALX-1::mKate animals proved to be inconclusive. Hermaphrodite and male animals had nearly indiscernible fluorescent punctae in the head and tail region, but nothing that appear to align with the location of ciliated sensory neurons (**Figure 29**).

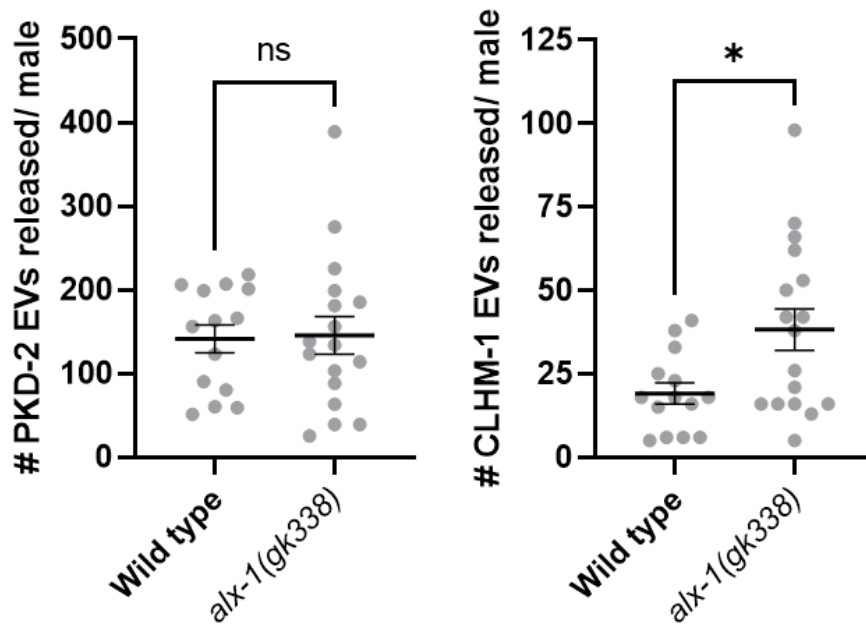


Figure 28: The average number of released environmental EVs containing CLHM-1 (right), but not PKD-2 (left), significantly increases in *alx-1(gk338)* mutant males. Error bars show SEM. Student's t-test;  $n \geq 14$ . \*=  $p < 0.05$ .

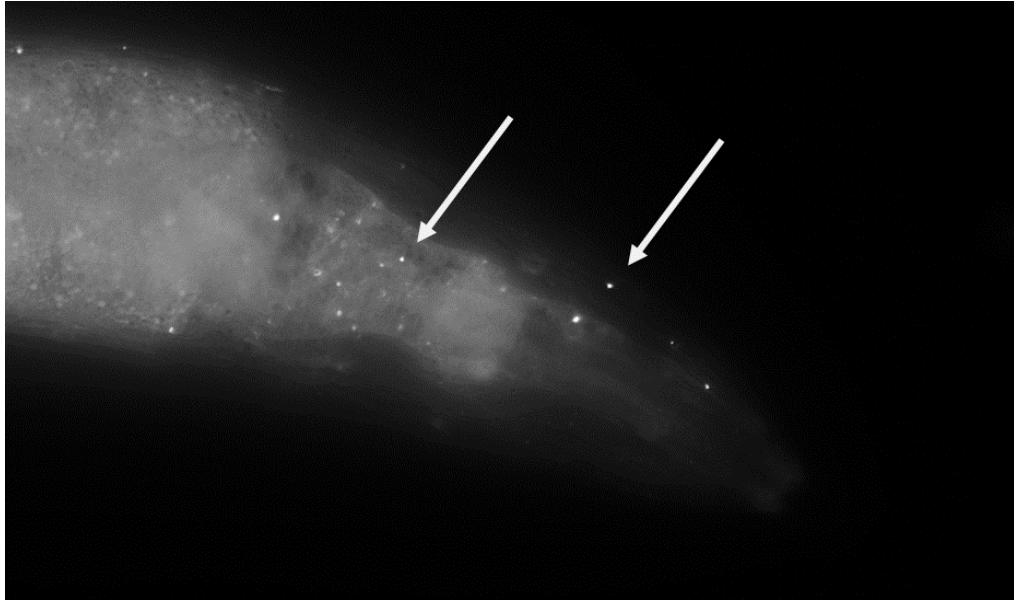


Figure 29: ALX-1::mKate shows nonspecific punctate distribution in the head of an adult male hermaphrodite (white arrow).

## 5.2 ARF-6 is required for biogenesis of CLHM-1 EVs

ADP-Ribosylation Factor 6 (ARF6) is a small GTPase factor that is involved in membrane receptor recycling via the endosomal recycling pathway (Claing et al., 2001). Recently, it was found that ARF6 is required for increase of MAPK signaling resulting in microvesicle shedding from tumor cells, linking it to ectosome biogenesis (Muralidharan-Chari et al., 2009). ARF6 is also found in PKD-positive EVs purified from urine, indicating its potential colocalization with PKD-2 in kidney epithelial cilia (Hogan et al., 2009).

*C. elegans* expresses a single ARF6 homolog, designated ARF-6. ARF-6 is not known to be heavily expressed in EVNs (Y. Li et al., 2004; J. Wang et al., 2015). However, I gauged that enough evidence existed to consider ARF-6 as a potential regulator of ciliary EV biogenesis. To test this possibility, I crossed a strain expressing CLHM-1::GFP with the *arf-6(tm1447)* loss-of-function mutant and imaged ciliary EVs released from the adult male tail. I found that loss of ARF-6 significantly decreases the average number of CLHM-1 EVs released from adult males. (**Figure 30**). This indicates that ARF-6 may play a role in ciliary EV biogenesis, cargo sorting, or cargo delivery.

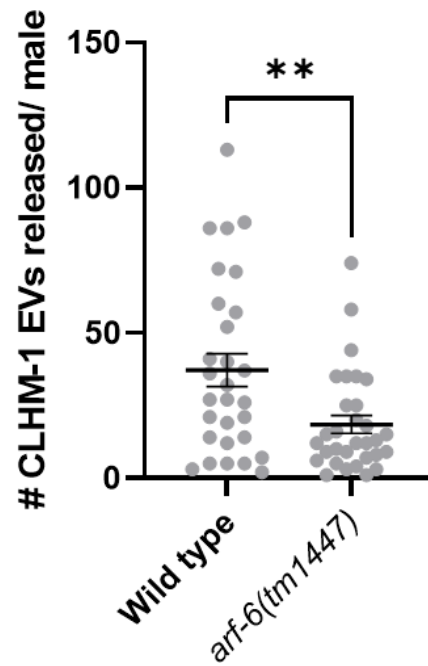


Figure 30: The average number of released environmental EVs containing CLHM-1, significantly decreases in *arf-6(tm1447)* mutant males. Error bars show SEM. Mann-Whitney test;  $n \geq 20$ . \* =  $p < 0.05$ , \*\* =  $p < 0.01$ .

## Chapter 6

### ISOLATION AND LC-MS/MS CHARACTERIZATION OF EV PARTICLES FROM *C. ELEGANS* CULTURE

#### 6.1 NTA and TEM characterization of EVs isolated from *C. elegans* culture using differential ultracentrifugation

My first three research aims rely primarily on super-resolution imaging and analysis to show that CLHM-1 is enriched in a distinct subpopulation of EVs released from sensory neuron cilia. However, I wished to explore an alternative approach to show that CLHM-1 EVs are distinct from other ciliary EVs. To do this, I planned to directly isolate all EV-sized particles released from *C. elegans*, then separate isolated EVs based on CLHM-1 enrichment and subsequently analyze the total proteomic contents of CLHM-1-enriched EVs using liquid chromatography tandem mass spectrometry (LC-MS/MS). This line of experimentation was particularly challenging as there was no existing literature describing how to isolate EVs from nematode culture for the purposes of LC-MS/MS, and thus I would be generating all protocols and experiments *de novo*.

TEM images indicate that ciliary EVs immunostained for the TRP polycystin LOV-1 are  $111.2 \pm 31.1$  nm in diameter (J. Wang et al., 2014), and thus comparable in size to large mammalian exosomes (van Niel et al., 2018). Thus, to isolate EVs from

*C. elegans*, I adapted a protocol to isolate exosomes from mammalian cell culture via differential ultracentrifugation (Greening et al., 2015). I scaled up culture of DR466, a strain containing the *him-5(e1490)* mutation, to produce a mixed population of approximately 200,000 adult males and hermaphrodites. I then washed these animals into M9 salt media, pelleted the animals, and subjected the supernatant to successive rounds of ultracentrifugation until I pelleted exosome-sized particles.

To confirm that particles attained via ultracentrifugation matched the morphological description of EVs, I provided sample to Shannon Modla of the Delaware Bio-imaging Center stained for TEM imaging. Analysis of the TEM images showed that isolated particles appeared circular in shape and contained membrane-like structures (**Figure 31**). These images resembled previously published images of *C. elegans* ciliary EVs as well as generally accepted morphology of EVs (J. Wang et al., 2014; Zabeo et al., 2017).

I then determined the size distribution of isolated EVs using nanoparticle tracking analysis (NTA), which tracks the Brownian motion of particles in liquid to approximate particle size. An average of 5 NTA technical replicates showed that the majority of isolated EVs were  $135.7 \pm 35.6$  nm in diameter (**Figure 32**). This would make isolated EVs slightly larger than previously reported but still within the potential size range of ectosomal EVs (van Niel et al., 2018; J. Wang et al., 2014).

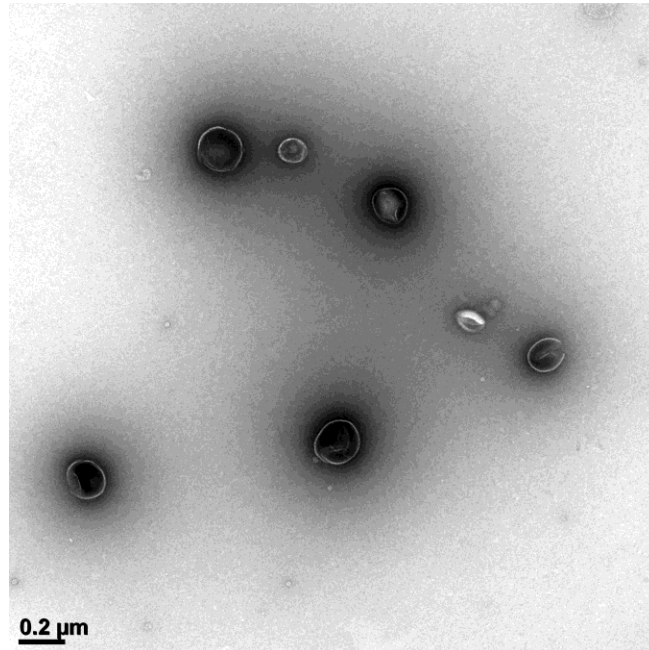


Figure 31: TEM image of pelleted EVs negative stained with uranyl acetate shows EVs are circular and wrapped in membrane-like structure. Scale bar = 0.2 μm.

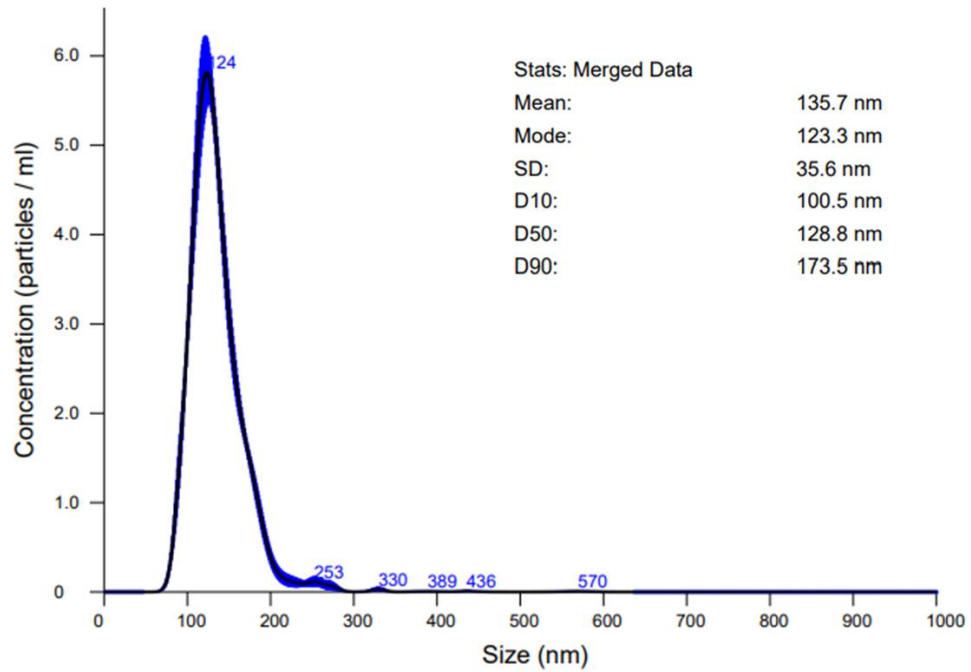


Figure 32: Nanoparticle Tracking Analysis shows that the majority of pelleted EVs are  $135.7 \pm 35.6$  nm in diameter. Graph is an average of 5 technical replicates.

## 6.2 LC-MS/MS analysis of EVs isolated from ultracentrifugation reveals presence of contaminating EVs

After determining that particles isolated from nematode culture were of the correct size and morphology, I sought to use LC-MS/MS analysis to determine if I had successfully retrieved ciliary EVs by identifying known ciliary EV proteins such as CLHM-1, PKD-2, CWP-1, CIL-7, LOV-1, or ASIC-2 (Maguire et al., 2015; J. Wang et al., 2014, 2015).

To prepare EV proteins for LC-MS/MS, I adapted a protocol describing trypsin digestion of peptides in a SDS-polyacrylamide gel (Gundry et al., 2010). Briefly, EVs were lysed in RIPA buffer to extract protein (Subedi et al., 2019), after which protein was denatured and separated using SDS-PAGE. The PA gel was stained to reveal protein bands; protein bands were cut and de-stained, and then treated with DTT, IAA, and trypsin for peptide reduction, alkylation, and digestion, respectively (Gundry et al., 2010). Digested peptides were cleaned using reverse-phase chromatography, dried, and submitted for LC-MS/MS analysis.

I used Proteome Discoverer Software (ThermoFisher) to compare identified peptide fragments against the Uniprot database of *C. elegans* proteins (<https://www.uniprot.org/proteomes/UP000001940>). A summary of *C. elegans* proteins identified via LC-MS/MS can be found in **Table 4**. The list included several aspartic proteases ASP-1, ASP-2, ASP-4, ASP-5, and ASP-6, which have predicted endopeptidase activity and are thought to be involved in necrotic cell death

(Syntichaki et al., 2002). The list also included ACT-4, an actin subunit protein. However, the list did not include any proteins known to be enriched in EVNs or cilia, nor any known ciliary EV markers (J. Wang et al., 2014, 2015)

I then wondered if any contaminating peptides were present by comparing identified peptide fragments against a database of *E. coli* proteins (**Table 5**). This showed a much more extensive list of proteins, including outer membrane protein A (OMPA), outer membrane protein F (OMPF), which are known to be markers of bacterial OMVs (Hong et al., 2019; van der Westhuizen et al., 2019). *E. coli* OMVs isolated via ultracentrifugation are approximately 130 nm in diameter (Reimer et al., 2021). Thus, I concluded that the majority of the EVs obtained from my experiment were not derived from nematodes, but from their *E. coli* food source.

These data showed proof-of-concept ability to extract EV particles of the correct size and successfully identify their protein contents. However, the data also revealed the overabundant presence of bacterial OMVs isolated from *C. elegans* and *E. coli* co-culture, this highlighted the need for a method to specifically enrich ciliary EVs.

Table 4: List of *C. elegans* proteins represented in LC-MS/MS samples

<b>UniProt Accession #</b>	<b>Polypeptide Description</b>	<b>Sequence Score</b>
O01532	ASpartyl Protease OS=Caenorhabditis elegans OX=6239 GN=asp-5 PE=1 SV=1 - [O01532_CAEEL]	6.19
Q95ZL1	Actin-4 OS=Caenorhabditis elegans OX=6239 GN=act-4 PE=1 SV=1 - [Q95ZL1_CAEEL]	5.67
Q86NE0	ASpartyl Protease OS=Caenorhabditis elegans OX=6239 GN=asp-2 PE=1 SV=1 - [Q86NE0_CAEEL]	4.88
G5ECU5	Uncharacterized protein OS=Caenorhabditis elegans OX=6239 GN=CELE_F44E5.4 PE=1 SV=1 - [G5ECU5_CAEEL]	3.63
Q93572	60S acidic ribosomal protein P0 OS=Caenorhabditis elegans OX=6239 GN=rla-0 PE=1 SV=3 - [RLA0_CAEEL]	3.16
G5EEI4	ASpartyl Protease OS=Caenorhabditis elegans OX=6239 GN=asp-1 PE=1 SV=1 - [G5EEI4_CAEEL]	3.07
O01530	Aspartic protease 6 OS=Caenorhabditis elegans OX=6239 GN=asp-6 PE=3 SV=1 - [ASP6_CAEEL]	2.95
P09446	Heat shock 70 kDa protein A OS=Caenorhabditis elegans OX=6239 GN=hsp-1 PE=1 SV=2 - [HSP7A_CAEEL]	2.92
O16198	Glutathione S-Transferase OS=Caenorhabditis elegans OX=6239 GN=gst-33 PE=1 SV=1 - [O16198_CAEEL]	2.71

Table 5: List of *E. coli* proteins represented in LC-MS/MS samples

UniProt Accession #	Peptide Description	Score
P02931	Outer membrane protein F OS=Escherichia coli (strain K12) OX=83333 GN=ompF PE=1 SV=1 - [OMPF_ECOLI]	128.37
P23843	Periplasmic oligopeptide-binding protein OS=Escherichia coli (strain K12) OX=83333 GN=oppA PE=1 SV=2 - [OPPA_ECOLI]	90.21
P02925	Ribose import binding protein RbsB OS=Escherichia coli (strain K12) OX=83333 GN=rbsB PE=1 SV=1 - [RBSB_ECOLI]	82.05
P0CE47	Elongation factor Tu 1 OS=Escherichia coli (strain K12) OX=83333 GN=tufA PE=1 SV=1 - [EFTU1_ECOLI]	76.24
P0AEE5	D-galactose-binding periplasmic protein OS=Escherichia coli (strain K12) OX=83333 GN=mglB PE=1 SV=1 - [DGAL_ECOLI]	61.08
P05825	Ferrienterobactin receptor OS=Escherichia coli (strain K12) OX=83333 GN=fepA PE=1 SV=2 - [FEPA_ECOLI]	60.80
P37902	Glutamate/aspartate import solute-binding protein OS=Escherichia coli (strain K12) OX=83333 GN=gltI PE=1 SV=2 - [GLTI_ECOLI]	57.14
P00509	Aspartate aminotransferase OS=Escherichia coli (strain K12) OX=83333 GN=aspC PE=1 SV=1 - [AAT_ECOLI]	55.58
P0AG67	30S ribosomal protein S1 OS=Escherichia coli (strain K12) OX=83333 GN=rpsA PE=1 SV=1 - [RS1_ECOLI]	47.65

P0A6M8	Elongation factor G OS=Escherichia coli (strain K12) OX=83333 GN=fusA PE=1 SV=2 - [EFG_ECOLI]	45.19
P25553	Lactaldehyde dehydrogenase OS=Escherichia coli (strain K12) OX=83333 GN=aldA PE=1 SV=2 - [ALDA_ECOLI]	44.86
P0A940	Outer membrane protein assembly factor BamA OS=Escherichia coli (strain K12) OX=83333 GN=bamA PE=1 SV=1 - [BAMA_ECOLI]	44.68
P31554	LPS-assembly protein LptD OS=Escherichia coli (strain K12) OX=83333 GN=lptD PE=1 SV=2 - [LPTD_ECOLI]	43.60
P27550	Acetyl-coenzyme A synthetase OS=Escherichia coli (strain K12) OX=83333 GN=acs PE=1 SV=2 - [ACSA_ECOLI]	43.53
P0A910	Outer membrane protein A OS=Escherichia coli (strain K12) OX=83333 GN=ompA PE=1 SV=1 - [OMPA_ECOLI]	41.95

### **6.3 Engineering a Strep-tag into CLHM-1 to pull down CLHM-1 EVs via Streptavidin affinity beads**

Multiple methods have been described to enrich for specific EV subtypes of a particular size or density, or for EVs containing specific protein surface markers. As exosomes and ectosomes populations can partially overlap in size, density, and presence of surface markers (Brennan et al., 2020; Kowal et al., 2016), careful consideration is required before selecting a method to enrich specific EVs.

Density gradient ultracentrifugation (DG-UC) and size exclusion chromatography (SEC) are used to separate EVs by density or size, respectively (Brennan et al., 2020). The overlap in size between ciliary EVs and *E. coli* EVs eliminated the possibility of using SEC. Using DG-UC to separate these EVs was theoretically possible. However, technical and ability limitations made this option unfavorable.

Another effective method of EV isolation is affinity purification against unique protein or lipids present on EV membranes (Nakai et al., 2016; Zhu et al., 2021). Unique affinity surface markers for mammalian EV subtypes have been described and utilized as substrates for affinity chromatography (Jeppesen et al., 2019; Zhu et al., 2021). Unfortunately, to my knowledge, similarly well-described surface markers for *C. elegans* ciliary EVs do not exist. TSP-6 and TSP-7, the *C. elegans* orthologs of mammalian EV affinity markers CD9 and CD63, respectively, are poorly described and are not enriched in known EVNs (J. Wang et al., 2015).

This led to me considering how to use CLHM-1 as a tool for specific EV enrichment. Previous attempts to raise an anti-CLHM-1 antibody provided difficulty due to the cytotoxic nature of CLHM-1 overexpression (Tanis et al., 2013). The N-terminus and C-terminus of the CLHM-1 monomer are contained within the cellular/EV lumen (Ma et al., 2012; Tanis et al., 2013), rendering them useless for adding any affinity chromatography tag for the purpose of isolating intact EVs (Kimple et al., 2013). However, unpublished data shows a region in the 2<sup>nd</sup> extracellular loop (EL2) of the CLHM-1 monomer that can be altered without affecting overall CLHM-1 channel physiology. Thus, I sought to insert a small affinity tag in CLHM-1 EL2 to isolate intact ciliary EVs enriched with CLHM-1. As the Strep-tag II (STII), an eight-AA peptide biotin analogue, shows high binding affinity for Streptactin, an engineered streptavidin analogue (Schmidt & Skerra, 2007), I sought to engineer the *stII* sequence into *clhm-1::gfp*.

To create this construct, I used Gibson assembly to insert the *stII* and linker sequences into both *Pclhm-1::clhm-1::gfp* and *Pclhm-1::clhm-1::tdTomato* miniMos vectors. I confirmed successful cloning with Sanger sequencing and inserted the *Pclhm-1::clhm-1(stII)::gfp* and *tdTomato* cassettes into the genome as previously described.

To confirm that Streptactin could recognize CLHM-1(STII)::tdTomato, I conducted a protein blot against whole worm lysate of transgenic animals using Streptactin conjugated to horseradish peroxidase (Streptactin-HRP). I found that Streptactin-HRP recognizes whole worm lysate of transgenic worms, but not wild-type

animals, at the predicted size of CLHM-1(STII)::tdTomato (**Figure 33**). An additional band was present in the transgenic lanes, but not the wild-type lanes, which I judged to potentially be a nonspecific lysis or denaturation product.

I then sought to confirm that inserting the *stII* sequence into the *clhm-1* sequence did not affect CLHM-1(STII)::GFP ciliary localization or EV biogenesis. Super-resolution imaging confirms that CLHM-1(STII)::GFP still localizes to the cilia of male head and tail EVNs (**Figure 34**). CLHM-1(STII)::GFP is also found in released environmental EVs in similar numbers to CLHM-1::GFP (**Figure 35**). Thus, it should be possible to isolate intact EVs by affinity chromatography against Strep-tagged CLHM-1 to isolate EVs for downstream proteomic analysis.

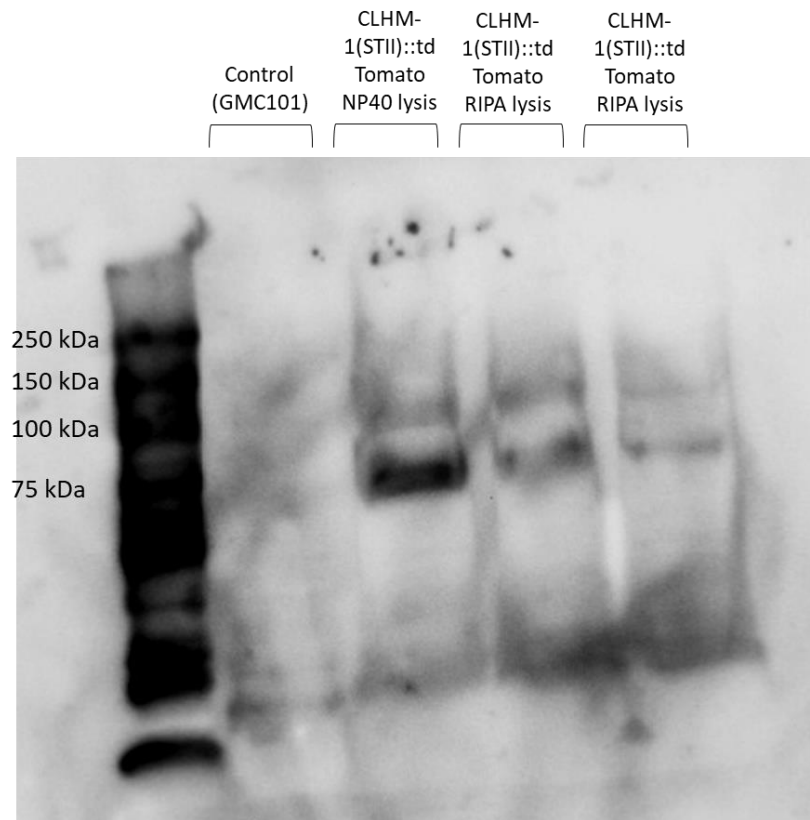


Figure 33: Protein blot shows Streptactin-HRP conjugate against lysate of animals expressing CLHM-1::tdTomato with internal Strep-tag. Bands appear at approximately 100 kDa and 75 kDa in transgenic lanes but not wild-type lane.



Figure 34: CLHM-1(STII)::GFP localizes to the cilia of adult male head and tail EVNs. Scale bars = 10  $\mu$ m.

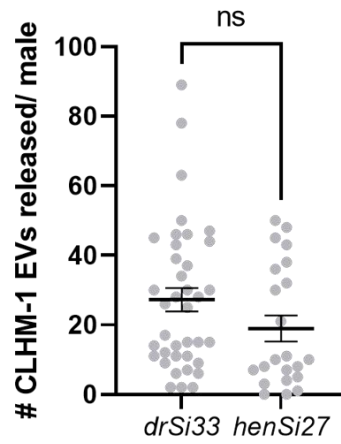
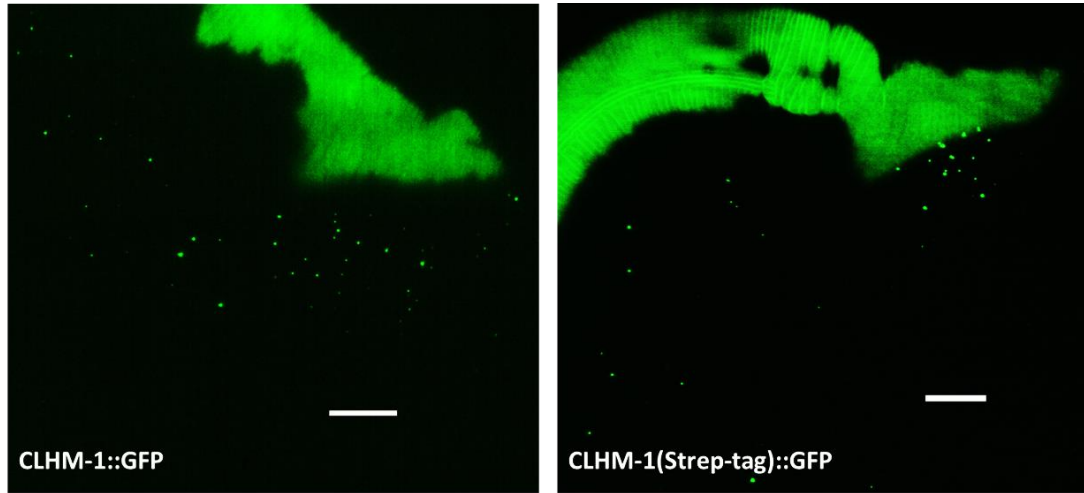


Figure 35: The average number of released environmental EVs containing CLHM-1(STII)::GFP is not significantly different than the number containing CLHM-1::GFP. Scale bars = 10  $\mu$ m.  $n \geq 20$ . Mann-Whitney test.

## Chapter 7

### DISCUSSION

Cilia protruding from cells are fundamentally important in receiving signals for signal transduction (Jiang et al., 2019; Lee & Chung, 2015; Wheway et al., 2018), but their ability to transmit signals via EVs is less well understood. It is important to understand how proteins become enriched in or excluded from specific ciliary EV subpopulations in order to ascertain the potential physiological functions or clinical relevance of these EVs.

Using the nematode *C. elegans* as an *in vivo* model to study ciliary EV biology, I identified the ion channel CLHM-1 as a new cargo in ciliary-derived EVs released from sensory neuron cilia into the environment. I discovered that CLHM-1 was enriched in a distinct subpopulation of EVs, separate from EVs carrying PKD-2, released from these neuron cilia and sought to determine the molecular mechanisms underlying this enrichment.

EVs are shed from the distal tip of neuron cilia. I found that CLHM-1 was excluded from this ciliary compartment and thus was not enriched into tip-derived EVs. The presence of mating partners caused an increase in tip-derived EV release, but a significant decrease in shedding of EVs containing CLHM-1. This indicates that differential localization of cargoes to ciliary compartments allows for heterogeneous

EV subpopulations to be dynamically and differentially shed in response to physiological stimuli.

Since there are multiple different ciliary-derived EVs subpopulations, this raises the question of how proteins are discretely localized to ensure enrichment into distinct subpopulations. Heterotrimeric kinesin-II and homomeric OSM-3 move IFT trains from the ciliary base, through the transition zone and up to the distal tip (Prevo et al., 2015). In the absence of these motors, many ciliary proteins accumulate at the ciliary base (Morsci & Barr, 2011), although not all proteins are dependent upon kinesin-II-mediated IFT for cilia entry (Belzile et al., 2013).

I found that PKD-2 often fails to enter the cilia proper and is not included in environmental EVs in *osm-3;klp-11* mutants, as previously reported (J. Wang et al., 2021). The myristoylated protein CIL-7, another ciliary EV cargo, does not require OSM-3 or the heterotrimeric kinesin-II to enter the cilia, but does depend on these IFT motors for inclusion in ciliary EVs (J. Wang et al., 2021). Interestingly, I found that CLHM-1 does not depend on OSM-3 and heterotrimeric kinesin-II for cilia entry or inclusion in ciliary EVs. This is consistent with CLHM-1 being excluded from tip-derived EVs and shows that anterograde IFT is required for EV shedding from the cilium distal tip, but not secondary sites. I also found differential roles for individual kinesin motors in regulating ciliary EV cargo enrichment, as loss of *osm-3* versus *klp-11* differentially affected colocalization of CLHM-1 and PKD-2 in the cilium and released EVs.

As IFT is inexorably linked to the translocation of proteins along the length of the cilia, I sought to understand how other factors that affect ciliary protein compartmentalization may affect EV cargo enrichment. Loss of the transition zone results in free diffusion of protein and lipid species into the cilium (Jensen et al., 2015a). I found that loss of this barrier in the *mks-5(tm3100)* mutant differentially impacted release of CLHM-1 and PDK-2 EV subpopulations.

Loss of the TZ in *mks-5(tm3100)* mutants has at least two molecular consequences that I posit may cause the observed changes in ciliary EV release. Firstly, in *mks-5(tm3100)* mutants, microtubule organization and axonemal structure is disrupted throughout the length of the cilia (Jensen et al., 2015b). Microtubules are the basis for IFT-related protein transport (O'Hagan et al., 2017; Prevo et al., 2017). My data shows that ciliary localization and EV inclusion of PKD-2, but not CLHM-1, is dependent upon kinesin-II-related IFT, meaning that the observed decrease of PKD-2 EVs in *mks-5(tm3100)* mutants may be a result of PKD-2 mislocalization. To confirm this, I will use super-resolution microscopy to image the cilia of *mks-5(tm3100)* mutant animals expressing PKD-2::GFP and CLHM-1::tdTomato and measure GFP fluorescence intensity along the cilia proper.

Loss of MKS-5 and the TZ also causes free diffusion of phosphoinositide lipid species throughout the cilia proper. Phosphoinositide 4,5 phosphate (PI(4,5)P<sub>2</sub> or PIP<sub>2</sub>) is concentrated at the PCMC and TZ but is largely absent from the cilia proper, and is involved in the targeting of membrane proteins to the ciliary pocket (Bae et al., 2009; Conduit et al., 2021; Jensen et al., 2015b). However, even in cilia with intact TZ,

disruption of PIP<sub>2</sub> equilibrium results in aberrant ciliary protein sublocalization (DiTirro et al., 2019), indicating that lipid distribution may be integral to ciliary EV protein enrichment. To test this, will examine cilia distribution and EV release of PKD-2::GFP and CLHM-1::tdTomato in an *inpp-1* loss-of-function mutant, which should have altered levels of ciliary PIP<sub>2</sub>.

I also found that molecular factors that are not been associated with cilia compartmentalization or protein translocation may be involved in ciliary EV protein cargo enrichment. Loss of the ESCRT-associated ubiquitin binding factor ALX-1 caused an increase in release of EVs containing CLHM-1, but not PKD-2, indicating that multiple molecular mechanisms exist to enrich proteins into specific EV subpopulations. I aimed to understand how ALX-1 affects CLHM-1 EV abundance by visualizing the localization of an ALX-1::mKate fusion protein, but was not able to yield any insights based on the particular transgenic model I used. To continue this experiment, I would confirm that ALX-1::mKate was able to rescue the specific increase in release of CLHM-1 EVs I observed in *alx-1* loss-of-function mutants, therefore confirming its functionality. I would also create a *Palx-1::gfp* transcriptional reporter to assess which, if any, EVNs express ALX-1.

I also showed that loss the small GTPase ARF-6 resulted in a decrease in the release of CLHM-1 EVs. In collaboration with undergraduate researcher Kate Wagner, the immediate future direction is to examine how loss of ARF-6 impacts release of PKD-2 EVs. Another future experiment will be to image the cilia in *arf-6*

mutants expressing CLHM-1::GFP to gauge whether the observed decrease in CLHM-1::GFP EV release is a consequence of decreased CLHM-1 ciliary abundance.

Ultimately, my work speaks to the potential overall physiological relevance of ciliary EVs. It has been suggested that packaging of proteins into EVs serves as a mechanism to reduce accumulation of cargoes resulting from disrupted IFT or protein overexpression (Razzauti & Laurent, 2021). However, my data are not consistent with all ciliary EVs being used only as vectors for disposal. The fluorescent EV cargoes I imaged were expressed at single copy, yet I still observed frequent and abundant shedding of EVs into the environment. I observed that CLHM-1 transport into the cilium proper was not dependent on kinesin-II activity, and did not observe an increase in shedding of CLHM-1 EVs in the *klp-11; osm-3* double mutant. Together, these results indicate that IFT disruption is not a main driver of ciliary EV shedding and environmental release. Shedding of EVs containing CLHM-1 was differentially altered not only in kinesin-II, *alx-1*, and *mks-5* mutants, but also by mating partner availability, suggesting that release of these EVs into the environment is physiologically significant.

I sought to design a method to specifically isolate EVs enriched with CLHM-1 by engineering a genetically encoded chimeric CLHM-1 protein with an extracellular Strep-tag for affinity purification. Although it appears that engineered CLHM-1/Strep-tag does not alter CLHM-1 ciliary localization or EV inclusion, I was unable to show that EVs containing this protein can be isolated with affinity purification due to time constraints. As a future direction, I would confirm that LC-MS/MS analysis of

transgenic animals expressing CLHM-1/ Strep-tag resulted in identification of CLHM-1 trypsin-digested polypeptides. This would indicate that large-scale affinity purification of worm EVs would yield intact particles.

An alternative to using Strep-tag affinity purification would be to use TurboID, a non-specific proximity-based biotin ligase that can be used as a tool to biotinylate proteins contained within EVs of interest (Branon et al., 2018). Dr. Inna Nikonorova, a postdoctoral researcher in the lab of Dr. Maureen Barr at Rutgers University, supplied me with a strain expressing an anti-GFP nanobody conjugated to TurboID and an mScarlet fluorescent transgene marker. I crossed this strain into a strain expressing CLHM-1::GFP. A future experimentalist can validate to see if mScarlet and GFP are colocalizing within environmental EVs, and then use streptavidin affinity isolation to pull down biotinylated EV proteins for LC-MS/MS identification.

As I was unable to characterize the CLHM-1 EV subpopulation, I was unable to gain insight into the specific physiological function of these EVs. However, I propose two possibilities, which I do not believe to be mutually exclusive. First, CLHM channels are permeable to  $\text{Ca}^{2+}$  and ATP (Ma et al., 2012; Taruno et al., 2013), thus CLHM-1 could act as a release channel for ions or small molecules stored in the EV lumen. Resting ciliary  $[\text{Ca}^{2+}]$  is significantly higher than resting cytoplasmic  $[\text{Ca}^{2+}]$  (Delling, Decaen, et al., 2013), and ATP synthase subunits localize to primary cilia (Hu & Barr, 2005; Lin et al., 2021), indicating that these molecules are concentrated in the cilia lumen and may be captured in ciliary EVs. The second possibility posits CLHM-1 as a modulator of primary cilia signaling, where it could

act to amplify signals. Excess CLHM-1 may need to be jettisoned from the cilia into EVs to prevent toxicity (Tanis et al., 2013), explaining its inclusion in specific EVs.

Regardless of the specific role for CLHM-1 in ciliary-derived EVs, my identification of this new EV subpopulation provides a new visual tool for exploring how specificity in ciliary EV biogenesis and cargo sorting is achieved. Innovations in super-resolution microscopy and labeling have made *in vivo* EV imaging feasible across a range of biological systems, although the most suitable techniques depend on the specific organism (Verweij et al., 2021). I performed imaging of EVs across three platforms equipped with different super-resolution capabilities: TIRF using the Andor Dragonfly, confocal with Airyscan detection using the Zeiss LSM880, and structured illumination using the Zeiss Elyra PS1. While all systems allowed for adequate detection of EVs containing fluorescent cargoes, use of the Andor Dragonfly coupled with a Zyla sCMOS detector provided the largest field of view and greatest resolution. Although I observed animal to animal variation, this platform provided robust and highly reproducible EV quantitation between different days and experimentalists. Our lab's *C. elegans* model, coupled with an imaging platform which enables visualization of EVs released from primary cilia *in vivo*, will continue to allow our lab to understand how specificity in ciliary EV biogenesis and cargo sorting is achieved.

## REFERENCES

- Admyre, C., Grunewald, J., Thyberg, J., Gripenbäck, S., Tornling, G., Eklund, A., Scheynius, A., & Gabrielsson, S. (2003). Exosomes with major histocompatibility complex class II and co-stimulatory molecules are present in human BAL fluid. *The European Respiratory Journal*, *22*(4), 578–583. <http://www.ncbi.nlm.nih.gov/pubmed/14582906>
- Akella, J. S., Carter, S. P., Nguyen, K., Tsiropoulou, S., Moran, A. L., Silva, M., Rizvi, F., Kennedy, B. N., Hall, D. H., Barr, M. M., & Blacque, O. E. (2020). Ciliary rab28 and the BBSome negatively regulate extracellular vesicle shedding. *ELife*, *9*. <https://doi.org/10.7554/ELIFE.50580>
- Anand, S., Foot, N., Ang, C.-S., Gembus, K. M., Keerthikumar, S., Adda, C. G., Mathivanan, S., & Kumar, S. (2018). Arrestin-Domain Containing Protein 1 (Arrdc1) Regulates the Protein Cargo and Release of Extracellular Vesicles. *PROTEOMICS*, *18*(17), 1800266. <https://doi.org/10.1002/pmic.201800266>
- Antonucci, F., Turola, E., Riganti, L., Caleo, M., Gabrielli, M., Perrotta, C., Novellino, L., Clementi, E., Giussani, P., Viani, P., Matteoli, M., & Verderio, C. (2012). Microvesicles released from microglia stimulate synaptic activity via enhanced sphingolipid metabolism. *The EMBO Journal*, *31*(5), 1231–1240. <https://doi.org/10.1038/emboj.2011.489>
- Bader, J. R., Kusik, B. W., & Besharse, J. C. (2012). Analysis of KIF17 distal tip trafficking in zebrafish cone photoreceptors. *Vision Research*, *75*, 37–43. <https://doi.org/10.1016/J.VISRES.2012.10.009>
- Bae, Y. K., Kim, E., L'Hernault, S. W., & Barr, M. M. (2009). The CIL-1 phosphoinositide 5-phosphatase regulates ciliary localization of the TRP polycystins and sperm function in *C. elegans*. *Current Biology : CB*, *19*(19), 1599. <https://doi.org/10.1016/J.CUB.2009.08.045>
- Bahrini, I., Song, J., Diez, D., & Hanayama, R. (2015). Neuronal exosomes facilitate synaptic pruning by up-regulating complement factors in microglia. *Scientific Reports*, *5*(1), 7989. <https://doi.org/10.1038/srep07989>
- Baietti, M. F., Zhang, Z., Mortier, E., Melchior, A., Degeest, G., Geeraerts, A.,

- Ivarsson, Y., Depoortere, F., Coomans, C., Vermeiren, E., Zimmermann, P., & David, G. (2012). Syndecan–syntenin–ALIX regulates the biogenesis of exosomes. *Nature Cell Biology*, *14*(7), 677–685. <https://doi.org/10.1038/ncb2502>
- Belzile, O., Hernandez-Lara, C. I., Wang, Q., & Snell, W. J. (2013). Regulated membrane protein entry into flagella is facilitated by cytoplasmic microtubules and does not require IFT. *Current Biology*, *23*(15), 1460–1465. <https://doi.org/10.1016/J.CUB.2013.06.025/ATTACHMENT/5556BCF6-CD43-46ED-B284-AD657A2A9006/MMC3.MP4>
- Berckmans, R. J., Nieuwland, R., Böing, A. N., Romijn, F. P., Hack, C. E., & Sturk, A. (2001). Cell-derived microparticles circulate in healthy humans and support low grade thrombin generation. *Thrombosis and Haemostasis*, *85*(4), 639–646. <http://www.ncbi.nlm.nih.gov/pubmed/11341498>
- Bissig, C., & Gruenberg, J. (2014). ALIX and the multivesicular endosome: ALIX in Wonderland. *Trends in Cell Biology*, *24*(1), 19–25. <https://doi.org/10.1016/j.tcb.2013.10.009>
- Blacque, O. E., Reardon, M. J., Li, C., McCarthy, J., Mahjoub, M. R., Ansley, S. J., Badano, J. L., Mah, A. K., Beales, P. L., Davidson, W. S., Johnsen, R. C., Audeh, M., Plasterk, R. H. A., Baillie, D. L., Katsanis, N., Quarmby, L. M., Wicks, S. R., & Leroux, M. R. (2004). Loss of *C. elegans* BBS-7 and BBS-8 protein function results in cilia defects and compromised intraflagellar transport. *Genes and Development*, *18*(13), 1630–1642. <https://doi.org/10.1101/gad.1194004>
- Blacque, O. E., & Sanders, A. A. (2014). Compartments within a compartment. *Organogenesis*, *10*(1), 126–137. <https://doi.org/10.4161/org.28830>
- Borges, F. T., Melo, S. A., Özdemir, B. C., Kato, N., Revuelta, I., Miller, C. A., Gattone, V. H., LeBleu, V. S., & Kalluri, R. (2013). TGF- $\beta$  1–Containing Exosomes from Injured Epithelial Cells Activate Fibroblasts to Initiate Tissue Regenerative Responses and Fibrosis. *Journal of the American Society of Nephrology*, *24*(3), 385–392. <https://doi.org/10.1681/ASN.2012101031>
- Branon, T. C., Bosch, J. A., Sanchez, A. D., Udeshi, N. D., Svinkina, T., Carr, S. A., Feldman, J. L., Perrimon, N., & Ting, A. Y. (2018). Efficient proximity labeling in living cells and organisms with TurboID. *Nature Biotechnology* *2018* *36*:9, *36*(9), 880–887. <https://doi.org/10.1038/nbt.4201>
- Brennan, K., Martin, K., FitzGerald, S. P., O’Sullivan, J., Wu, Y., Blanco, A., Richardson, C., & Mc Gee, M. M. (2020). A comparison of methods for the isolation and separation of extracellular vesicles from protein and lipid particles in human serum. *Scientific Reports* *2020* *10*:1, *10*(1), 1–13.

<https://doi.org/10.1038/s41598-020-57497-7>

- Brenner, S. (1974). The genetics of *Caenorhabditis elegans*. *Genetics*, 77(1), 71–94. <http://www.ncbi.nlm.nih.gov/pubmed/4366476>
- Bulloj, A., Leal, M. C., Xu, H., Castaño, E. M., & Morelli, L. (2010). Insulin-Degrading Enzyme Sorting in Exosomes: A Secretory Pathway for a Key Brain Amyloid- $\beta$  Degrading Protease. *Journal of Alzheimer's Disease*, 19(1), 79–95. <https://doi.org/10.3233/JAD-2010-1206>
- Castaman, G., Yu-Feng, L., & Rodeghiero, F. (1996). A bleeding disorder characterised by isolated deficiency of platelet microvesicle generation. *Lancet (London, England)*, 347(9002), 700–701. [https://doi.org/10.1016/s0140-6736\(96\)91259-3](https://doi.org/10.1016/s0140-6736(96)91259-3)
- Chivet, M., Javalet, C., Laulagnier, K., Blot, B., Hemming, F. J., & Sadoul, R. (2014). Exosomes secreted by cortical neurons upon glutamatergic synapse activation specifically interact with neurons. *Journal of Extracellular Vesicles*, 3(1), 24722. <https://doi.org/10.3402/jev.v3.24722>
- Claing, A., Chen, W., Miller, W. E., Vitale, N., Moss, J., Premont, R. T., & Lefkowitz, R. J. (2001).  $\beta$ -Arrestin-mediated ADP-ribosylation Factor 6 Activation and  $\beta$ 2-Adrenergic Receptor Endocytosis \*. *Journal of Biological Chemistry*, 276(45), 42509–42513. <https://doi.org/10.1074/JBC.M108399200>
- Colombo, M., Raposo, G., & Théry, C. (2014). Biogenesis, Secretion, and Intercellular Interactions of Exosomes and Other Extracellular Vesicles. *Annu. Rev. Cell Dev. Biol*, 30, 255–289. <https://doi.org/10.1146/annurev-cellbio-101512-122326>
- Conduit, S. E., Davies, E. M., Fulcher, A. J., Oorschot, V., & Mitchell, C. A. (2021). Superresolution Microscopy Reveals Distinct Phosphoinositide Subdomains Within the Cilia Transition Zone. *Frontiers in Cell and Developmental Biology*, 9, 1020. <https://doi.org/10.3389/FCELL.2021.634649/BIBTEX>
- Corrigan, L., Redhai, S., Leiblich, A., Fan, S.-J., Perera, S. M. W., Patel, R., Gandy, C., Wainwright, S. M., Morris, J. F., Hamdy, F., Goberdhan, D. C. I., & Wilson, C. (2014). BMP-regulated exosomes from *Drosophila* male reproductive glands reprogram female behavior. *The Journal of Cell Biology*, 206(5), 671–688. <https://doi.org/10.1083/jcb.201401072>
- Corsi, A. K., Wightman, B., & Chalfie, M. (2015). *Caenorhabditis elegans*. <https://doi.org/10.1895/wormbook.1.177.1>

- Delling, M., Decaen, P. G., Doerner, J. F., Febvay, S., & Clapham, D. E. (2013). Primary cilia are specialized calcium signalling organelles. *Nature* 2013 504:7479, 504(7479), 311–314. <https://doi.org/10.1038/nature12833>
- Delling, M., DeCaen, P. G., Doerner, J. F., Febvay, S., & Clapham, D. E. (2013). Primary cilia are specialized calcium signalling organelles. *Nature* 2013 504:7479, 504(7479), 311–314. <https://doi.org/10.1038/nature12833>
- DiTirro, D., Philbrook, A., Rubino, K., & Sengupta, P. (2019). The *Caenorhabditis elegans* tubby homolog dynamically modulates olfactory cilia membrane morphogenesis and phospholipid composition. *ELife*, 8. <https://doi.org/10.7554/ELIFE.48789>
- Dores, M. R., Chen, B., Lin, H., Soh, U. J. K., Paing, M. M., Montagne, W. A., Meerloo, T., & Trejo, J. (2012). ALIX binds a YPX<sub>3</sub>L motif of the GPCR PAR1 and mediates ubiquitin-independent ESCRT-III/MVB sorting. *The Journal of Cell Biology*, 197(3), 407–419. <https://doi.org/10.1083/jcb.201110031>
- Doroquez, D. B., Berciu, C., Anderson, J. R., Sengupta, P., & Nicastro, D. (2014). A high-resolution morphological and ultrastructural map of anterior sensory cilia and glia in *Caenorhabditis elegans*. *ELife*, 2014(3). <https://doi.org/10.7554/ELIFE.01948>
- Dreses-Werringloer, U., Lambert, J.-C., Vingtdoux, V., Zhao, H., Vais, H., Siebert, A., Jain, A., Koppel, J., Rovelet-Lecrux, A., Hannequin, D., Pasquier, F., Galimberti, D., Scarpini, E., Mann, D., Lendon, C., Campion, D., Amouyel, P., Davies, P., Foskett, J. K., ... Marambaud, P. (2008). A Polymorphism in CALHM1 Influences Ca<sup>2+</sup> Homeostasis, A $\beta$  Levels, and Alzheimer's Disease Risk. *Cell*, 133(7), 1149–1161. <https://doi.org/10.1016/j.cell.2008.05.048>
- Frohlich, D., Kuo, W. P., Fruhbeis, C., Sun, J.-J., Zehendner, C. M., Luhmann, H. J., Pinto, S., Toedling, J., Trotter, J., & Kramer-Albers, E.-M. (2014). Multifaceted effects of oligodendroglial exosomes on neurons: impact on neuronal firing rate, signal transduction and gene regulation. *Philosophical Transactions of the Royal Society B: Biological Sciences*, 369(1652), 20130510–20130510. <https://doi.org/10.1098/rstb.2013.0510>
- Frøkjær-Jensen, C., Davis, M. W., Sarov, M., Taylor, J., Flibotte, S., LaBella, M., Pozniakovsky, A., Moerman, D. G., & Jorgensen, E. M. (2014). Random and targeted transgene insertion in *Caenorhabditis elegans* using a modified Mos1 transposon. *Nature Methods*, 11(5), 529–534. <https://doi.org/10.1038/nmeth.2889>
- Frühbeis, C., Fröhlich, D., Kuo, W. P., Amphornrat, J., Thilemann, S., Saab, A. S., Kirchhoff, F., Möbius, W., Goebbels, S., Nave, K.-A., Schneider, A., Simons,

- M., Klugmann, M., Trotter, J., & Krämer-Albers, E.-M. (2013). Neurotransmitter-Triggered Transfer of Exosomes Mediates Oligodendrocyte–Neuron Communication. *PLoS Biology*, *11*(7), e1001604. <https://doi.org/10.1371/journal.pbio.1001604>
- Fu, W., Wang, L., Kim, S., Li, J., & Dynlacht, B. D. (2016). Role for the IFT-A Complex in Selective Transport to the Primary Cilium. *Cell Reports*, *17*(6), 1505–1517. <https://doi.org/10.1016/J.CELREP.2016.10.018>
- Gabrielli, M., Battista, N., Riganti, L., Prada, I., Antonucci, F., Cantone, L., Matteoli, M., Maccarrone, M., & Verderio, C. (2015). Active endocannabinoids are secreted on extracellular membrane vesicles. *EMBO Reports*, *16*(2), 213–220. <https://doi.org/10.15252/embr.201439668>
- Giri, P. K., & Schorey, J. S. (2008). Exosomes Derived from M. Bovis BCG Infected Macrophages Activate Antigen-Specific CD4+ and CD8+ T Cells In Vitro and In Vivo. *PLoS ONE*, *3*(6), e2461. <https://doi.org/10.1371/journal.pone.0002461>
- Gonzalez-Begne, M., Lu, B., Han, X., Hagen, F. K., Hand, A. R., Melvin, J. E., & Yates, J. R. (2009). Proteomic Analysis of Human Parotid Gland Exosomes by Multidimensional Protein Identification Technology (MudPIT). *Journal of Proteome Research*, *8*(3), 1304–1314. <https://doi.org/10.1021/pr800658c>
- Greening, D. W., Xu, R., Ji, H., Tauro, B. J., & Simpson, R. J. (2015). A protocol for exosome isolation and characterization: evaluation of ultracentrifugation, density-gradient separation, and immunoaffinity capture methods. *Methods in Molecular Biology (Clifton, N.J.)*, *1295*, 179–209. [https://doi.org/10.1007/978-1-4939-2550-6\\_15](https://doi.org/10.1007/978-1-4939-2550-6_15)
- Gross, J. C., Chaudhary, V., Bartscherer, K., & Boutros, M. (2012). Active Wnt proteins are secreted on exosomes. *Nature Cell Biology*, *14*(10), 1036–1045. <https://doi.org/10.1038/ncb2574>
- Gundry, R. L., White, M. Y., Murray, C. I., Kane, L. A., Fu, Q., Stanley, B. A., & Van Eyk, J. E. (2010). Preparation of Proteins and Peptides for Mass Spectrometry Analysis in a Bottom-Up Proteomics Workflow. *Current Protocols in Molecular Biology*, *90*(1), 10.25.1-10.25.23. <https://doi.org/10.1002/0471142727.MB1025S88>
- Guo, J. L., & Lee, V. M.-Y. (2011). Seeding of Normal Tau by Pathological Tau Conformers Drives Pathogenesis of Alzheimer-like Tangles. *Journal of Biological Chemistry*, *286*(17), 15317–15331. <https://doi.org/10.1074/jbc.M110.209296>

- Halkein, J., Tabruyn, S. P., Ricke-Hoch, M., Haghikia, A., Nguyen, N.-Q.-N., Scherr, M., Castermans, K., Malvaux, L., Lambert, V., Thiry, M., Sliwa, K., Noel, A., Martial, J. A., Hilfiker-Kleiner, D., & Struman, I. (2013). MicroRNA-146a is a therapeutic target and biomarker for peripartum cardiomyopathy. *The Journal of Clinical Investigation*, *123*(5), 2143–2154. <https://doi.org/10.1172/JCI64365>
- Han, H., & Hill, C. P. (2019). Structure and mechanism of the ESCRT pathway AAA+ ATPase Vps4. *Biochemical Society Transactions*, *47*(1), 37–45. <https://doi.org/10.1042/BST20180260>
- Harding, C. (1983). Receptor-mediated endocytosis of transferrin and recycling of the transferrin receptor in rat reticulocytes. *The Journal of Cell Biology*, *97*(2), 329–339. <https://doi.org/10.1083/jcb.97.2.329>
- Hirano, T., Katoh, Y., Nakayama, K., & Marshall, W. (2017). Intraflagellar transport - A complex mediates ciliary entry and retrograde trafficking of ciliary G protein-coupled receptors. *Molecular Biology of the Cell*, *28*(3), 429–439. <https://doi.org/10.1091/MBC.E16-11-0813/ASSET/IMAGES/LARGE/429FIG7.JPEG>
- Hodgkin, J., Horvitz, H. R., & Brenner, S. (1979). Nondisjunction Mutants of the Nematode CAENORHABDITIS ELEGANS. *Genetics*, *91*(1), 67. [/pmc/articles/PMC1213932/?report=abstract](https://pmc/articles/PMC1213932/?report=abstract)
- Hogan, M. C., Manganelli, L., Woollard, J. R., Masyuk, A. I., Masyuk, T. V., Tammachote, R., Huang, B. Q., Leontovich, A. A., Beito, T. G., Madden, B. J., Charlesworth, M. C., Torres, V. E., Larusso, N. F., Harris, P. C., & Ward, C. J. (2009). Characterization of PKD Protein-Positive Exosome-Like Vesicles. *Journal of the American Society of Nephrology*, *20*(2), 278–288. <https://doi.org/10.1681/ASN.2008060564>
- Hong, J., Dauros-Singorenko, P., Whitcombe, A., Payne, L., Blenkiron, C., Phillips, A., & Swift, S. (2019). Analysis of the Escherichia coli extracellular vesicle proteome identifies markers of purity and culture conditions. *Journal of Extracellular Vesicles*, *8*(1). <https://doi.org/10.1080/20013078.2019.1632099>
- Hu, J., & Barr, M. M. (2005). ATP-2 interacts with the PLAT domain of LOV-1 and is involved in Caenorhabditis elegans polycystin signaling. *Molecular Biology of the Cell*, *16*(2), 458–469. <https://doi.org/10.1091/MBC.E04-09-0851>
- Hurley, J. H. (2015). ESCRTs are everywhere. *The EMBO Journal*, *34*(19), 2398–2407. <https://doi.org/10.15252/embj.201592484>
- Hyenne, V., Apaydin, A., Rodriguez, D., Spiegelhalter, C., Hoff-Yoessle, S., Diem,

- M., Tak, S., Lefebvre, O., Schwab, Y., Goetz, J. G., & Labouesse, M. (2015). RAL-1 controls multivesicular body biogenesis and exosome secretion. *The Journal of Cell Biology*, *211*(1), 27–37. <https://doi.org/10.1083/jcb.201504136>
- Im, Y. J., & Hurley, J. H. (2008). Integrated Structural Model and Membrane Targeting Mechanism of the Human ESCRT-II Complex. *Developmental Cell*, *14*(6), 902–913. <https://doi.org/10.1016/j.devcel.2008.04.004>
- Izquierdo-Useros, N., Lorizate, M., Puertas, M. C., Rodriguez-Plata, M. T., Zangger, N., Erikson, E., Pino, M., Erkizia, I., Glass, B., Clotet, B., Keppler, O. T., Telenti, A., Kräusslich, H.-G., & Martinez-Picado, J. (2012). Siglec-1 Is a Novel Dendritic Cell Receptor That Mediates HIV-1 Trans-Infection Through Recognition of Viral Membrane Gangliosides. *PLoS Biology*, *10*(12), e1001448. <https://doi.org/10.1371/journal.pbio.1001448>
- Jensen, V. L., Lambacher, N. J., Li, C., Mohan, S., Williams, C. L., Inglis, P. N., Yoder, B. K., Blacque, O. E., & Leroux, M. R. (2018). Role for intraflagellar transport in building a functional transition zone. *EMBO Reports*, *19*(12). <https://doi.org/10.15252/EMBR.201845862>
- Jensen, V. L., & Leroux, M. R. (2017). Gates for soluble and membrane proteins, and two trafficking systems (IFT and LIFT), establish a dynamic ciliary signaling compartment. *Current Opinion in Cell Biology*, *47*, 83–91. <https://doi.org/10.1016/J.CEB.2017.03.012>
- Jensen, V. L., Li, C., Bowie, R. V, Clarke, L., Mohan, S., Blacque, O. E., & Leroux, M. R. (2015a). Formation of the transition zone by Mks5/Rpgrip1L establishes a ciliary zone of exclusion (CIZE) that compartmentalises ciliary signalling proteins and controls PIP2 ciliary abundance. *The EMBO Journal*, *34*(20), 2537–2556. <https://doi.org/10.15252/EMBJ.201488044>
- Jensen, V. L., Li, C., Bowie, R. V, Clarke, L., Mohan, S., Blacque, O. E., & Leroux, M. R. (2015b). Formation of the transition zone by Mks5/Rpgrip1L establishes a ciliary zone of exclusion (CIZE) that compartmentalises ciliary signalling proteins and controls PIP2 ciliary abundance. *The EMBO Journal*, *34*(20), 2537–2556. <https://doi.org/10.15252/EMBJ.201488044>
- Jeppesen, D. K., Fenix, A. M., Franklin, J. L., Higginbotham, J. N., Zhang, Q., Zimmerman, L. J., Liebler, D. C., Ping, J., Liu, Q., Evans, R., Fissell, W. H., Patton, J. G., Rome, L. H., Burnette, D. T., & Coffey, R. J. (2019). Reassessment of Exosome Composition. *Cell*, *177*(2), 428–445.e18. <https://doi.org/10.1016/J.CELL.2019.02.029>
- Jiang, J. Y., Falcone, J. L., Curci, S., & Hofer, A. M. (2019). Direct visualization of

- cAMP signaling in primary cilia reveals up-regulation of ciliary GPCR activity following Hedgehog activation. *Proceedings of the National Academy of Sciences*, 116(24), 12066–12071. <https://doi.org/10.1073/PNAS.1819730116>
- Johnson, J. R., Edwards, M. R., Davies, H., Newman, D., Holden, W., Jenkins, R. E., Burgoyne, R. D., Lucas, R. J., & Barclay, J. W. (2017). Ethanol stimulates locomotion via a  $\text{g}\alpha\text{s}$ -signaling pathway in IL2 neurons in *Caenorhabditis elegans*. *Genetics*, 207(3), 1023–1039. <https://doi.org/10.1534/GENETICS.117.300119/-/DC1>
- Joshi, P., Turola, E., Ruiz, A., Bergami, A., Libera, D. D., Benussi, L., Giussani, P., Magnani, G., Comi, G., Legname, G., Ghidoni, R., Furlan, R., Matteoli, M., & Verderio, C. (2014). Microglia convert aggregated amyloid- $\beta$  into neurotoxic forms through the shedding of microvesicles. *Cell Death and Differentiation*, 21(4), 582–593. <https://doi.org/10.1038/cdd.2013.180>
- Kaplan, O. I., Doroquez, D. B., Cevik, S., Bowie, R. V., Clarke, L., Sanders, A. A. W. M., Kida, K., Rappoport, J. Z., Sengupta, P., & Blacque, O. E. (2012). Endocytosis genes facilitate protein and membrane transport in *C. elegans* sensory cilia. *Current Biology*, 22(6), 451–460. <https://doi.org/10.1016/j.cub.2012.01.060>
- Kimple, M. E., Brill, A. L., & Pasker, R. L. (2013). Overview of affinity tags for protein purification. *Current Protocols in Protein Science*, 73, Unit 9.9. <https://doi.org/10.1002/0471140864.ps0909s73>
- Kobayashi, T., Ishida, Y., Hirano, T., Katoh, Y., & Nakayama, K. (2020). Cooperation of the IFT-A complex with the IFT-B complex is required for ciliary retrograde protein trafficking and GPCR import. <https://doi.org/10.1091/mbc.E20-08-0556>, 32(1), 45–56. <https://doi.org/10.1091/mbc.E20-08-0556>
- Koles, K., Nunnari, J., Korkut, C., Barria, R., Brewer, C., Li, Y., Leszyk, J., Zhang, B., & Budnik, V. (2012). Mechanism of Evenness Interrupted (Evi)-Exosome Release at Synaptic Boutons. *Journal of Biological Chemistry*, 287(20), 16820–16834. <https://doi.org/10.1074/jbc.M112.342667>
- Kolhe, R., Hunter, M., Liu, S., Jadeja, R. N., Pundkar, C., Mondal, A. K., Mendhe, B., Drewry, M., Rojiani, M. V., Liu, Y., Isales, C. M., Guldborg, R. E., Hamrick, M. W., & Fulzele, S. (2017). Gender-specific differential expression of exosomal miRNA in synovial fluid of patients with osteoarthritis. *Scientific Reports*, 7(1), 2029. <https://doi.org/10.1038/s41598-017-01905-y>
- Kostelansky, M. S., Schluter, C., Tam, Y. Y. C., Lee, S., Ghirlando, R., Beach, B., Conibear, E., & Hurley, J. H. (2007). Molecular Architecture and Functional

- Model of the Complete Yeast ESCRT-I Heterotetramer. *Cell*, 129(3), 485–498.  
<https://doi.org/10.1016/j.cell.2007.03.016>
- Kowal, J., Arras, G., Colombo, M., Jouve, M., Morath, J. P., Primdal-Bengtson, B., Dingli, F., Loew, D., Tkach, M., & Théry, C. (2016). Proteomic comparison defines novel markers to characterize heterogeneous populations of extracellular vesicle subtypes. *Proceedings of the National Academy of Sciences*, 113(8), E968–E977. <https://doi.org/10.1073/pnas.1521230113>
- Kucharzewska, P., Christianson, H. C., Welch, J. E., Svensson, K. J., Fredlund, E., Ringnér, M., Mörgelin, M., Bourseau-Guilmain, E., Bengzon, J., & Belting, M. (2013). Exosomes reflect the hypoxic status of glioma cells and mediate hypoxia-dependent activation of vascular cells during tumor development. *Proceedings of the National Academy of Sciences of the United States of America*, 110(18), 7312–7317. <https://doi.org/10.1073/pnas.1220998110>
- Lachenal, G., Pernet-Gallay, K., Chivet, M., Hemming, F. J., Belly, A., Bodon, G., Blot, B., Haase, G., Goldberg, Y., & Sadoul, R. (2011). Release of exosomes from differentiated neurons and its regulation by synaptic glutamatergic activity. *Molecular and Cellular Neuroscience*, 46(2), 409–418.  
<https://doi.org/10.1016/j.mcn.2010.11.004>
- Lambert, J.-C., Sleegers, K., González-Pérez, A., Ingelsson, M., Beecham, G. W., Hiltunen, M., Combarros, O., Bullido, M. J., Brouwers, N., Bettens, K., Berr, C., Pasquier, F., Richard, F., Dekosky, S. T., Hannequin, D., Haines, J. L., Tognoni, G., Fiévet, N., Dartigues, J.-F., ... Amouyel, P. (2010). The CALHM1 P86L polymorphism is a genetic modifier of age at onset in Alzheimer's disease: A meta-analysis study. *Journal of Alzheimer's Disease*, 22(1), 247–255.  
<https://doi.org/10.3233/JAD-2010-100933>
- Lane, R. E., Korbie, D., Hill, M. M., & Trau, M. (2018). Extracellular vesicles as circulating cancer biomarkers: opportunities and challenges. *Clinical and Translational Medicine*, 7(1), 14. <https://doi.org/10.1186/s40169-018-0192-7>
- Lee, J., & Chung, Y. D. (2015). Ciliary subcompartments: how are they established and what are their functions? *BMB Reports*, 48(7), 380.  
<https://doi.org/10.5483/BMBREP.2015.48.7.084>
- Lespagnol, A., Duflaut, D., Beekman, C., Blanc, L., Fiucci, G., Marine, J.-C., Vidal, M., Amson, R., & Telerman, A. (2008). Exosome secretion, including the DNA damage-induced p53-dependent secretory pathway, is severely compromised in TSAP6/Steap3-null mice. *Cell Death & Differentiation*, 15(11), 1723–1733.  
<https://doi.org/10.1038/cdd.2008.104>

- Li, C., Jensen, V. L., Park, K., Kennedy, J., Garcia-Gonzalo, F. R., Romani, M., De Mori, R., Bruel, A. L., Gaillard, D., Doray, B., Lopez, E., Rivière, J. B., Faivre, L., Thauvin-Robinet, C., Reiter, J. F., Blacque, O. E., Valente, E. M., & Leroux, M. R. (2016). MKS5 and CEP290 Dependent Assembly Pathway of the Ciliary Transition Zone. *PLOS Biology*, *14*(3), e1002416. <https://doi.org/10.1371/JOURNAL.PBIO.1002416>
- Li, Y., Kelly, W. G., Logsdon, J. M., Schurko, A. M., Harfe, B. D., Hill-Harfe, K. L., & Kahn, R. A. (2004). Functional genomic analysis of the ADP-ribosylation factor family of GTPases: phylogeny among diverse eukaryotes and function in *C. elegans*. *The FASEB Journal*, *18*(15), 1834–1850. <https://doi.org/10.1096/FJ.04-2273COM>
- Lin, W., Qiao, C., Hu, J., Wei, Q., & Xu, T. (2021). Conserved role of ATP synthase in mammalian cilia. *Experimental Cell Research*, *401*(1), 112520. <https://doi.org/10.1016/J.YEXCR.2021.112520>
- Liu, K. S., & Sternberg, P. W. (1995). Sensory regulation of male mating behavior in *caenorhabditis elegans*. *Neuron*, *14*(1), 79–89. [https://doi.org/10.1016/0896-6273\(95\)90242-2](https://doi.org/10.1016/0896-6273(95)90242-2)
- Loktev, A. V., & Jackson, P. K. (2013). Neuropeptide Y Family Receptors Traffic via the Bardet-Biedl Syndrome Pathway to Signal in Neuronal Primary Cilia. *Cell Reports*, *5*(5), 1316–1329. <https://doi.org/10.1016/J.CELREP.2013.11.011>
- Lombardi, M., Gabrielli, M., Adinolfi, E., & Verderio, C. (2021). Role of ATP in Extracellular Vesicle Biogenesis and Dynamics. *Frontiers in Pharmacology*, *12*, 356. <https://doi.org/10.3389/FPHAR.2021.654023/BIBTEX>
- Long, H., Zhang, F., Xu, N., Liu, G., Diener, D. R., Rosenbaum, J. L., & Huang, K. (2016). Comparative Analysis of Ciliary Membranes and Ectosomes. *Current Biology*, *26*(24), 3327–3335. <https://doi.org/10.1016/J.CUB.2016.09.055>
- Lopez-Verrilli, M. A., Picou, F., & Court, F. A. (2013). Schwann cell-derived exosomes enhance axonal regeneration in the peripheral nervous system. *Glia*, *61*(11), 1795–1806. <https://doi.org/10.1002/glia.22558>
- Ma, Z., Siebert, A. P., Cheung, K.-H., Lee, R. J., Johnson, B., Cohen, A. S., Vingtdeux, V., Marambaud, P., & Foskett, J. K. (2012). Calcium homeostasis modulator 1 (CALHM1) is the pore-forming subunit of an ion channel that mediates extracellular Ca<sup>2+</sup> regulation of neuronal excitability. *Proceedings of the National Academy of Sciences*, *109*(28), E1963–E1971. <https://doi.org/10.1073/pnas.1204023109>

- Maguire, J. E., Silva, M., Nguyen, K. C. Q., Hellen, E., Kern, A. D., Hall, D. H., & Barr, M. M. (2015). Myristoylated CIL-7 regulates ciliary extracellular vesicle biogenesis. *Molecular Biology of the Cell*, *26*(15), 2823–2832. <https://doi.org/10.1091/mbc.E15-01-0009>
- Mayers, J. R., Fyfe, I., Schuh, A. L., Chapman, E. R., Edwardson, J. M., & Audhya, A. (2011). ESCRT-0 Assembles as a Heterotetrameric Complex on Membranes and Binds Multiple Ubiquitinated Cargoes Simultaneously. *Journal of Biological Chemistry*, *286*(11), 9636–9645. <https://doi.org/10.1074/jbc.M110.185363>
- Mello, C. C., Kramer, J. M., Stinchcomb, D., & Ambros, V. (1991). Efficient gene transfer in *C.elegans*: extrachromosomal maintenance and integration of transforming sequences. *The EMBO Journal*, *10*(12), 3959–3970. <http://www.ncbi.nlm.nih.gov/pubmed/1935914>
- Monguió-Tortajada, M., Gálvez-Montón, C., Bayes-Genis, A., Roura, S., & Borràs, F. E. (2019). Extracellular vesicle isolation methods: rising impact of size-exclusion chromatography. *Cellular and Molecular Life Sciences*, *76*(12), 2369–2382. <https://doi.org/10.1007/S00018-019-03071-Y/FIGURES/4>
- Montecalvo, A., Larregina, A. T., Shufesky, W. J., Beer Stolz, D., Sullivan, M. L. G., Karlsson, J. M., Baty, C. J., Gibson, G. A., Erdos, G., Wang, Z., Milosevic, J., Tkacheva, O. A., Divito, S. J., Jordan, R., Lyons-Weiler, J., Watkins, S. C., & Morelli, A. E. (2012). Mechanism of transfer of functional microRNAs between mouse dendritic cells via exosomes. *Blood*, *119*(3), 756–766. <https://doi.org/10.1182/blood-2011-02-338004>
- Morelli, A. E., Larregina, A. T., Shufesky, W. J., Sullivan, M. L. G., Stolz, D. B., Papworth, G. D., Zahorchak, A. F., Logar, A. J., Wang, Z., Watkins, S. C., Falo, L. D., & Thomson, A. W. (2004). Endocytosis, intracellular sorting, and processing of exosomes by dendritic cells. *Blood*, *104*(10), 3257–3266. <https://doi.org/10.1182/blood-2004-03-0824>
- Morita, E., Sandrin, V., McCullough, J., Katsuyama, A., Baci Hamilton, I., & Sundquist, W. I. (2011). ESCRT-III Protein Requirements for HIV-1 Budding. *Cell Host & Microbe*, *9*(3), 235–242. <https://doi.org/10.1016/j.chom.2011.02.004>
- Morsci, N. S., & Barr, M. M. (2011). Kinesin-3 KLP-6 Regulates Intraflagellar Transport in Male-Specific Cilia of *Caenorhabditis elegans*. *Current Biology*, *21*(14), 1239–1244. <https://doi.org/10.1016/J.CUB.2011.06.027>
- Muralidharan-Chari, V., Clancy, J., Plou, C., Romao, M., Chavrier, P., Raposo, G., & D'Souza-Schorey, C. (2009). ARF6-Regulated Shedding of Tumor Cell-Derived

- Plasma Membrane Microvesicles. *Current Biology*, 19(22), 1875–1885.  
<https://doi.org/10.1016/j.cub.2009.09.059>
- Nabhan, J. F., Hu, R., Oh, R. S., Cohen, S. N., & Lu, Q. (2012). Formation and release of arrestin domain-containing protein 1-mediated microvesicles (ARMMs) at plasma membrane by recruitment of TSG101 protein. *Proceedings of the National Academy of Sciences*, 109(11), 4146–4151.  
<https://doi.org/10.1073/pnas.1200448109>
- Nager, A. R., Goldstein, J. S., Herranz-Pérez, V., Portran, D., Ye, F., Garcia-Verdugo, J. M., & Nachury, M. V. (2017). An Actin Network Dispatches Ciliary GPCRs into Extracellular Vesicles to Modulate Signaling. *Cell*, 168(1–2), 252–263.e14.  
<https://doi.org/10.1016/J.CELL.2016.11.036>
- Nakai, W., Yoshida, T., Diez, D., Miyatake, Y., Nishibu, T., Imawaka, N., Naruse, K., Sadamura, Y., & Hanayama, R. (2016). A novel affinity-based method for the isolation of highly purified extracellular vesicles. *Scientific Reports* 2016 6:1, 6(1), 1–11. <https://doi.org/10.1038/srep33935>
- Nikonorova, I. A., Wang, J., Cope, A. L., Tilton, P., Power, K. M., Walsh, J. D., Akella, J. S., Krauchunas, A. R., Shah, P., & Barr, M. M. (2021). Tracking extracellular vesicle (EV) cargo as a platform for studying EVomics, signaling, and targeting in vivo. *BioRxiv*, 2021.09.23.461577.  
<https://doi.org/10.1101/2021.09.23.461577>
- O'Hagan, R., Silva, M., Nguyen, K. C. Q., Zhang, W., Bellotti, S., Ramadan, Y. H., Hall, D. H., & Barr, M. M. (2017). Glutamylation Regulates Transport, Specializes Function, and Sculptures the Structure of Cilia. *Current Biology*, 27(22), 3430–3441.e6. <https://doi.org/10.1016/j.cub.2017.09.066>
- Odorizzi, G. (2006). The multiple personalities of Alix. *Journal of Cell Science*, 119(Pt 15), 3025–3032. <https://doi.org/10.1242/jcs.03072>
- Palma, J., Yaddanapudi, S. C., Pigati, L., Havens, M. A., Jeong, S., Weiner, G. A., Weimer, K. M. E., Stern, B., Hastings, M. L., & Duelli, D. M. (2012). MicroRNAs are exported from malignant cells in customized particles. *Nucleic Acids Research*, 40(18), 9125–9138. <https://doi.org/10.1093/nar/gks656>
- Palmerini, C. A., Saccardi, C., Carlini, E., Fabiani, R., & Arienti, G. (2003). Fusion of prostasomes to human spermatozoa stimulates the acrosome reaction. *Fertility and Sterility*, 80(5), 1181–1184. [https://doi.org/10.1016/S0015-0282\(03\)02160-5](https://doi.org/10.1016/S0015-0282(03)02160-5)
- Pan, X., Ou, G., Civelekoglu-Scholey, G., Blacque, O. E., Endres, N. F., Tao, L., Mogilner, A., Leroux, M. R., Vale, R. D., & Scholey, J. M. (2006). Mechanism

- of transport of IFT particles in *C. elegans* cilia by the concerted action of kinesin-II and OSM-3 motors. *The Journal of Cell Biology*, 174(7), 1035. <https://doi.org/10.1083/JCB.200606003>
- Peden, E. M., & Barr, M. M. (2005). The KLP-6 Kinesin Is Required for Male Mating Behaviors and Polycystin Localization in *Caenorhabditis elegans*. *Current Biology*, 15(5), 394–404. <https://doi.org/10.1016/J.CUB.2004.12.073>
- Phua, S. C., Chiba, S., Suzuki, M., Su, E., Roberson, E. C., Pusapati, G. V., Setou, M., Rohatgi, R., Reiter, J. F., Ikegami, K., & Inoue, T. (2017). Dynamic Remodeling of Membrane Composition Drives Cell Cycle through Primary Cilia Excision. *Cell*, 168(1–2), 264–279.e15. <https://doi.org/10.1016/J.CELL.2016.12.032>
- Pisitkun, T., Shen, R.-F., & Knepper, M. A. (2004). Identification and proteomic profiling of exosomes in human urine. *Proceedings of the National Academy of Sciences*, 101(36), 13368–13373. <https://doi.org/10.1073/pnas.0403453101>
- Prabu, P., Rome, S., Sathishkumar, C., Gastebois, C., Meugnier, E., Mohan, V., & Balasubramanyam, M. (2019). MicroRNAs from urinary extracellular vesicles are non-invasive early biomarkers of diabetic nephropathy in type 2 diabetes patients with the ‘Asian Indian phenotype.’ *Diabetes & Metabolism*, 45(3), 276–285. <https://doi.org/10.1016/j.diabet.2018.08.004>
- Prevo, B., Mangeol, P., Oswald, F., Scholey, J. M., & Peterman, E. J. G. (2015). Functional differentiation of cooperating kinesin-2 motors orchestrates cargo import and transport in *C. elegans* cilia. *Nature Cell Biology* 2015 17:12, 17(12), 1536–1545. <https://doi.org/10.1038/ncb3263>
- Prevo, B., Scholey, J. M., & Peterman, E. J. G. (2017). Intraflagellar transport: mechanisms of motor action, cooperation, and cargo delivery. *FEBS Journal*, 284(18), 2905–2931. <https://doi.org/10.1111/febs.14068>
- Qin, H., Burnette, D. T., Bae, Y. K., Forscher, P., Barr, M. M., & Rosenbaum, J. L. (2005). Intraflagellar transport is required for the vectorial movement of TRPV channels in the ciliary membrane. *Current Biology*, 15(18), 1695–1699. <https://doi.org/10.1016/j.cub.2005.08.047>
- Ramirez, M. I., Amorim, M. G., Gadelha, C., Milic, I., Welsh, J. A., Freitas, V. M., Nawaz, M., Akbar, N., Couch, Y., Makin, L., Cooke, F., Vettore, A. L., Batista, P. X., Freezor, R., Pezuk, J. A., Rosa-Fernandes, L., Claudia, A., Carreira, O., Devitt, A., ... Dias-Neto, E. (2018). Technical challenges of working with extracellular vesicles. *Nanoscale*, 10, 881. <https://doi.org/10.1039/c7nr08360b>
- Razzauti, A., & Laurent, P. (2021). Ectocytosis prevents accumulation of ciliary cargo

- in *C. elegans* sensory neurons. *ELife*, *10*. <https://doi.org/10.7554/ELIFE.67670>
- Reimer, S. L., Beniac, D. R., Hiebert, S. L., Booth, T. F., Chong, P. M., Westmacott, G. R., Zhanel, G. G., & Bay, D. C. (2021). Comparative Analysis of Outer Membrane Vesicle Isolation Methods With an *Escherichia coli* tolA Mutant Reveals a Hypervesiculating Phenotype With Outer-Inner Membrane Vesicle Content. *Frontiers in Microbiology*, *12*, 383. <https://doi.org/10.3389/FMICB.2021.628801/BIBTEX>
- Rieu, S., Géminard, C., Rabesandratana, H., Sainte-Marie, J., & Vidal, M. (2000). Exosomes released during reticulocyte maturation bind to fibronectin via integrin  $\alpha 4\beta 1$ . *European Journal of Biochemistry*, *267*(2), 583–590. <https://doi.org/10.1046/j.1432-1327.2000.01036.x>
- Russell, J. C., Kim, T.-K., Noori, A., Merrihew, G. E., Robbins, J. E., Golubeva, A., Wang, K., MacCoss, M. J., & Kaeberlein, M. (2020). Composition of *Caenorhabditis elegans* extracellular vesicles suggests roles in metabolism, immunity, and aging. *GeroScience* *2020* *42*:4, *42*(4), 1133–1145. <https://doi.org/10.1007/S11357-020-00204-1>
- Schmidt, T. G. M., & Skerra, A. (2007). The Strep-tag system for one-step purification and high-affinity detection or capturing of proteins. *Nature Protocols* *2007* *2*:6, *2*(6), 1528–1535. <https://doi.org/10.1038/nprot.2007.209>
- Schwarz, A., Wennemuth, G., Post, H., Brandenburger, T., Aumüller, G., & Wilhelm, B. (2013). Vesicular transfer of membrane components to bovine epididymal spermatozoa. *Cell and Tissue Research*, *353*(3), 549–561. <https://doi.org/10.1007/s00441-013-1633-7>
- Schwechheimer, C., & Kuehn, M. J. (2015). Outer-membrane vesicles from Gram-negative bacteria: biogenesis and functions. *Nature Publishing Group*, *13*. <https://doi.org/10.1038/nrmicro3525>
- Scott, A., Gaspar, J., Stuchell-Brereton, M. D., Alam, S. L., Skalicky, J. J., & Sundquist, W. I. (2005). Structure and ESCRT-III protein interactions of the MIT domain of human VPS4A. *Proceedings of the National Academy of Sciences*, *102*(39), 13813–13818. <https://doi.org/10.1073/pnas.0502165102>
- Shi, A., Pant, S., Balklava, Z., Chen, C. C. H., Figueroa, V., & Grant, B. D. (2007). A novel requirement for *C. elegans* Alix/ALX-1 in RME-1-mediated membrane transport. *Current Biology : CB*, *17*(22), 1913–1924. <https://doi.org/10.1016/J.CUB.2007.10.045>
- Silva, M., Morsci, N., Nguyen, K. C. Q., Rizvi, A., Rongo, C., Hall, D. H., & Barr, M.

- M. (2017). Cell-Specific  $\alpha$ -Tubulin Isoform Regulates Ciliary Microtubule Ultrastructure, Intraflagellar Transport, and Extracellular Vesicle Biology. *Current Biology*, 27(7), 968–980. <https://doi.org/10.1016/j.cub.2017.02.039>
- Singh, S., Gui, M., Koh, F., Yip, M. C. J., & Brown, A. (2020). Structure and activation mechanism of the BBosome membrane protein trafficking complex. *ELife*, 9. <https://doi.org/10.7554/ELIFE.53322>
- Skibinski, G., Kelly, R. W., Harkiss, D., & James, K. (1992). Immunosuppression by human seminal plasma--extracellular organelles (prostasomes) modulate activity of phagocytic cells. *American Journal of Reproductive Immunology (New York, N.Y. : 1989)*, 28(2), 97–103. <http://www.ncbi.nlm.nih.gov/pubmed/1337434>
- Snow, J. J., Ou, G., Gunnarson, A. L., Walker, M. R. S., Zhou, H. M., Brust-Mascher, I., & Scholey, J. M. (2004). Two anterograde intraflagellar transport motors cooperate to build sensory cilia on *C. elegans* neurons. *Nature Cell Biology* 2004 6:11, 6(11), 1109–1113. <https://doi.org/10.1038/ncb1186>
- Spitzer, P., Mulzer, L.-M., Oberstein, T. J., Munoz, L. E., Lewczuk, P., Kornhuber, J., Herrmann, M., & Maler, J. M. (2019). Microvesicles from cerebrospinal fluid of patients with Alzheimer's disease display reduced concentrations of tau and APP protein. *Scientific Reports*, 9(1), 7089. <https://doi.org/10.1038/s41598-019-43607-7>
- Street, J. M., Barran, P. E., Mackay, C. L., Weidt, S., Balmforth, C., Walsh, T. S., Chalmers, R. T., Webb, D. J., & Dear, J. W. (2012). Identification and proteomic profiling of exosomes in human cerebrospinal fluid. *Journal of Translational Medicine*, 10(1), 5. <https://doi.org/10.1186/1479-5876-10-5>
- Subedi, P., Schneider, M., Philipp, J., Azimzadeh, O., Metzger, F., Moertl, S., Atkinson, M. J., & Tapio, S. (2019). Comparison of methods to isolate proteins from extracellular vesicles for mass spectrometry-based proteomic analyses. *Analytical Biochemistry*, 584, 113390. <https://doi.org/10.1016/J.AB.2019.113390>
- Syntichaki, P., Xu, K., Driscoll, M., & Tavernarakis, N. (2002). Specific aspartyl and calpain proteases are required for neurodegeneration in *C. elegans*. *Nature* 2002 419:6910, 419(6910), 939–944. <https://doi.org/10.1038/nature01108>
- Tanis, J. E., Ma, Z., Krajacic, P., He, L., Foskett, J. K., & Lamitina, T. (2013). CLHM-1 is a Functionally Conserved and Conditionally Toxic Ca<sup>2+</sup>-Permeable Ion Channel in *Caenorhabditis elegans*. *Journal of Neuroscience*, 33(30), 12275–12286. <https://doi.org/10.1523/JNEUROSCI.5919-12.2013>
- Taruno, A., Vingtdoux, V., Ohmoto, M., Ma, Z., Dvoryanchikov, G., Li, A., Adrien,

- L., Zhao, H., Leung, S., Abernethy, M., Koppel, J., Davies, P., Civan, M. M., Chaudhari, N., Matsumoto, I., Hellekant, G., Tordoff, M. G., Marambaud, P., & Foskett, J. K. (2013). CALHM1 ion channel mediates purinergic neurotransmission of sweet, bitter and umami tastes. *Nature*, *495*(7440), 223–226. <https://doi.org/10.1038/nature11906>
- Taylor, J., Azimi, I., Monteith, G., & Bebawy, M. (2020). Ca<sup>2+</sup> mediates extracellular vesicle biogenesis through alternate pathways in malignancy. *https://doi.org/10.1080/20013078.2020.1734326*, *9*(1). <https://doi.org/10.1080/20013078.2020.1734326>
- Théry, C., Regnault, A., Garin, J., Wolfers, J., Zitvogel, L., Ricciardi-Castagnoli, P., Raposo, G., & Amigorena, S. (1999). Molecular Characterization of Dendritic Cell-Derived Exosomes. *The Journal of Cell Biology*, *147*(3), 599–610. <https://doi.org/10.1083/jcb.147.3.599>
- Toti, F., Satta, N., Fressinaud, E., Meyer, D., & Freyssinet, J. (1996). Scott syndrome, characterized by impaired transmembrane migration of procoagulant phosphatidylserine and hemorrhagic complications, is an inherited disorder. *Blood*, *87*(4). <http://www.bloodjournal.org/content/87/4/1409.long?sso-checked=true>
- Touroutine, D., & Tanis, J. E. (2020). A Rapid, SuperSelective Method for Detection of Single Nucleotide Variants in *Caenorhabditis elegans*. *Genetics*, *216*(2), 343–352. <https://doi.org/10.1534/GENETICS.120.303553>
- van der Burght, S. N., Rademakers, S., Johnson, J. L., Li, C., Kremers, G. J., Houtsmuller, A. B., Leroux, M. R., & Jansen, G. (2020). Ciliary Tip Signaling Compartment Is Formed and Maintained by Intraflagellar Transport. *Current Biology*, *30*(21), 4299–4306.e5. <https://doi.org/10.1016/J.CUB.2020.08.032>
- van der Westhuizen, W. A., Theron, C. W., Boucher, C. E., & Bragg, R. R. (2019). Regulation of outer-membrane proteins (OMPs) A and F, during hlyF-induced outer-membrane vesicle (OMV) biosynthesis. *Heliyon*, *5*(7), e02014. <https://doi.org/10.1016/J.HELIYON.2019.E02014>
- van Niel, G., Charrin, S., Simoes, S., Romao, M., Rochin, L., Saftig, P., Marks, M. S., Rubinstein, E., & Raposo, G. (2011). The tetraspanin CD63 regulates ESCRT-independent and -dependent endosomal sorting during melanogenesis. *Developmental Cell*, *21*(4), 708–721. <https://doi.org/10.1016/j.devcel.2011.08.019>
- van Niel, G., D'Angelo, G., & Raposo, G. (2018). Shedding light on the cell biology of extracellular vesicles. *Nature Reviews Molecular Cell Biology*, *19*(4), 213–

228. <https://doi.org/10.1038/nrm.2017.125>

- Verweij, F. J., Balaj, L., Boulanger, C. M., Carter, D. R. F., Compeer, E. B., D'Angelo, G., El Andaloussi, S., Goetz, J. G., Gross, J. C., Hyenne, V., Krämer-Albers, E. M., Lai, C. P., Loyer, X., Marki, A., Momma, S., Nolte-'t Hoen, E. N. M., Pegtel, D. M., Peinado, H., Raposo, G., ... van Niel, G. (2021). The power of imaging to understand extracellular vesicle biology in vivo. *Nature Methods* 2021 18:9, 18(9), 1013–1026. <https://doi.org/10.1038/s41592-021-01206-3>
- Vingtdeux, V., Chang, E. H., Frattini, S. A., Zhao, H., Chandakkar, P., Adrien, L., Strohl, J. J., Gibson, E. L., Ohmoto, M., Matsumoto, I., Huerta, P. T., & Marambaud, P. (2016). CALHM1 deficiency impairs cerebral neuron activity and memory flexibility in mice. *Scientific Reports*, 6. <https://doi.org/10.1038/srep24250>
- Volz, A.-K., Frei, A., Kretschmer, V., de Jesus Domingues, A. M., Ketting, R. F., Ueffing, M., Boldt, K., Krämer-Albers, E.-M., & May-Simera, H. L. (2021). Bardet-Biedl syndrome proteins modulate the release of bioactive extracellular vesicles. *Nature Communications* 2021 12:1, 12(1), 1–16. <https://doi.org/10.1038/s41467-021-25929-1>
- Wang, J., & Barr, M. M. (2016). Ciliary Extracellular Vesicles : Txt Msg Organelles. *Cellular and Molecular Neurobiology*, 36(3), 449–457. <https://doi.org/10.1007/s10571-016-0345-4>
- Wang, J., Kaletsky, R., Silva, M., Williams, A., Haas, L. A., Androwski, R. J., Landis, J. N., Patrick, C., Rashid, A., Santiago-Martinez, D., Gravato-Nobre, M., Hodgkin, J., Hall, D. H., Murphy, C. T., & Barr, M. M. (2015). Cell-Specific Transcriptional Profiling of Ciliated Sensory Neurons Reveals Regulators of Behavior and Extracellular Vesicle Biogenesis. *Current Biology*, 25(24), 3232–3238. <https://doi.org/10.1016/J.CUB.2015.10.057>
- Wang, J., Nikonorova, I. A., Gu, A., Sternberg, P. W., & Barr, M. M. (2020). Release and targeting of polycystin-2-carrying ciliary extracellular vesicles. *Current Biology*, 30(13), R755–R756. <https://doi.org/10.1016/J.CUB.2020.05.079>
- Wang, J., Nikonorova, I. A., Silva, M., Walsh, J. D., Tilton, P. E., Gu, A., Akella, J. S., & Barr, M. M. (2021). Sensory cilia act as a specialized venue for regulated extracellular vesicle biogenesis and signaling. *Current Biology*. <https://doi.org/10.1016/J.CUB.2021.06.040>
- Wang, J., Silva, M., Haas, L. A., Morsci, N. S., Nguyen, K. C. Q., Hall, D. H., & Barr, M. M. (2014). C. elegans Ciliated Sensory Neurons Release Extracellular Vesicles that Function in Animal Communication. *Current Biology*, 24(5), 519–

525. <https://doi.org/10.1016/j.cub.2014.01.002>

- Wang, Q., & Lu, Q. (2017). Plasma membrane-derived extracellular microvesicles mediate non-canonical intercellular NOTCH signaling. *Nature Communications* 2017 8:1, 8(1), 1–9. <https://doi.org/10.1038/s41467-017-00767-2>
- Webber, J., Steadman, R., Mason, M. D., Tabi, Z., & Clayton, A. (2010). Cancer Exosomes Trigger Fibroblast to Myofibroblast Differentiation. *Cancer Research*, 70(23), 9621–9630. <https://doi.org/10.1158/0008-5472.CAN-10-1722>
- Wehman, A. M., Poggioli, C., Schweinsberg, P., Grant, B. D., & Nance, J. (2011). The P4-ATPase TAT-5 Inhibits the Budding of Extracellular Vesicles in *C. elegans* Embryos. *Current Biology*, 21(23), 1951–1959. <https://doi.org/10.1016/j.cub.2011.10.040>
- Wheway, G., Nazlamova, L., & Hancock, J. T. (2018). Signaling through the Primary Cilium. *Frontiers in Cell and Developmental Biology*, 0(FEB), 8. <https://doi.org/10.3389/FCELL.2018.00008>
- White, J. Q., Nicholas, T. J., Gritton, J., Truong, L., Davidson, E. R., & Jorgensen, E. M. (2007). The Sensory Circuitry for Sexual Attraction in *C. elegans* Males. *Current Biology*, 17(21), 1847–1857. <https://doi.org/10.1016/J.CUB.2007.09.011>
- Willms, E., Johansson, H. J., Mäger, I., Lee, Y., Blomberg, K. E. M., Sadik, M., Alaarg, A., Smith, C. I. E., Lehtiö, J., EL Andaloussi, S., Wood, M. J. A., & Vader, P. (2016). Cells release subpopulations of exosomes with distinct molecular and biological properties. *Scientific Reports*, 6(1), 22519. <https://doi.org/10.1038/srep22519>
- Wollert, T., Wunder, C., Lippincott-Schwartz, J., & Hurley, J. H. (2009). Membrane scission by the ESCRT-III complex. *Nature*, 458(7235), 172–177. <https://doi.org/10.1038/nature07836>
- Wood, C. R., Huang, K., Diener, D. R., & Rosenbaum, J. L. (2013). The Cilium Secretes Bioactive Ectosomes. *Current Biology*, 23(10), 906–911. <https://doi.org/10.1016/J.CUB.2013.04.019>
- Yáñez-Mó, M., Siljander, P. R.-M., Andreu, Z., Bedina Zavec, A., Borràs, F. E., Buzas, E. I., Buzas, K., Casal, E., Cappello, F., Carvalho, J., Colás, E., Cordeiro-da Silva, A., Fais, S., Falcon-Perez, J. M., Ghobrial, I. M., Giebel, B., Gimona, M., Graner, M., Gursel, I., ... De Wever, O. (2015). Biological properties of extracellular vesicles and their physiological functions. *Journal of Extracellular Vesicles*, 4(1), 27066. <https://doi.org/10.3402/jev.v4.27066>

Zabeo, D., Cvjetkovic, A., Lässer, C., Schorb, M., Lötval, J., & Höög, J. L. (2017). Exosomes purified from a single cell type have diverse morphology. *Journal of Extracellular Vesicles*, 6(1). <https://doi.org/10.1080/20013078.2017.1329476>

Zhu, J., Zhang, J., Ji, X., Tan, Z., & Lubman, D. M. (2021). Column-based Technology for CD9-HPLC Immunoaffinity Isolation of Serum Extracellular Vesicles. *Journal of Proteome Research*, 20, 4911. [https://doi.org/10.1021/ACS.JPROTEOME.1C00549/SUPPL\\_FILE/PR1C00549\\_SI\\_001.PDF](https://doi.org/10.1021/ACS.JPROTEOME.1C00549/SUPPL_FILE/PR1C00549_SI_001.PDF)